THIRD SEMI-ANNUAL

radiation effects symposium

Sponsored by Air Research and Development Command
UNITED STATES AIR FORCE

LOCKHEED NUCLEAR PRODUCTS
Lockheed Aircraft Corporation, Georgia Division

VOLUME 3 OF 6

Aircraft Systems and Materials Papers

Third Semi-annual

radiation effects symposium

28-30 October 1958

Sponsored by
Air Research and Development Command
UNITED STATES AIR FORCE

LOCKHEED NUCLEAR PRODUCTS
LOCKHEED AIRCRAFT CORPORATION
GEORGIA DIVISION – MARIETTA, GEORGIA

FOREWORD

The proceedings of the Third Semi-Annual ANP Radiation Effects Symposium, held at the Dinkler-Plaza Hotel in Atlanta, Georgia, October 28 through 30, 1958, are in six volumes. Each of the first five volumes presents the unclassified papers from one of the five sessions; the sixth volume presents classified papers from all five sessions.

Each volume contains a complete table of contents and an index of authors. Volume One contains a list of the names of all who attended the Symposium.

VOLUME 1

GENERAL SESSION

1. APPLICATION OF RADIATION EFFECTS DATA TO NUCLEAR AIRCRAFT PROBLEMS by C. G. Collins, Aircraft Nuclear Propulsion Department, General Electric Company, Cincinnati, Ohio

2. RADIATION EFFECTS TESTING OF AIRCRAFT SUBSYSTEMS AND COMPONENTS AT AIR FORCE PLANT No. 67 FOR THE ANP PROGRAM by W. L. Bridges, Lockheed Nuclear Products, Lockheed Aircraft Corporation, Georgia Division, Marietta, Georgia

3. *MISSION AND TRAFFIC CONTROL REQUIREMENTS FOR THE WS/125A by James R. Burnett, Bendix Systems Division, Bendix Aviation Corporation, Ann Arbor, Michigan

4. NEW RADIATION TEST FACILITIES IN THE GENERAL ELECTRIC COMPANY by S. S. Jones, Vallecitos Atomic Laboratory, General Electric Company, San Jose, California, and W. R. Langdon and T. T. Naydan, General Electric Company, Schenectady, New York.

5. THE CONVAIR RADIATION EFFECTS TESTING SYSTEM by J. W. Allen, Convair, A Division of General Dynamics Corporation, Fort Worth, Texas

6. RADIATION EFFECTS REACTOR by W. T. Scarborough, Lockheed Nuclear Products, Lockheed Aircraft Corporation, Georgia Division, Marietta, Georgia

7. A DESCRIPTION OF A MULTI-KILOCURIE IRRADIATION FACILITY AND THE ASSOCIATED RADIATION DOSIMETRY by R. E. Simpson, Lockheed Nuclear Products, Lockheed Aircraft Corporation, Georgia Division, Marietta, Georgia, and M. Z. Fainman, M. E. Krasnow, E. R. Rathbun, C. R. Memhardt, Inland Testing Laboratories and Cook Research, Morton Grove, Illinois

8. START-UP OF THE CRITICAL EXPERIMENT REACTOR by M. A. Dewar, Lockheed Nuclear Products, Lockheed Aircraft Corporation, Georgia Division, Marietta, Georgia

9. REMOTE AREA MONITORING SYSTEM AT AIR FORCE PLANT No. 67 by E. N. Lide, Lockheed Nuclear Products, Lockheed Aircraft Corporation, Georgia Division, Marietta, Georgia

* This paper is classified and is bound in Volume Six.

10. AREA MONITORING FOR RADIOACTIVITY by Roy Shipp, Lockheed Nuclear Products, Lockheed Aircraft Corporation, Georgia Division, Marietta, Georgia

11. LOGARITHMIC CIRCUITS FOR RADIATION DOSIMETRY by L. A. Turner, Lockheed Nuclear Products, Lockheed Aircraft Corporation, Georgia Division, Marietta, Georgia

VOLUME 2

DOSIMETRY AND NUCLEAR MEASUREMENTS

12. INFLUENCE OF ENERGY SPECTRA ON RADIATION EFFECTS by F. C. Maienschein, Oak Ridge National Laboratory, Oak Ridge, Tennessee

13. CROSS SECTION AVERAGES FOR TYPICAL REACTOR SPECTRA by Walter R. Burrus and Russell P. Sullivan, Physics Department, Ohio State University, Columbus, Ohio

14. NUCLEAR UNITS AND MEASUREMENTS by R. S. Caswell and S. W. Smith, Atomic and Radiation Physics Division, National Bureau of Standards, Washington, District of Columbia

15. COMPARISON OF RADIATION EFFECTS IN DIFFERENT FACILITIES by W. T. Harper, Lockheed Aircraft Corporation, Lockheed Missile Systems Division, Palo Alto, California, and W. R. Burrus, Ohio State University, Columbus, Ohio

16. THE DETERMINATION OF NUCLEAR PARAMETERS FOR EXPERIMENTAL RADIATION EFFECTS by G. A. Wheeler, Convair, A Division of General Dynamics Corporation, Fort Worth, Texas

17. CALORIMETRIC DOSIMETRY PROGRAM AT LOCKHEED by Roger L. Gamble, Lockheed Nuclear Products, Lockheed Aircraft Corporation, Georgia Division, Marietta, Georgia

18. DOSIMETRY AND ENERGY DISTRIBUTION OF FAST NEUTRONS USING Li I by F. D. Schupp and S. L. Ruby, Radiation & Nucleonics Laboratory, Materials Engineering Department, Westinghouse Electric Corporation, East Pittsburgh, Pennsylvania

19. NEUTRON FLUX ENERGY DISTRIBUTION OF THE BNL REACTOR SHIELDING FACILITY by M. M. Weiss and M. M. Donnelly, Bell Telephone Laboratories, Whippany, New Jersey

20. THE EFFECTS OF NUCLEAR RADIATION ON SPARK GAPS by G. I. Duncan, Special Transformer Department, General Electric Company, Fort Wayne, Indiana, and J. C. Fraser and B. Valachovic, General Engineering Laboratory, General Electric Company, Schenectady, New York

21. RADIATION TESTING AND PROPERTIES OF A BORON NITRIDE DIELECTRIC CAPACITOR by G. R. Van Houten, T. C. O'Nan and J. T. Hood, P. R. Mallory and Company, Incorporated, Indianapolis, Indiana

VOLUME 3

AIRCRAFT SYSTEMS AND MATERIALS

22. THE PERFORMANCE OF IRRADIATED ELECTRONIC SYSTEMS BY ANALOG COMPUTER SIMULATION by V. C. Brown and N. M. Peterson, Convair, A Division of General Dynamics Corporation, Fort Worth, Texas

23. COMBINED TIME, TEMPERATURE, AND RADIATION EFFECTS ON ORGANIC MATERIALS by C. G. Collins, Aircraft Nuclear Propulsion Department, General Electric Company, Cincinnati, Ohio

24. RADIATION DAMAGE OF AIRPLANE TIRE MATERIALS by T. C. Gregson and S. D. Gehman, The Goodyear Tire and Rubber Company, Akron, Ohio

25. RADIATION EFFECTS ON FLIGHT CONTROLS SUBSYSTEM DESIGN by D. O. Gunson, Lockheed Aircraft Corporation, Georgia Division, Marietta, Georgia

26. PNEUMATICS - A TOOL FOR THE DESIGNER OF NUCLEAR POWERED AIRCRAFT by John A. Osterman, Lockheed Aircraft Corporation, Georgia Division, Marietta, Georgia

27. AIRCRAFT RADOME DESIGN PROBLEMS ASSOCIATED WITH A NUCLEAR ENVIRONMENT by Frank W. Thomas, Lockheed Nuclear Products, Lockheed Aircraft Corporation, Georgia Division, Marietta, Georgia

28. *EFFECTS OF HIGH ALTITUDE NUCLEAR DETONATIONS ON PROPAGATION OF ELECTROMAGNETIC WAVES by Samuel Horowitz and Lt. Richard Sugarman, U. S. Air Force Cambridge Research Center, Bedford, Massachusetts

29. *THE EFFECTS OF GAMMA RAY AND REACTOR IRRADIATIONS ON THE SENSITIVITY OF EXPLOSIVES by Paul W. Levy, Brookhaven National Laboratory, Upton, Long Island, New York, and J. V. R. Kaufman and James E. Abel, Explosives Research Section, Picatinny Arsenal, Dover, New Jersey

30. ON THE ENERGY LEVELS IN NEUTRON IRRADIATED SILICON by C. A. Klein and W. D. Straub, Research Division, Raytheon Manufacturing Company, Waltham, Massachusetts

31. EFFECT OF RADIATION ON THE CRITICAL SHEAR STRESS OF A METAL SINGLE CRYSTAL by C. E. Morgan, Convair, A Division of General Dynamics Corporation, Fort Worth, Texas

32. MEASUREMENT OF THE RANGE OF RECOIL ATOMS by R. A. Schmitt and R. A. Sharp, General Atomic, A Division of General Dynamics Corporation, San Diego, California

33. THE EFFECTS OF NUCLEAR ENVIRONMENT ON METALLIC AND NONMETALLIC MAGNETIC MATERIALS by E. I. Salkovitz and A. I. Schindler, U. S. Naval Research Laboratory, Washington, District of Columbia

34. *THE EFFECT OF NUCLEAR RADIATION ON COMMUNICATIONS SET AN/ARC-34 by D. L. Jacobs, Convair, A Division of General Dynamics, Fort Worth, Texas

35. RADIATION TESTING OF J-79 ORGANIC ENGINEERING MATERIALS AND COMPONENTS by D. E. Barnett, Aircraft Nuclear Propulsion Department, General Electric Company, Cincinnati, Ohio

36. *THE EFFECT OF NUCLEAR RADIATION DURING ESCAPE ON F-104 by F. L. Bouquet, Jr., Lockheed Aircraft Corporation, California Division, Burbank, California

* This paper is classified and is bound in Volume Six.

VOLUME 4

ELECTRONICS AND SEMI-CONDUCTORS

37. THE EFFECTS OF RADIATION ON VARIOUS RESISTOR TYPES by E. R. Pfaff and R. D. Shelton, Admiral Corporation, Chicago, Illinois

38. RADIATION EFFECTS IN COMPOUND SEMICONDUCTORS by L. W. Aukerman and R. K. Willardson, Battelle Memorial Institute, Columbus, Ohio

39. A CRITICAL SURVEY OF RADIATION DAMAGE TO CIRCUITS by W. W. Happ and S. R. Hawkins, Lockheed Aircraft Corporation, Lockheed Missile Systems Division, Palo Alto, California

40. RADIATION STABILIZATION OF TRANSISTOR CIRCUITS BY ACTIVE FEEDBACK by S. R. Hawkins and W. W. Happ, Lockheed Aircraft Corporation, Lockheed Missile Systems Division, Palo Alto, California

41. COMPARISON OF NEUTRON DAMAGE IN GERMANIUM AND SILICON TRANSISTORS by J. W. Easley, Bell Telephone Laboratories, Whippany, New Jersey

42. PULSED RADIATION EFFECTS IN SEMICONDUCTORS by J. M. Denney, C. W. Perkins, and J. R. Wieneke, Nuclear Electronics Department, Hughes Aircraft Company, Culver City, California

43. THE EFFECT OF VARIATION OF THE WIDTH OF THE BASE REGION ON THE RADIATION TOLERANCE OF SILICON DIODES by Gerald C. Huth, Aircraft Nuclear Propulsion Department, General Electric Company, Cincinnati, Ohio

44. THE EFFECT OF NUCLEAR RADIATION ON COMMERCIAL SILICON DIODES by John R. Crittenden, Aircraft Nuclear Propulsion Department, General Electric Company, Cincinnati, Ohio

45. EVALUATION OF SILICON DIODE IRRADIATION RESULTS IN TERMS OF MAGNETIC AMPLIFIER PERFORMANCE by J. A. Russell, Aircraft Nuclear Propulsion Department, General Electric Company, Cincinnati, Ohio

46. GAMMA RADIATION EFFECTS IN SILICON SOLAR CELLS by G. Enslow, F. Junga, and W. W. Happ, Lockheed Aircraft Corporation, Lockheed Missile Systems Division, Palo Alto, California

47. THE EFFECTS OF NUCLEAR RADIATION ON POWER TRANSISTORS by Frederick Gordon, Jr., U. S. Army Signal Corps, Research and Development Laboratories, Fort Monmouth, New Jersey

48. THE PERFORMANCE OF SOME ZENER REFERENCE ELEMENTS DURING EXPOSURE TO NUCLEAR RADIATION by M. A. Xavier, Cook Research Laboratory Division, Cook Electric Company, Morton Grove, Illinois

49. EFFECTS OF ELECTRON BOMBARDMENT ON CADMIUM SULFIDE WHISKERS by B. A. Kulp and D. C. Reynolds, Aeronautical Research Laboratory, Wright Air Development Center, Wright-Patterson Air Force Base, Ohio

VOLUME 5

LUBRICANTS AND PLASTICS

50. THE BEHAVIOR OF FUELS AND LUBRICANTS IN DYNAMIC TEST EQUIPMENT OPERATING IN THE PRESENCE OF GAMMA RADIATION by M. Z. Fainman, Inland Testing Laboratory, Morton Grove, Illinois

51. THE DEVELOPMENT OF NUCLEAR RADIATION RESISTANT SOLID FILM LUBRICANTS by William L. R. Rice and Lieutenant William L. Cox, Materials Laboratory, Wright Air Development Center, Wright-Patterson Air Force Base, Ohio

52. INTEREFFECTS BETWEEN REACTOR RADIATION AND MIL-L-7808C AIRCRAFT TURBINE OIL by F. A. Haley, Convair, A Division of General Dynamics Corporation, Fort Worth, Texas

53. DEVELOPMENT OF RADIATION-RESISTANT HIGH-TEMPERATURE LUBRICANTS by C. L. Mahoney, W. S. Saari, K. J. Sax, W. W. Kerlin, E. R. Barnum, P. H. Williams Shell Development Company, Emeryville, California

54. ELECTRICAL EFFECTS OF HIGH-INTENSITY IONIZING RADIATION ON NONMETALS by V. A. J. Van Lint and P. H. Miller, Jr., General Atomic, A Division of General Dynamics Corporation, San Diego, California

55. STUDY OF RADIATION EFFECTS ON ELECTRICAL INSULATION by J. F. Hansen, Battelle Memorial Institute, Columbus, Ohio, and M. L. Shatzen, Lockheed Nuclear Products, Lockheed Aircraft Corporation, Georgia Division, Marietta, Georgia

56. A STUDY OF RADIATION EFFECTS ON FUEL TANK SEALANTS AND BLADDER CELL MATERIAL by M. L. Shatzen, Lockheed Nuclear Products, Lockheed Aircraft Corporation, Georgia Division, Marietta, Georgia, and R. S. Tope, C. W. Cooper, and R. G. Heiligmann, Sealants and Elastomers Division, Battelle Memorial Institute, Columbus, Ohio

57. THE EFFECT OF ELECTRON RADIATION ON THE COMPLEX DYNAMIC MODULUS OF POLYSTYRENE AND HIGH DENSITY POLYETHYLENE by R. H. Chambers, General Atomic, A Division of General Dynamics Corporation, San Diego, California

58. RADIATION RESISTANT SILICONES by E. L. Warrick, D. J. Fischer, and J. F. Zack, Dow Corning Corporation, Midland, Michigan

59. RADIATION EFFECTS ON ORGANO-SILICONS by T. W. Albrecht, Convair, A Division of General Dynamics Corporation, Fort Worth, Texas

60. EFFECTS OF GAMMA RADIATION ON FLUOROCARBON POLYMERS by Leo A. Wall, Roland E. Florin, and D. W. Brown, National Bureau of Standards, Washington, District of Columbia

61. *FAST NEUTRON ACTIVATION OF SEAPLANE MATERIALS by L. Brandeis Wehle, Jr., Michael D. D'Agostino, and Anthony J. Favale, Grumman Aircraft Engineering Corporation, Bethpage, Long Island, New York

62. EFFECTS OF NUCLEAR RADIATION ON CORK, LEATHER, AND ELASTOMERS by Chester J. De Zeih, Boeing Airplane Company, Seattle, Washington

63. THE "PLATE SHEAR METHOD" OF DETERMINING THE MODULUS OF RIGIDITY OF SANDWICH PANELS by R. R. Bauerlein, Convair, A Division of General Dynamics Corporation, Fort Worth, Texas

64. "O" RING TESTING IN A MIXED FIELD IRRADIATION by E. E. Kerlin, Convair, A Division of General Dynamics Corporation, Fort Worth, Texas

* This paper is classified and is bound in Volume Six.

65. RADIATION EFFECTS ON 23 SILICONE RUBBERS AT AMBIENT TEMPERATURE by D. M. Newell, Convair, A Division of General Dynamics Corporation, Fort Worth, Texas

66. *THE RADIATION ENVIRONMENT DUE TO ACTIVATION AND SCATTERING EFFECTS NEAR BASED SEAPLANES by F. L. Bouquet, Jr., Lockheed Aircraft Corporation, California Division, Burbank, California

* This paper is classified and is bound in Volume Six.

VOLUME 6

CLASSIFIED PAPERS

3. MISSION AND TRAFFIC CONTROL REQUIREMENTS FOR THE WS/125A by James R. Burnett, Bendix Systems Division, Bendix Aviation Corporation, Ann Arbor, Michigan

28. EFFECTS OF HIGH ALTITUDE NUCLEAR DETONATIONS ON PROPAGATION OF ELECTROMAGNETIC WAVES by Samuel Horowitz and Lt. Richard Sugarman, U. S. Air Force Cambridge Research Center, Bedford, Massachusetts

29. THE EFFECTS OF GAMMA RAY AND REACTOR IRRADIATIONS ON THE SENSITIVITY OF EXPLOSIVES by Paul W. Levy, Brookhaven National Laboratory, Upton, Long Island, New York,and J. V. R. Kaufman and James E. Abel, Explosives Research Section, Picatinny Arsenal, Dover, New Jersey

34. THE EFFECT OF NUCLEAR RADIATION ON COMMUNICATIONS SET AN/ARC-34 by D. L. Jacobs, Convair, A Division of General Dynamics, Fort Worth, Texas

36. THE EFFECT OF NUCLEAR RADIATION DURING ESCAPE ON F-104 by F. L. Bouquet, Jr., Lockheed Aircraft Corporation, California Division, Burbank, California

61. FAST NEUTRON ACTIVATION OF SEAPLANE MATERIALS by L. Brandeis Wehle, Jr., Michael D. D'Agostino, and Anthony J. Favale, Grumman Aircraft Engineering Corporation, Bethpage, Long Island, New York

66. THE RADIATION ENVIRONMENT DUE TO ACTIVATION AND SCATTERING EFFECTS NEAR BASED SEAPLANES by F. L. Bouquet, Jr., Lockheed Aircraft Corporation, California Division, Burbank, California

INDEX OF AUTHORS

NAME	PAPER NO.	NAME	PAPER NO.
1. Abel, J. E.	29	42. Hawkins, S. R.	39, 40
2. Albrecht, T. W.	59	43. Heiligmann, R. G.	56
3. Allen, J. W.	5	44. Hood, J. T.	21
4. Aukerman, L. W.	38	45. Horowitz, S.	28
5. Barnett, D. E.	35	46. Huth, G. C.	43
6. Barnum, E. R.	53	47. Jacobs, D. L.	34
7. Bauerlein, R. R.	63	48. Jones, S. S.	4
8. Bouquet, F. L.	36, 66	49. Junga, F.	46
9. Bridges, W. L.	2	50. Kaufman, J. V. R.	29
10. Brown, D. W.	60	51. Kerlin, E. E.	64
11. Brown, V. C.	22	52. Kerlin, W. W.	53
12. Burnett, J. R.	3	53. Klein, C. A.	30
13. Burrus, W. R.	13, 15	54. Krasnow, M. E.	7
14. Caswell, R. S.	14	55. Kulp, B. A.	49
15. Chambers, R. H.	57	56. Langdon, W. R.	4
16. Collins, C. G.	1, 23	57. Levy, P. W.	29
17. Cooper, C. W.	56	58. Lide, E. N.	9
18. Cox, Lt. W. L.	51	59. Mahoney, C. L.	53
19. Crittenden, J. R.	44	60. Maienschein, F. C.	12
20. D'Agostino, M. D.	61	61. Memhardt, C. R.	7
21. Denney, J. M.	42	62. Miller, P. H., Jr.	54
22. Dewar, M. A.	8	63. Morgan, C. E.	31
23. DeZeih, C. J.	62	64. Naydan, T. T.	4
24. Donnelly, M. M.	19	65. Newell, D. M.	65
25. Duncan, G. I.	20	66. O'Nan, T. C.	21
26. Easley, J. W.	41	67. Osterman, J. A.	26
27. Enslow, G.	46	68. Perkins, C. W.	42
28. Fainman, M. Z.	7, 50	69. Peterson, N. M.	22
29. Favale, A. J.	61	70. Pfaff, E. R.	37
30. Fischer, D. J.	58	71. Rathbun, E. R.	7
31. Florin, R. E.	60	72. Reynolds, D. C.	49
32. Fraser, J. C.	20	73. Rice, W.L.R.	51
33. Gamble, R. L.	17	74. Ruby, S. L.	18
34. Gehman, S. D.	24	75. Russell, J. A.	45
35. Gordon, F., Jr.	47	76. Saari, W. S.	53
36. Gregson, T. C.	24	77. Salkovitz, E. I.	33
37. Gunson, D. O.	25	78. Sax, K. J.	53
38. Haley, F. A.	52	79. Scarborough, W. T.	6
39. Hansen, J. F.	55	80. Schindler, A. I.	33
40. Happ, W. W.	39, 40, 46	81. Schmitt, R. A.	32
41. Harper, W. T.	15	82. Schupp, F. D.	18

83. Sharp, R. A. 32
84. Shatzen, M. L. 55, 56
85. Shelton, R. D. 37
86. Shipp, R. L. 10
87. Simpson, R. E. 7
88. Smith, S. W. 14
89. Straub, W. D. 30
90. Sugarman, Lt. R. 28
91. Sullivan, R. P. 13
92. Thomas, F. W. 27
93. Tope, R. S. 56
94. Turner, L. A. 11
95. Valachovic, B. 20
96. Van Houten, G. R. 21
97. Van Lint, V.A.J. 54
98. Wall, L. A. 60
99. Warrick, E. L. 58
100. Wehle, L. B. 61
101. Weiss, M. M. 19
102. Wheeler, G. A. 16
103. Wieneke, J. R. 42
104. Willardson, R. K. 38
105. Williams, P. H. 53
106. Xavier, M. A. 48
107. Zack, J. F. 58

PREDICTING THE PERFORMANCE OF IRRADIATED ELECTRONICS SYSTEMS BY SIMULATION ON THE ANALOG COMPUTER

by

V. C. Brown and N. M. Peterson

CONVAIR

A Division of General Dynamics Corporation
Fort Worth, Texas

The method of simulating electronics systems on analog computers for the purpose of studying the effects of radiation is described and a comparison made between the results obtained by the simulation technique and data obtained in an actual irradiation. The results show that, by combining proper statistical methods with computer simulation, the performance of electronics systems under radiation may be successfully predicted.

INTRODUCTION

Literally thousands of components are available today to the military electronics designer; unfortunately, only a few will ever be adequately tested in the many possible combinations of electronic application, temperature, humidity, and pressure. For this reason, the functioning of a mechanism as complex as many of the present-day electronic systems is always a question. When the system is exposed, in addition, to such a new and heretofore unstudied environment as nuclear radiation, the question is compounded.

Predictions of the effects of radiation on electronic systems must take into direct account the radiation-induced changes in the operating characteristics of the components. The tolerance of the system to these changes and the possibility of feedback or cumulative effects - that is, effects not directly associated with the radiation damage itself, but changes caused by a damage to one component affecting the operation of another - must be considered.

One approach to this problem has been through the use of simulation techniques on the analog computer. The method consists essentially of simulating the system to be studied and then varying the characteristics of the components as they are found to vary under irradiation.

SIMULATION TECHNIQUES

Analog computers may be used to simulate physical systems in several ways, depending on the nature of the problem. In general, as shown in Figure 1, the principal means of simulation are the following:

(1) Solution of the equations governing the system;

(2) Direct substitution for system components, i.e., system components are replaced with analog computer elements directly.

(3) Simulation of system output, in which the output from the computer simulates that of the physical system. The method of obtaining the simulated output, however, bears no direct resemblance to the physical system.

The solution of system equations is the most widely used method; however, it usually requires the largest number of computing elements and, therefore, is the most expensive method of simulation.

On the other hand, the method of direct substitution for the system components is simpler and easier to apply. It has the added advantage that the equations of the system need not be written. The simulation of system output is generally used when either of the other methods is impractical or impossible to apply. The advantage of this method is that very complex equipment need not be simulated in its entirety.

Of the three methods generally used, experience has indicated that the direct substitution method is the one most suited for electronic systems. Obviously, it is simpler to simulate one LC network with another LC network than it would be to write the equations and then study the behavior of the equations. In effect, then, in the case of passive elements, the simulation consists of building the system under study out of the precision variable components of the computer.

Operation of the vacuum tubes and other active elements in an electrical circuit may be accurately simulated, as in Figure 2, with current generators or voltage amplifiers connected to give the familiar equivalent circuits. To take into account the nonlinearities in the transfer characteristics of such elements, a function generator may be used in conjunction with the other elements.

METHODS OF SIMULATION

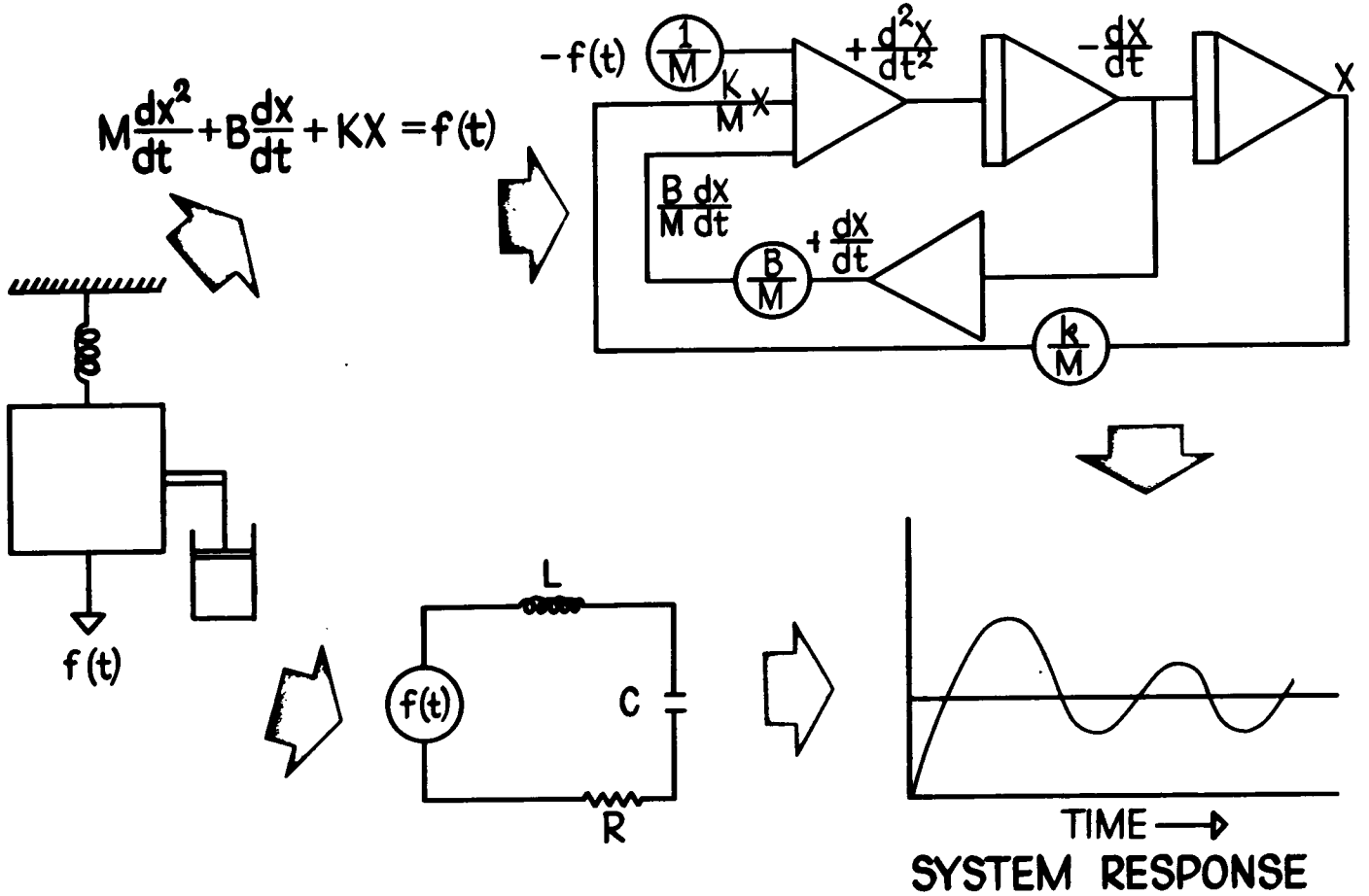

NPC 7434

FIGURE 1

AMPLIFIER WITH INTERELECTRODE CAPACITANCE

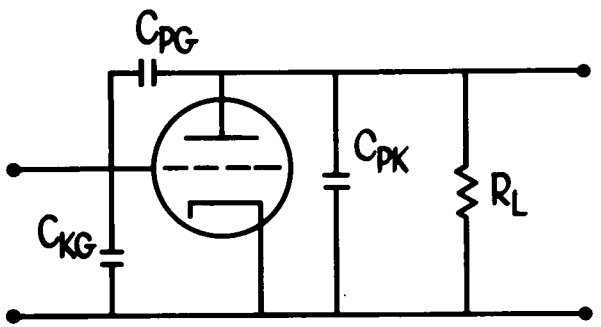

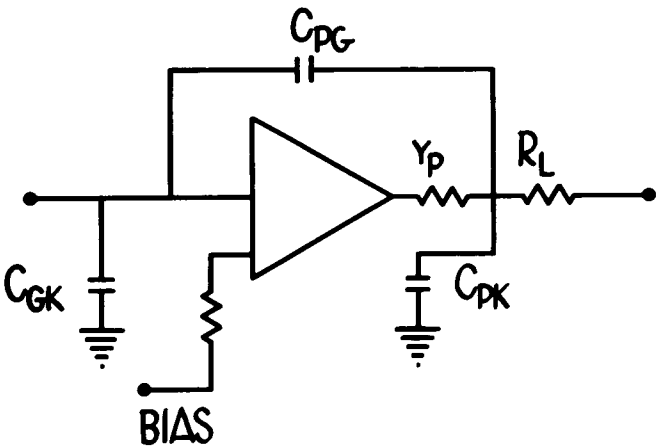

LINEAR SIMULATION

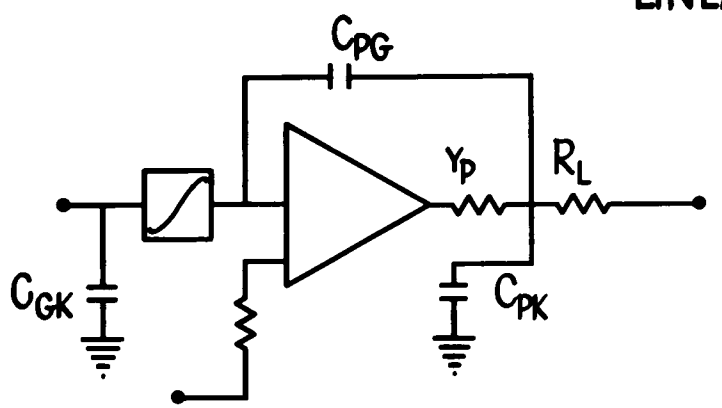

NONLINEAR SIMULATION

NPC 7435

FIGURE 2

Figure 3 illustrates how a biasing arrangement is used to simulate the cutoff point of a tube. Notice the similarity between the actual and the simulated systems. The "feel" for the system is not lost, and each component in the original system has a counterpart in the simulated system. The value of any of the components, or the characteristics of the tubes, may be varied as needed.

APPLICATION TO SYSTEMS

The reliability of the predictions is only as good as the data that are used. In this respect, the analysis of a system begins with an analysis of the available irradiation data on the components used in the system.

Suppose, for purposes of illustration, that a group of resistors of a certain type have been irradiated. Then the mean resistance of the group may be plotted as a function of irradiation. Next, by standard statistical methods, a confidence envelope may be drawn around the mean value of resistance, within which a given percent of all the resistors of that class would lie, as in Figure 4. The width of the confidence band depends upon the percent of the total number of components that we want to fall within the band and upon the confidence desired in the predictions.

Now suppose that we have simulated a system on a computer, the output of which is a function of the resistors within it. By varying the values of these resistors, there may be either an increase or a decrease in the quality of the system performance. In other words, the partial derivative of the system output with respect to the resistance is either positive or negative. If it is positive, the values of the resistance used in the simulated irradiated system will be those taken from the bottom of the confidence envelope. If the partial derivative is negative, the top of the confidence band is used. In this way, by taking the values at the extreme of the envelope, we have ensured with, say, 90 or 95 percent confidence that the resistor in the actual system will be in better condition than in the simulated system. Incidentally, in the determination of the partial deviatives one finds immediately the most critical components where the system will require close parametric control.

Figure 5 gives the results of an analysis of a video transistor amplifier. The actual amplifier was irradiated in the Penn State reactor and was a two-stage, capacitance-coupled amplifier with voltage feedback and unbypassed emitter resistors. The deviation between the curves given for the simulated and actual system is believed to be caused partly by the lack

SIMULATED MULTIVIBRATOR AND OUTPUT

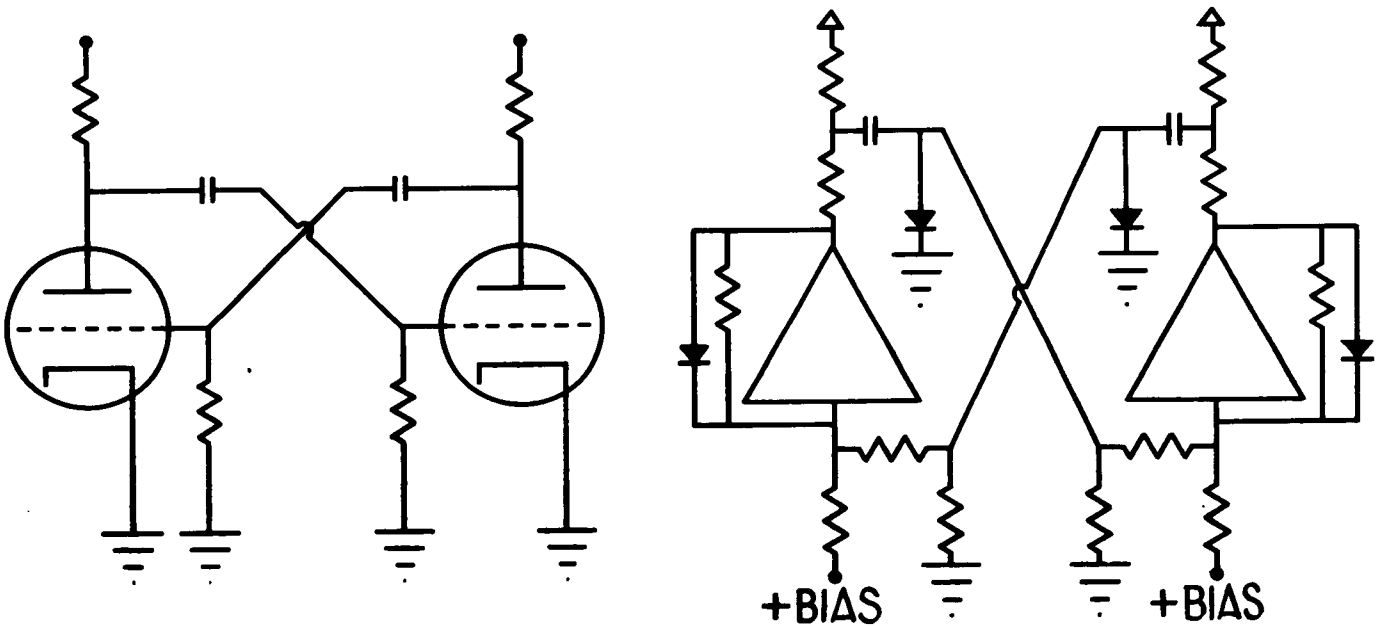

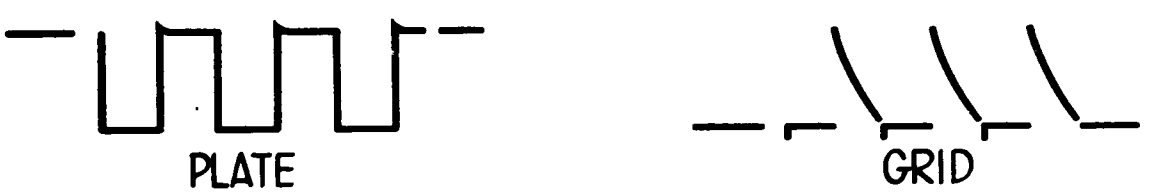

NPC 7436

FIGURE 3

EFFECT OF IRRADIATION ON THE RESISTANCE OF A GROUP OF RESISTORS

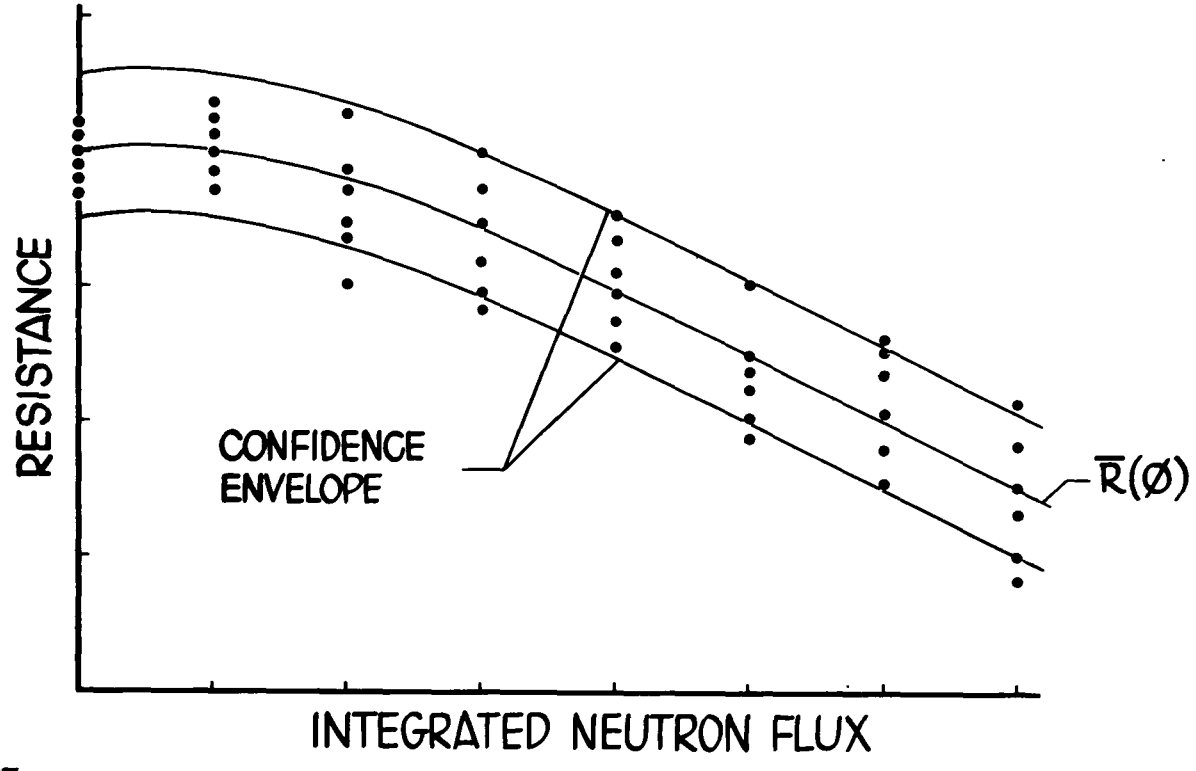

NPC 7437

FIGURE 4

TRANSFER RATIO OF VIDEO AMPLIFIERS

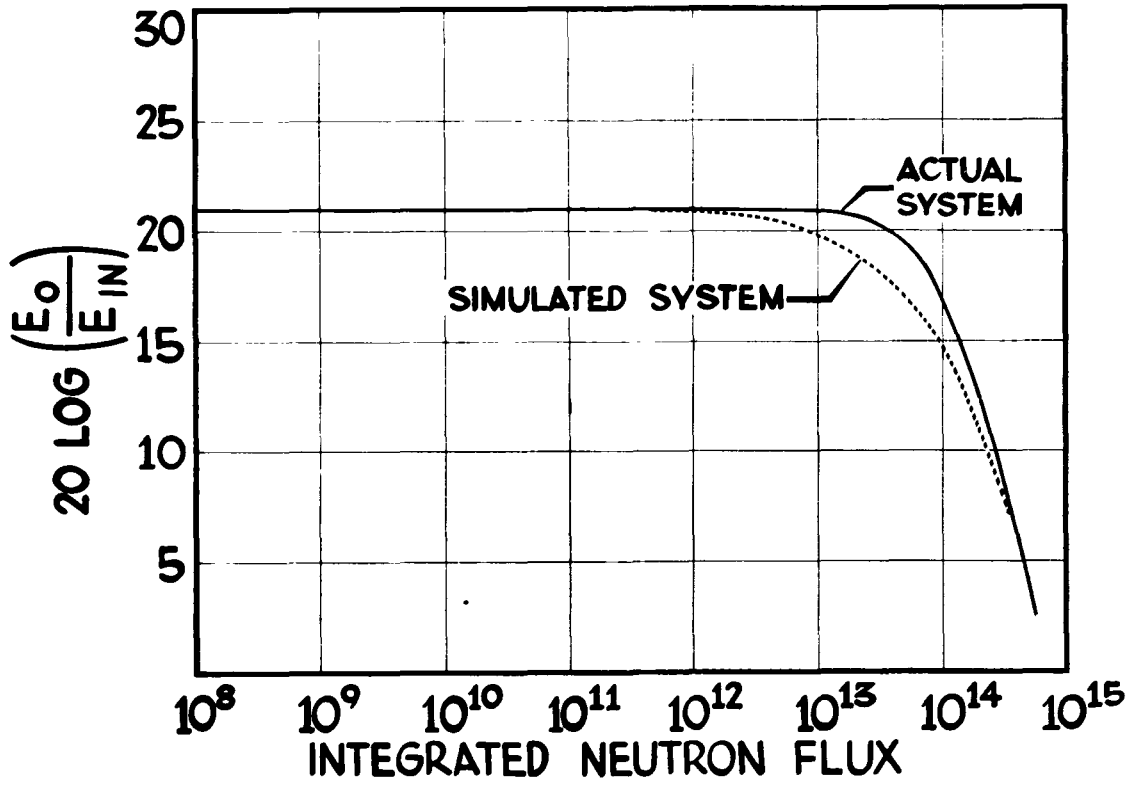

NPC 7458

FIGURE 5

of uniformity normally found in transistors. In addition, some healing of the amplifier, when the irradiation of the real system was interrupted overnight, was apparent. The healing effect was not included in the data used in simulating the system on the computer.

OVER-ALL PERFORMANCE

Finally, it must be recognized at some time the system may refuse to perform at all. That is, there may be a "catastrophic" component failure, such as a capacitor short which renders the system completely inoperative.

Ordinarily, standard statistical methods are used to evaluate a system subject to catastrophic failures and the reliability is given as an exponential function of time (Fig. 6). In irradiated systems the picture is altered somewhat, the probability of failure in a system being not only a function of time but of the radiation administered to the system.

If it is assumed that the catastrophic failure rate of the components in a system can be approximated by

$$f(t) = kt^{\alpha},$$

then, when the system is operated continuously under radiation, the reliability may be given by

$$P(t) = e^{-kt^{\alpha}},$$

where $P(t)$ represents the probability of the system operating for a time t without failing, and α and k are parameters which are functions of the integrated dose administered to the system. The development of this expression is discussed in the Appendix. Portions of the failure rate curve may be approximated by this function, and the reliability may be calculated if the failure rates for the various components are known.

Figure 7 gives the results of an analysis on a closed circuit television system, whose camera is subjected to radiation. Curve 2 shows the magnitude of the optical signal into the camera, and Curve 3 is an approximation of the reliability of the system. The electronic performance (the gain-bandwidth product) was obtained by the computer simulation technique

FAILURE RATE OF ELECTRONIC COMPONENTS

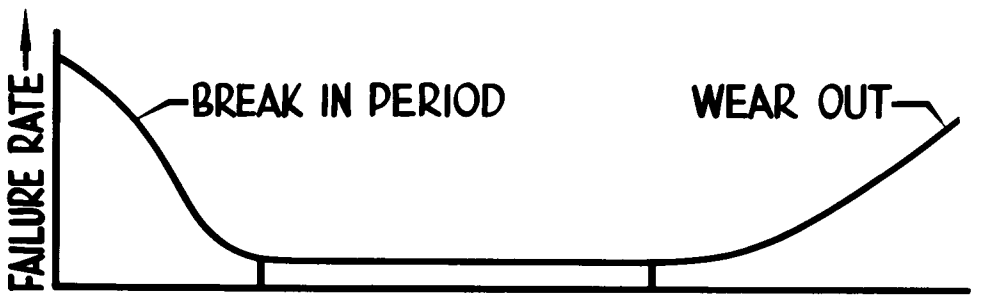

NORMAL FAILURE RATES

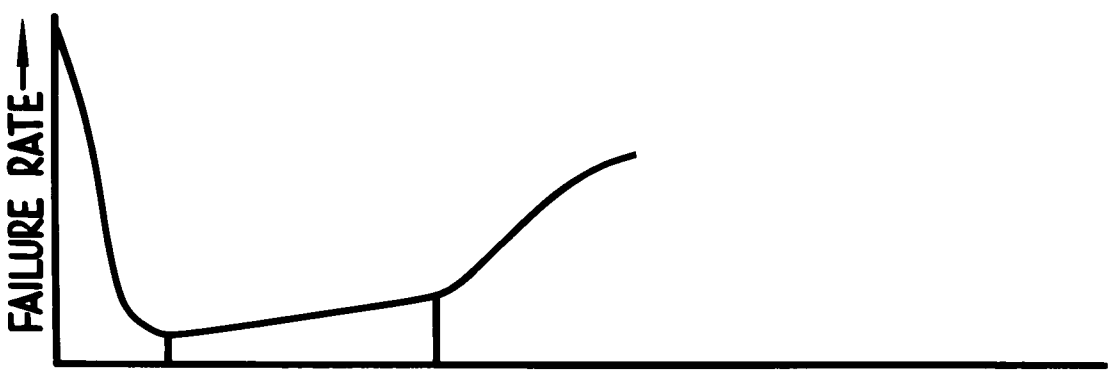

UNDER RADIATION

NPC 7439

FIGURE 6

PERFORMANCE OF A CLOSED CIRCUIT TELEVISION SYSTEM

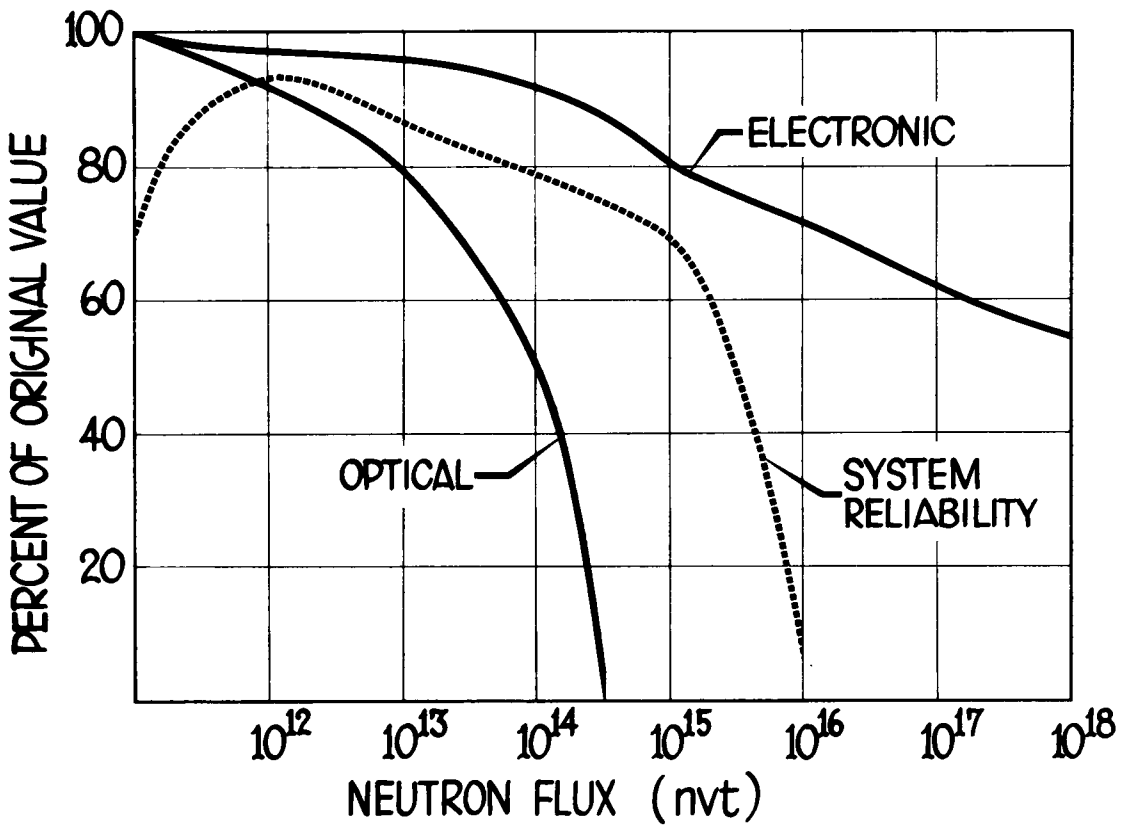

NPC 7440

FIGURE 7

and the optical performance from data on irradiated optical glasses.

Such an analysis of a system is based on answering three questions.

1. As the system is irradiated, how will it operate?

2. What is the chance of its operating at all?

3. When is the system expected to fail?

If the failure of the system is caused by the catastrophic failure of components, then its mean time to failure is simply the mean time to failure of the most susceptible components. If the performance of the system is considered unsatisfactory at some arbitrary level, then its mean time to failure may be found approximately by following the mean-value curves of the components under irradiation.

The reliability curve in Figure 7 is somewhat arbitrary in that it was computed from the probability that the system is to operate for a specified length of time without a failure. By taking shorter or longer periods of time, the curve may be raised or lowered.

Of the three such systems irradiated to date, the response seems to follow the optical performance curve given in the figure. There are, however, other considerations to be taken into account, such as lighting and optics adjustments, that were not included in the analysis. These could shift the optical curve either one way or another. Of the three cameras irradiated to a total integrated neutron flux of about 8×10^{14} nvt, no change in electronic performance was discernible. There were, however, several failures in the camera control unit.

CONCLUSIONS

It is believed that, by combining proper statistical methods with computor simulation of electronic systems, electronic performance under irradiation may be successfully predicted. The accuracy of these predictions depends of course upon the quality and quantity of the available data on the components and upon the application of these data to a particular situation. When only trends can be found in the component data, the simulation can still give valuable insight into system stability and performance in a nuclear environment.

APPENDIX A

FAILURE DATA AND RELIABILITY

A failure is here defined as any deviation of the functioning of a part or subsystem from requirements of the specifications, drawings, purchase descriptions, contracts, or order. A critical failure is one which could prevent the performance of the tactical function of the system.

Generally, it is assumed that the probability of failure is small, and that failures are distributed according to Poissón's formula

$$P(x) = e^{-t/T} \left(\frac{t}{T}\right)^x \Big/ x!$$

where: x = the number of failures and

T = mean time to failure

Any test or run of the system can have the possible outcome of "failure" or "no failure". Each run is then a Poissón Trial, and the probability of no failures in a time t of the trial or run is

$$P(0) = e^{-t/T}, \qquad (1)$$

a continuous, exponential distribution.

Hence the probability of one or more failures in time t is:

$$Q(0) = 1 - P(0) = 1 - e^{-t/T}$$

and the probability of failure in time dt is the rate of occurrence of failures:

$$dQ = \frac{1}{T} e^{-t/T} dt.$$

Another way of saying this is that the instantaneous probability rate of failure at time t conditional on no failure before time t is:

$$Z(t) = P\left[\, t \leqslant \tau < t + dt / \tau \geqslant t \,\right] = \frac{f(t)}{1 - F(t)}$$

where:

$f(t)$ = probability of failure in time t.

If

$$Z(t) = k, \text{ a constant}$$

then

$$\int_0^t Z(t)dt = \int_0^t kdt = kt$$

and

$$\ell n \left[1 - F(t) \right]_0^t = - kt$$

or

$$1 - F(t) = e^{-kt} = \text{reliability of the system;}$$

hence

$$F(t) = 1 - e^{-kt}$$

and

$$dF(t) = f(t) = ke^{-kt}$$

or

$$f(t) = \frac{1}{T} e^{-\frac{t}{T}}$$

Thus

$$\int_0^t f(t)dt = 1-e^{-\frac{t}{T}} = \frac{t}{T} - \left(\frac{t}{T}\right)^2 \frac{1}{2!} + \left(\frac{t}{T}\right)^3 \frac{1}{3!} - \cdots \approx \frac{t}{T} \text{ for large } T$$

If $k = 1/T$ is not constant with respect to time, then Figure 6A would show a slope $\neq 0$. Suppose $1/T = kt^{\alpha}$, then the distribution of failures instead of following the simple exponential distribution, would adhere to the Weibull distribution

$$Z(t) = kt^{\alpha}$$

$$\ell n \left[1 - F(T) \right] = - kt^{\alpha} \text{ and } 1 - F(t) = e^{-kt^{\alpha}},$$

which may be taken as defining the reliability of the system under study.

COMBINED TIME, TEMPERATURE, AND RADIATION EFFECTS ON ORGANIC MATERIALS

by

C. G. Collins
General Electric Company
Aircraft Nuclear Propulsion Department
Cincinnati 15, Ohio

Experimental observations of combined time, temperature, and radiation effects on a lubricating oil and Teflon aircraft engine hoses are described for the temperature range from 80° to 400°F and for radiation rates of 10^6 to 5×10^7 ergs $(gmC)^{-1}$ hr^{-1}.

The results show that at a constant radiation rate the failure time - as judged by the oxidation-induction period of the oil and by leaks in the Teflon hoses - follows an Arrhenius-type relationship with temperature. At a constant temperature, failure time was found to follow a logarithmic relationship with radiation dose rate. The over-all results can be described in a summary equation in terms of time, absolute temperature, and radiation dose rate.

Several implications of the summary equation are discussed in reference to radiation effects in organic materials. One implication is that observations of equal damage at constant dosage irrespective of dose rate may be valid at only one temperature or at high dose rates.

INTRODUCTION

One of the major problem areas confronting radiation effects investigators at present is that of defining materials performance under combined radiation and temperature environments. Since time-at-temperature is an important factor in the deterioration of organic materials, the importance of temperature in radiation effects has been suspected - and demonstrated - in a number of instances. Progress in this area, however, has been impeded by the lack of mathematical methods of treating the data, and large numbers of experiments have been necessary to obtain data for each parameter over a range of values of practical interest.

This report discusses experiments in which the time required for occurence of a constant amount of oxidation of an organic liquid was studied over a range of dose rates and temperatures. The quantity - time required for constant amount of reaction - is readily analyzable with the familiar logarithm time versus absolute temperature relationship of accelerated life tests. It proved fairly straight-forward to analyze the radiation experiments in a similar manner and the results of the experiments can be described by an equation involving terms for time, temperature, and radiation rate. Further experimentation is necessary to clearly establish the validity of the equation; however, the general form of the equation seems clear and bears sufficient resemblance to fundamental relationships that it may be applicable to other materials. In this respect, the implications were considered of sufficient interest to warrant discussion despite limited experimental verification. Some of the implications of the equation regarding the relationships between radiation rate, radiation dosage, temperature, and time in the degradation of organic materials are discussed following a description of the experimental procedure and results. A few data that indicate that the same type of equation applies to the life of Teflon hoses are included.

EXPERIMENTAL PROCEDURE

Experiments were performed on a di-ester oil and utilized the oxidation-induction period as the indicator of the occurrence of a given amount of chemical reaction. The oxidation-induction period is defined as the time required to reach the "break" in the curve of oxygen absorption versus time, as shown by curve a of Figure 1. At high temperatures, the oxygen absorption curve rises without a definite break, as in curve b of Figure 1, so that the induction period is usually defined as the time to absorb the same amount of oxygen that is absorbed in a true induction period (curve a). In these experiments, the effect of increasing radiation rate was observed to affect the curves in a manner similar to that of high temperature and the usual definition of the induction period was followed. This corresponded to the absorption of 0.4 mole of oxygen per 426 grams of fluid.

The apparatus employed was of the type described by Dornte. This consisted of circulating oxygen through the oil in a closed system containing a bellows pump, adsorbent tubes for oxidation products (water, CO_2), and a mercury valve for admitting oxygen. The oxygen flow rate, intended to be 5.0 liters per hour, was found to be 3.5 liters per hour after a few measurements were completed. All of the experiments reported here were conducted at this flow rate.

Samples consisted of 250 milliliters of di-2-ethylhexyl sebacate containing 0.5 weight percent phenothiazine. This quantity of oil filled the 2 inch diameter stainless steel irradiation capsules to a height of approximately 5 inches. Oxygen bubbled through about $4\frac{1}{2}$ inches of this height from perforations in a horizontal portion of the gas inlet tube.

Dosimetry for the irradiations, which were performed in a cobalt-60 source, was determined by means of the cerous-ceric sulfate oxidation. Measurements were made inside the furnace-capsule arrangement used with the oil and corrections applied for the thickness of the walls of the glass cerous sulfate container. Energy absorption in the samples was computed by graphically integrating the curve of dose rate versus distance (from the source) for the sample geometry. An average energy of 1.25 mev was assumed for the gamma rays, and the absorption coefficients were those reported by Snyder and Powell.(1)

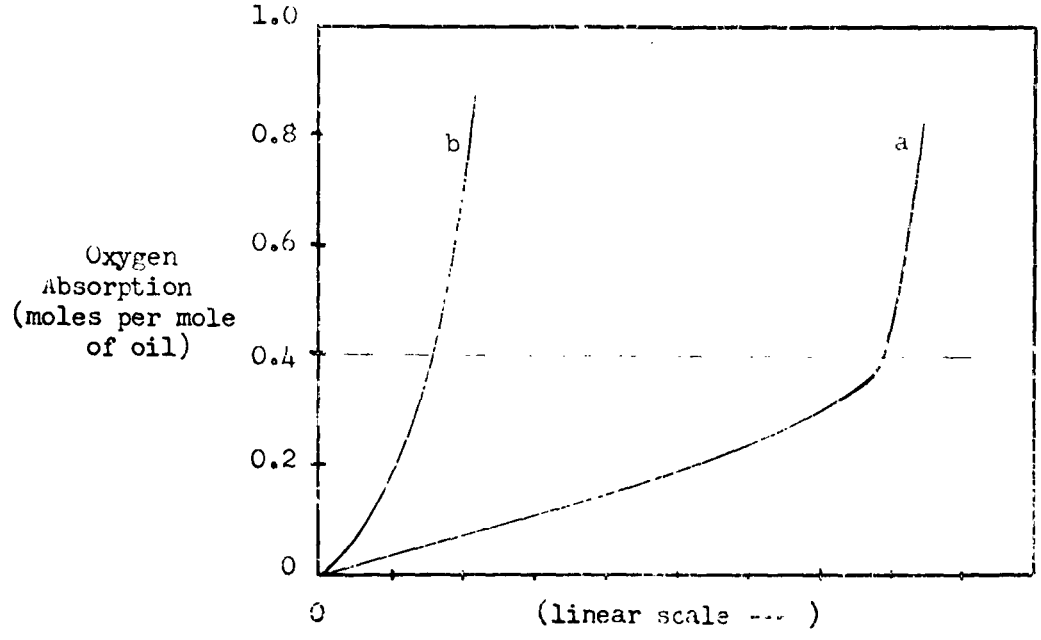

Figure 1

TYPICAL OXYGEN ABSORPTION CURVES IN OXIDATION INDUCTION PERIOD MEASUREMENTS

Curve (a), at low temperature or low radiation dose rate

Curve (b), at high temperature or high radiation dose rate

RESULTS

The results of the measurements are summarized in Table I. Since the oxidation reaction is significantly affected by temperature, it is not surprising that the results are not simply correlated in terms of radiation dosage.

Figure 2 is a plot of the results in the type of graph employed in accelerated life tests. The logarithm of the time required for the constant amount of reaction indicated by the induction-period is plotted versus the reciprocal of absolute temperature (°Kelvin), results at any one radiation rate being connected by a straight line. That the lines are straight is demonstrated for only a limited temperature range by these data but the idea is supported by the results of M. A. Golub on the cis-trans isomerization of poly-butadiene,[2] by the Teflon data of Figure 6, and follows from the laws of chemical kinetics.

Under non-radiation conditions, the time, t, required for a given constant amount of reaction is related to temperature by the equation

$$\ln t = \frac{E^*}{RT} + \text{constant} \qquad (I)$$

where E* is an experimental activation energy, R is the molar gas constant, T is absolute temperature, and the constant involves, in part at least, the ratio of the concentration of a reacting species initially and after time t. This equation is derived from Arrhenius relationship between reaction velocity and temperature, and is the familiar basis of all accelerated life tests of materials and components.

An equation of this same form

$$\ln t = \frac{a}{T} + b \qquad (II)$$

is applicable to the experimental points obtained at constant radiation dose rate. Considering that a given dose rate produces the reactant species at a constant rate, the reaction velocity will be accelerated over that occurring with temperature alone. The reaction velocity enters (I) in the terms for activation energy and in the constant, hence, one would expect the basic form of I to be the same, and the effect of radiation rate in the empirical relationships to be apparent in the values of E* and the constant, i.e. in a and b. On this basis, also, it would be expected that since the reaction rate is accelerated more by a higher radiation rate, an increase in dose rate should decrease the numerical value of a.

In formulating an over-all equation for the experimental results, the relationship between dose rate and the acceleration of reaction velocity is necessary; this proved to be fairly simple. Straight lines

TABLE I

OXIDATION-INDUCTION PERIOD OF AN INHIBITED DI-ESTER OIL*
DURING IRRADIATION

OXIDATION INDUCTION PERIOD (hrs.)	TEMPERATURE °F	RADIATION DOSE RATE (absorbed) ergs gm^{-1} hr^{-1}	RADIATION DOSAGE (absorbed) ergs gm^{-1}
77	300	2.2×10^{7}	1.69×10^{9}
49	"	5.3×10^{7}	2.6×10^{9}
106	347	1.1×10^{7}	1.17×10^{8}
79	"	2.7×10^{6}	2.13×10^{8}
36	"	2.2×10^{7}	7.92×10^{8}
23.5	"	5.6×10^{7}	1.32×10^{9}
31.5	400	1.0×10^{6}	3.15×10^{7}
16	"	2.1×10^{7}	3.36×10^{8}

*Di-2-ethylhexyl-sebacate plus 0.5 per cent (weight) phenoghiazine. Oxygen flow rate was 3.5 liters per hour through 250 cc.

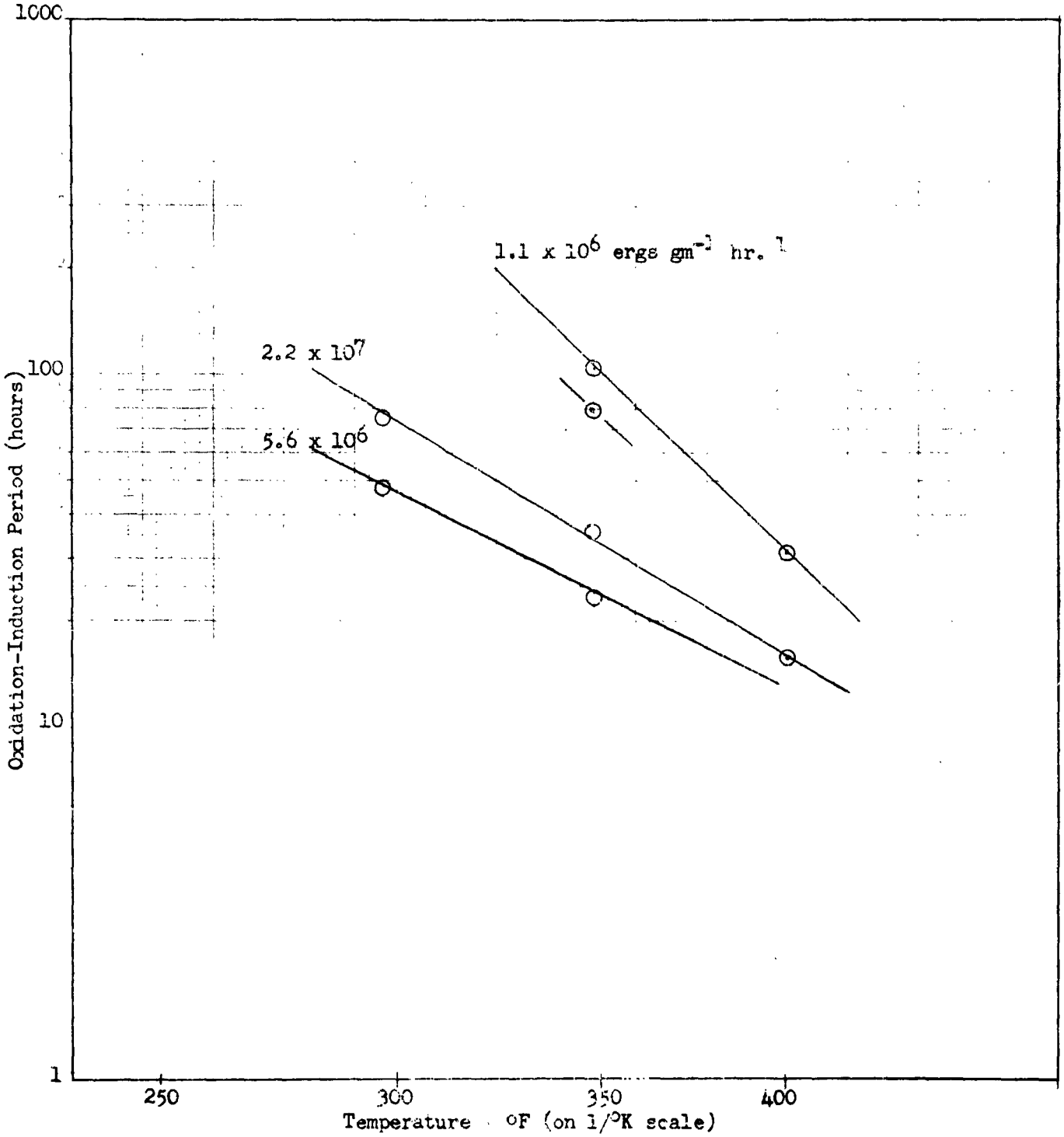

Figure 2

OXIDATION-INDUCTION PERIOD OF LUBRICATING OIL AS FUNCTION OF TEMPERATURE AT CONSTANT RADIATION RATE

were obtained when the constants a and b of equation II were plotted versus thelogarithm of radiation rate; the constants are therefore of the form:

$$a = c_1 \ln r + c_2$$

$$b = c_3 \ln r + c_3$$

where r is dose rate and the "c's" are empirical constants. Substituting these values for a and b in equation II yields the summary equation:

$$\ln t = \frac{23469.6}{T} - \left(\frac{1045.79}{T} - 1.95434\right) \ln r - 42.40723 \qquad \text{III}$$

where t is hours, r is radiation rate (ergs per gram absorbed per hour), and T is absolute temperature (°K). This equation fits the experimental data shown in Figure 2 within ± 3.5%.

DISCUSSION

While a more fundamental approach to reaction rates might have yielded a somewhat less complicated-appearing relationship, the empirical equation derived here does not conflict with the basic ideas of photochemistry and bears sufficient resemblance to fundamental relationships that an equation of the same general type possibly will apply to many organic materials under radiation conditions. In this respect, it is of interest to consider the "view" of radiation damage presented by the equation and its implications regarding the relationships between time, temperature, dose rate, and dosage.

Over-all Indications - The results obtained from calculations with the equation provide the over-all "picture" of radiation effects shown in Figure 3. The heavy lines on the right and at the bottom of the figure represent the apparent limits of applicability of the equation and are discussed below. Within the region bounded by the limits, the combined temperature and radiation effects are indicated by the lines shown for a few selected radiation rates. At constant dose rate, straight lines are obtained when ln t is plotted versus 1/T. The slope of these lines is greatest at low dose rates, thermal activation being the major factor influencing the reaction. At successively higher dose rates, the lines tend to a slope of zero, the indication being that radiation effects completely over-ride thermal effects.

The limits of the region over which the equation is applicable are related to both temperature and dose rate. The slanting line on the right represents results obtained with temperature alone.(a) Since the lines representing radiation results extrapolate across this line, they lead to the obviously erroneous conclusion that the time required for a given amount of reaction under certain combined radiation and temperature conditions is less than that required under temperature alone. The

(a) The line representing results without radiation was not measured in these experiments; the results shown are quoted from reference 3 and are for slightly different experimental conditions, i.e. for an oxygen flow rate of 5 liters per hour.

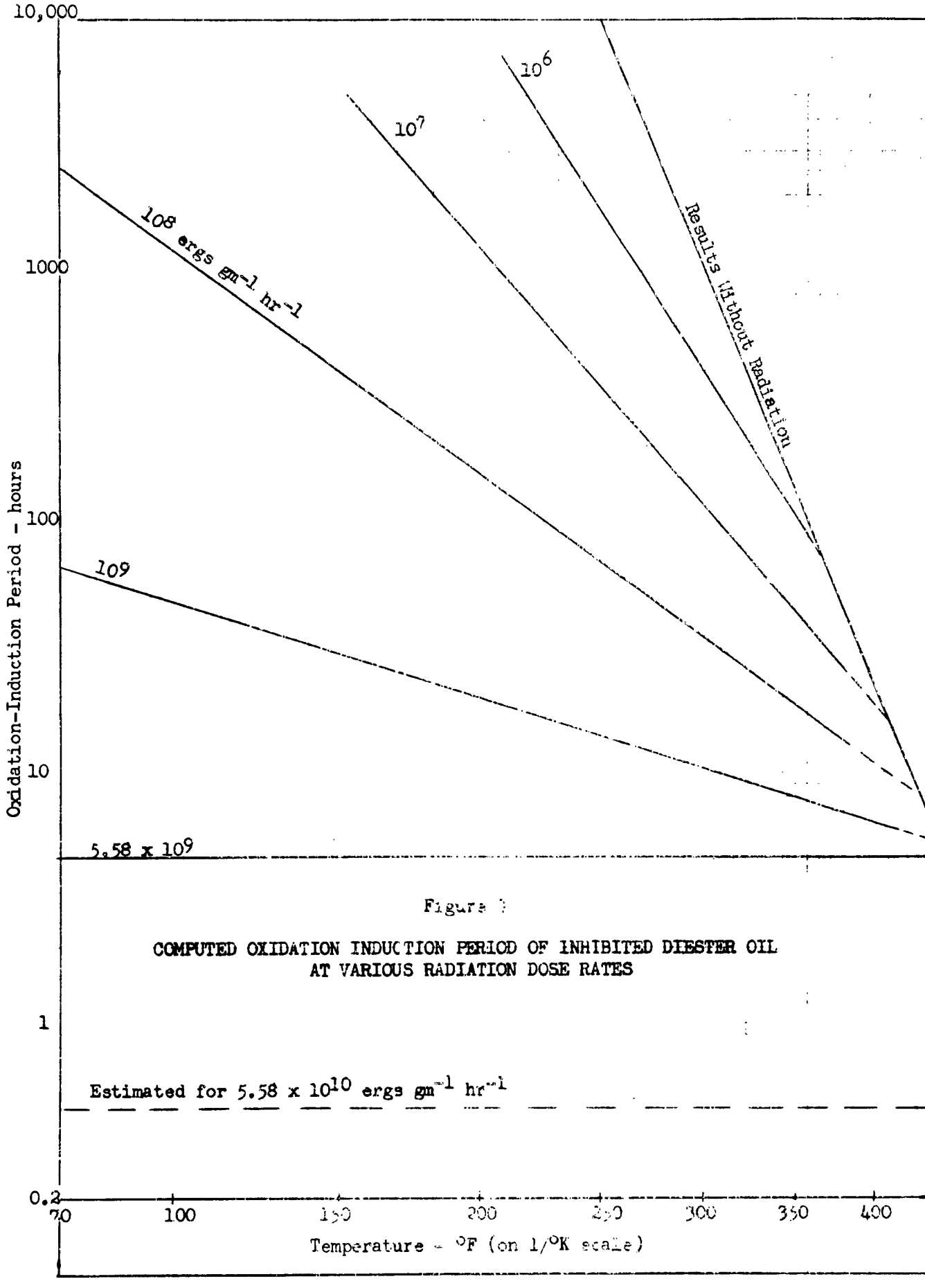

Figure 7

COMPUTED OXIDATION INDUCTION PERIOD OF INHIBITED DIESTER OIL
AT VARIOUS RADIATION DOSE RATES

temperature only line, therefore, is the upper temperature limit of the equation's applicability; it is unfortunate that this limit cannot be determined from the radiation results alone or from the equation.(b)

The second limit is related to radiation rate. This is indicated by the heavy horizontal line - at the bottom of Figure 3 - which represents a radiation rate (5.58×10^9 ergs gm^{-1} hr^{-1}) of such magnitude that thermal effects are negligible. Whether such a condition actually exists is indeterminate with the existing data. However, mathematically, the equation predicts a line of positive slope, i.e. a lesser effect at a high temperature than at a low temperature, if computations are made for radiation rates greater than 5.58×10^9 ergs gm^{-1} hr^{-1} for the oil oxidation. Hence, it is presumed that the dose rate that yields - by computation - constant time irrespective of temperature is the dose rate limit.

The region of the excessively high dose rates is certain to be of practical interest in some instances, but relationships between time and dose rate in this region are strictly a matter of conjecture at present. It might be presumed that one would obtain a series of horizontal lines in this region with at least two possibilities for the time-dose-rate relationship. First, the time for a given amount of reaction may be inversely proportional to the dose rate, i.e. the dosage required for a given amount of reaction would be the same irrespective of the dose rate. Second, the reaction under study might possess a finite reaction velocity occasioned by concentration, mobility of the reacting species, or other factors, such that much of the energy provided by radiation is not utilized in the particular reaction being studied. In this instance, the dosage for a constant amount of damage may vary for different radiation rates.

Radiation Rate and Radiation Dosage - Radiation dosage rather than radiation rate, has been the basis on which the limits of radiation tolerance of many materials have been established, the basis being supported by many experimental observations. The indications of the summary equation are such, however, as to raise the possibility that the experimental observations may be applicable only under specific conditions. The relationship indicated by the equation between time and radiation rate at constant temperature is

$$\ln t \sim - a \ln r$$

or

$$t \sim \frac{1}{r^a}$$

where the constant "a" is a function of temperature. This relationship is shown in Figure 4. Multiplying by r to obtain dosage (rt) gives

(b) Presumably, the slope of the temperature-only line would be given by the first term of the summary equation if the empirical constants were determined for the proper units of time and radiation rate, e.g. seconds and ergs $mole^{-1}$ sec^{-1}. Since temperature-only experiments were not completed, this point could not be checked.

Figure 4

OXIDATION-INDUCTION PERIOD OF LUBRICATING OIL AS FUNCTION OF RADIATION DOSE RATE AT CONSTANT TEMPERATURE

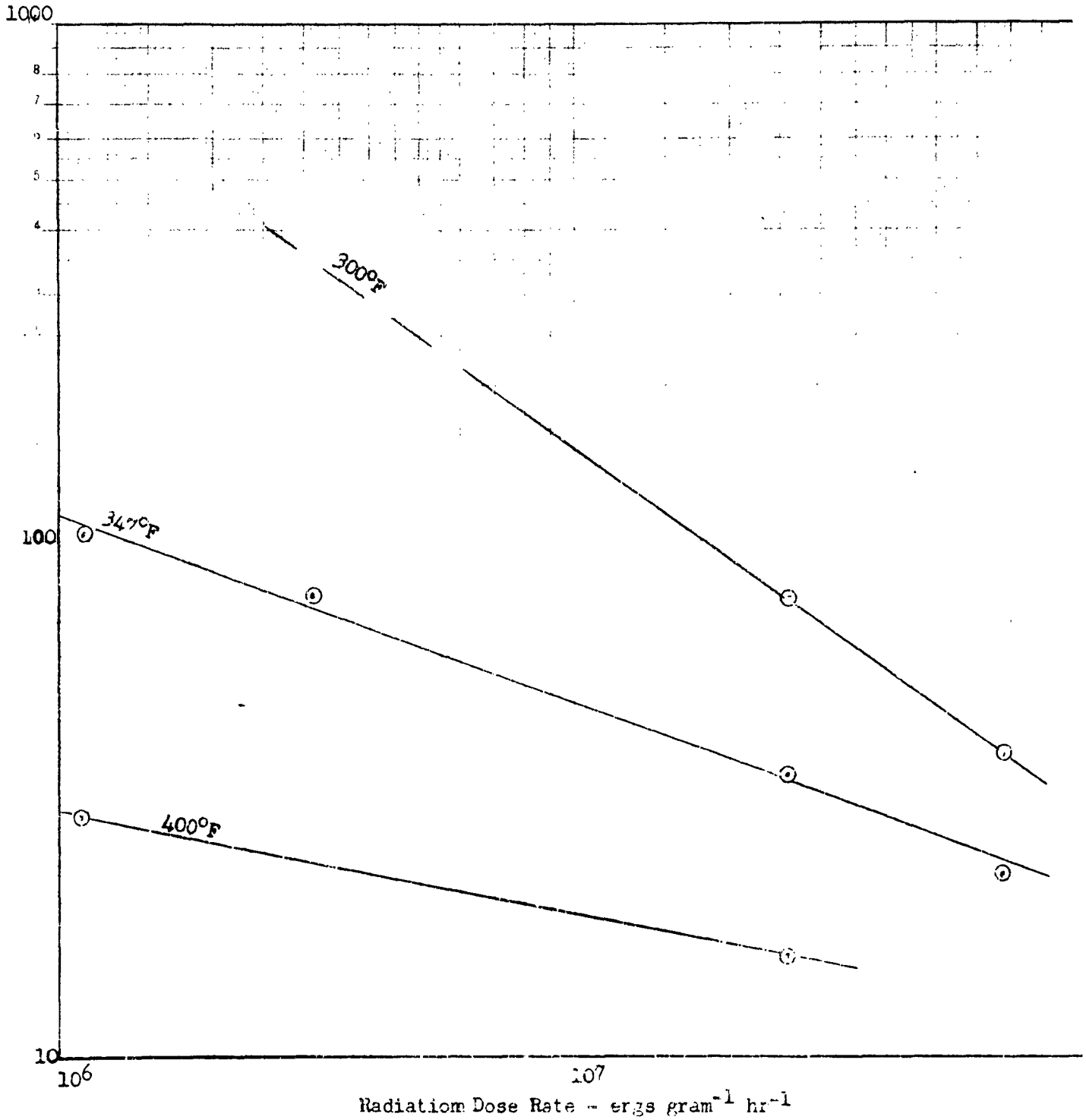

$$rt \propto \frac{r}{ra} \quad \text{or} \quad rt \cdot r^{1-a}$$

Therefore, at different temperatures, the dosage is proportional to a power function of radiation rate and straight lines are obtained when ln dosage is plotted versus ln radiation rate, as shown in Figure 5. A relationship of this type has been reported by Goodman and Coleman[4] who noted that the dosage-to-failure of Kel-F as a dielectric was proportional to the square root of radiation rate at temperatures of 30° to 90°C.

At a temperature at which "a" equals one, the dosage is proportional to a constant, i.e. the dosage at a constant amount of damage is the same irrespective of dose rate. Measurements at this temperature and in the region of "excessive" radiation rate (the region below the horizontal line of Figure 3) appear to be two conditions under which the dosage corresponding to a given amount of reaction is independent of dose rate.

APPLICABILITY TO OTHER MATERIALS

At the time of this report, studies of other materials in the frame of a reference of a constant amount of reaction had not been pursued to a point that an over-all equation could be derived with confidence. A few results obtained with Teflon aircraft engine hoses are discussed here for the comparison they provide with the oil oxidation data.

Test results are shown in Figure 6 in which the time-to-failure is plotted versus the reciprocal absolute temperature. Failure of the hoses was determined by leakage or rupture, the samples being held under a static pressure of 1100 psig with MIL-L-7808 lubricating oil during the test. Most of the measurements were made at a radiation exposure rate of 1.3×10^6 ergs $(gmC)^{-1}$ hr^{-1}; because of poor performance, especially in a subsequent test in which the pressure was cycled (c), only two additional tests were made under the static conditions for the purpose of checking the applicability of the equation. The experimental measurements are describable by the equation

$$\ln t = \frac{2679.25}{T} - \left(\frac{156.45}{T} + 0.26291\right) \ln r + 7.00331$$

where r = exposure dose rate, ergs $(gmC)^{-1}$ hr^{-1}. Calculations with this equation yield the results shown in Figure 7. Although the "picture" presented is self-consistent, there are too few data to assure its validity. Certainly, the computed results qualitatively disagree with the data of Harrington(5) who concluded from experiments with a number of elastomers and plastics, including Teflon, that damage is dependent only on total dosage at dose rates from 10^4 to 10^7 roentgen hr^{-1}. There may be no

(c) Teflon hoses tested at 350°F and a radiation rate of 1.3×10^4 ergs $(gmC)^{-1}$ hr^{-1} failed after 9.7 hours when the pressure was cycled from 0 to 1000 psig at 15 minute intervals.

Figure 5

RADIATION DOSAGE AS A FUNCTION OF DOSE RATE
FOR OXIDATION-INDUCTION PERIOD MEASUREMENTS

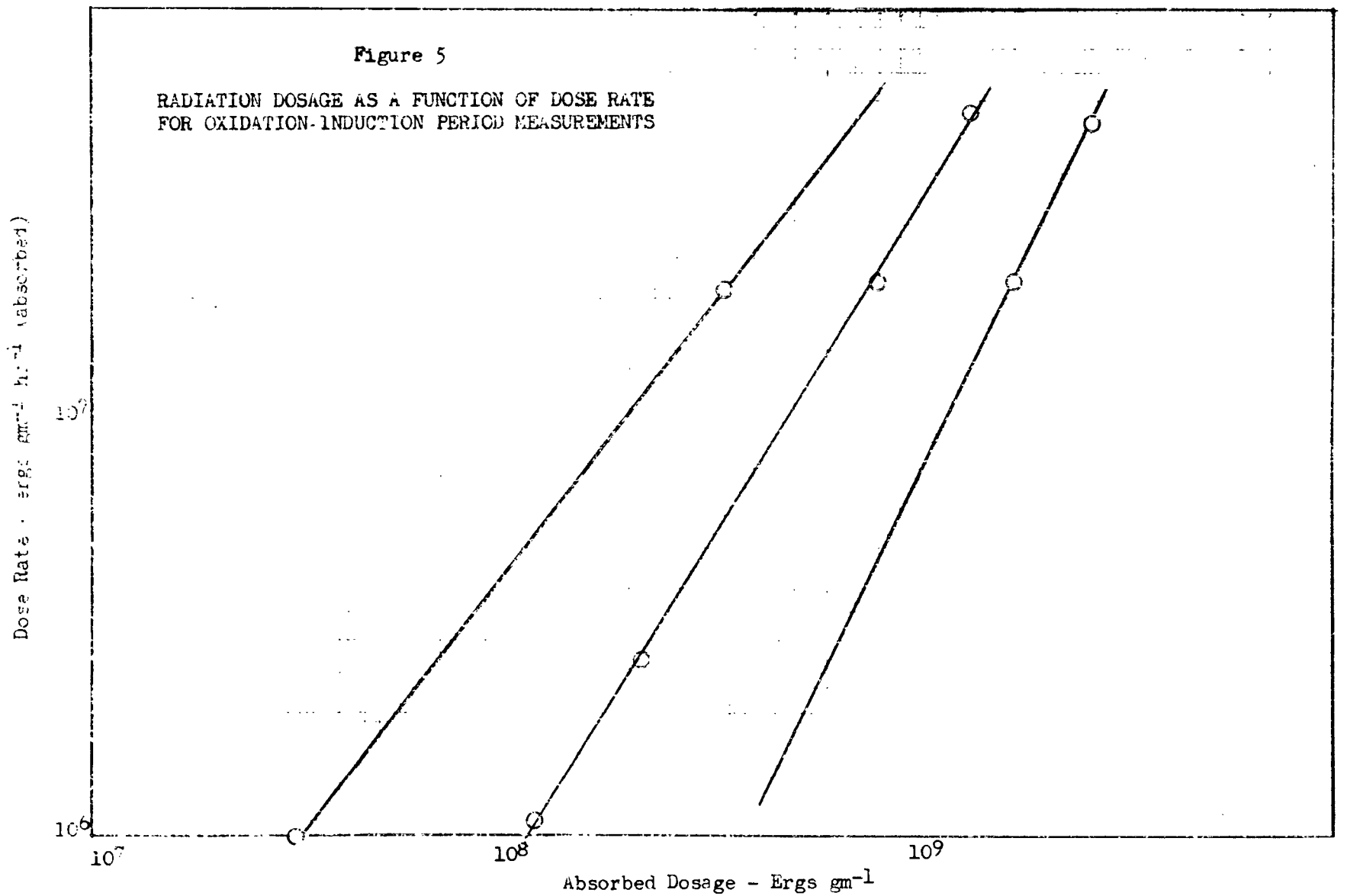

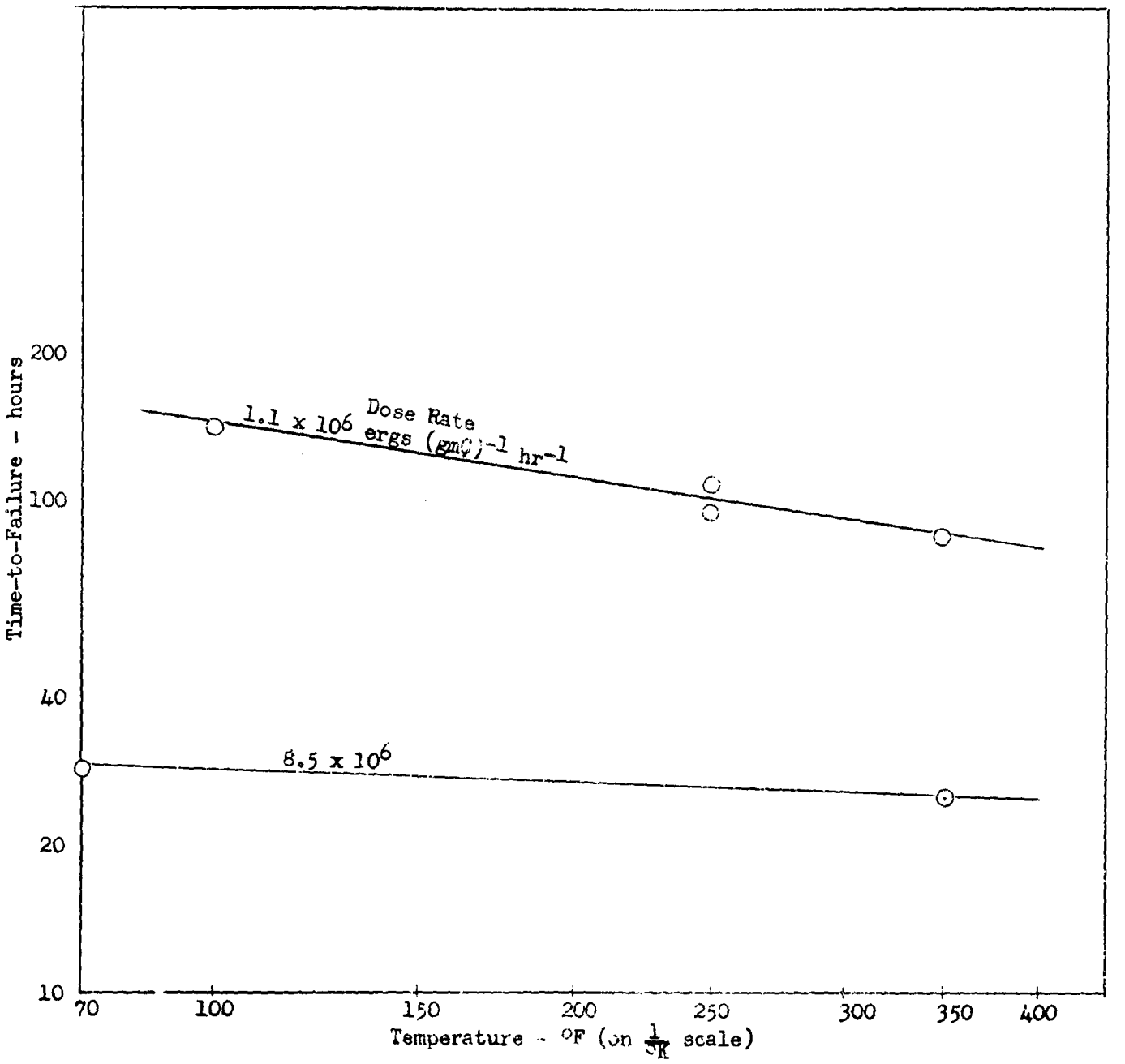

Figure 6

EXPERIMENTAL MEASUREMENTS OF TIME-TO-FAILURE OF
TEFLON AIRCRAFT ENGINE HOSES

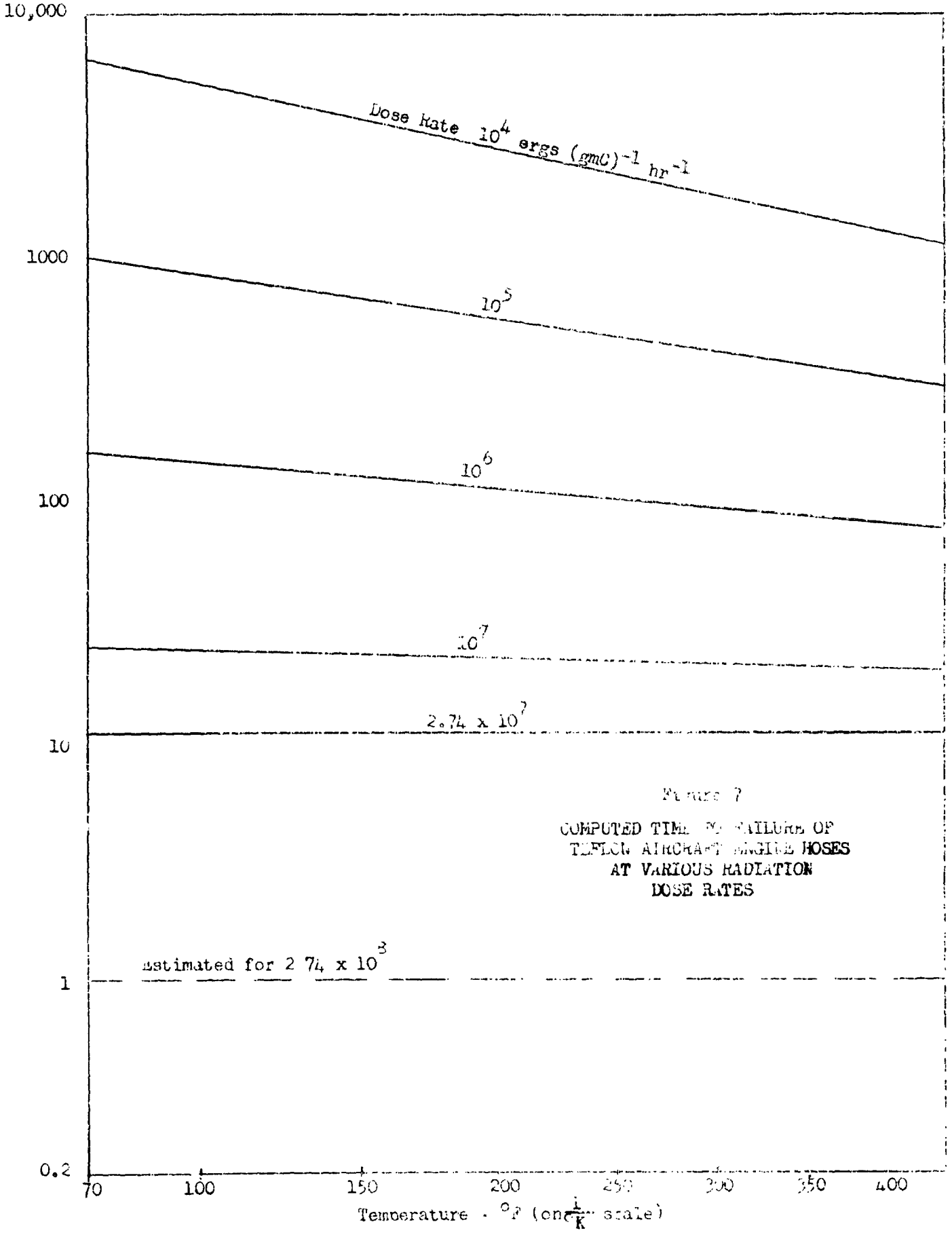

FIGURE 7

COMPUTED TIME TO FAILURE OF TEFLON AIRCRAFT ENGINE HOSES AT VARIOUS RADIATION DOSE RATES

disagreement at high dose rates. As discussed previously, the damage may be dependent only on total dosage if the degradation reactions are not time dependent and the dose rate is equal to or greater than that at which thermal effects are negligible. In Teflon, this dose rate is 2.74 $\times 10^7$ ergs $(gmC)^{-1}$ hr^{-1} ($\sim 3.19 \times 10^5$ r hr^{-1}) - if the equation is correct. The disagreement at the lower dose rates may be due to sample geometry, dosimetry, or other factors; but the writer tends to the belief that differences in the mechanical stress levels during the two types of irradiation experiments are responsible.

Since Teflon has excellent thermal and oxidation stability under non-radiation conditions, the thermal effects apparent in the experimental results can probably be ascribed to the reactions initiated by the radiation. In this respect, it is interesting to note that thermal effects in the Teflon are minor in comparison to those in the oil oxidation over the temperature range considered. In fact, the computed results for a dose rate of 10^7 ergs $(gmC)^{-1}$ hr^{-1} indicate such a small thermal effect that good experimental statistics would be required for its detection.

SUMMARY AND CONCLUSIONS

An analysis of experimental results has been described which indicates that, where the time required for a constant amount of reaction is the variable studied, the combined time, temperature, and radiation effects in organic materials can be described by an equation of the form

$$\ln t = \frac{c_1}{T} + \left(\frac{c_2}{T} + c_3\right) \ln r + c_4$$

where t is elapsed time, T is absolute temperature, r is radiation dose rate, and the c's empirical constants. Several relationships between time, temperature and radiation dose rate are apparent in the equation. The relationship between the dosage corresponding to a given amount of damage and dose rate can be derived and is indicated to be: dosage $\sim r^{1-a}$, where a is equal to $c_2/T + c_3$ and is temperature dependent. The implications of the equation are that there are two conditions under which the dosage for a given amount of damage is independent of dose rate; these include a specific temperature and high dose rates, both being dependent on the particular material under study.

Although the validity of the over-all equation and its applicability to a variety of organic materials are yet to be established, it appears reasonably certain that combined radiation and temperature effects can profitably be studied in terms of a constant amount of reaction. The constant amount of reaction, which can be interpreted as the "life" of materials, appears to obey, under constant dose rate conditions, the logarithm time

versus absolute temperature relationship familiar in accelerated life tests. Accelerated life tests have been found to be applicable to numerous materials and components such as o-ring seals, electrical insulation, electric motors, solenoids, and other components whose failure is dependent on the deterioration of a "weak-link" material. Such an approach to radiation testing would appear to offer the advantages of yielding results of practical value and of opening up the possibility of extrapolating experimental results by mathematical analysis.

BIBLIOGRAPHY

(1) Snyder, W. S., and Powell, J. L., "Absorption of Gamma Rays,"ORNL 421, Supplement 4, March (1950).

(2) Born, J. W., "A Study of the Effects of Nuclear Radiations on Elastomeric Compounds and Compounding Materials," Quarterly Progress Report No. 1, B. F. Goodrich Company Research Center, Materials Laboratory, Contract No. AF33(616)-5646, July (1958).

(3) Klaus, E. E., and Fenske, M. R., "Fluids, Lubricants, Fuels, and Related Materials," WADC TR 55-30, Part V, (1957) (ASTIA AD 130907).

(4) Goodman, J., and Coleman, J. H., "Dose-Rate Dependence of Kel-F Degradation by Ionizing Radiation," J. Polymer Science, 25, 253 (1957).

(5) Harrington, Robert, "Elastomers for Use in Radiation Fields," Rubber Age, 81, No. 6, pp. 971-980, Sept. (1957).

RADIATION DAMAGE OF AIRPLANE TIRE MATERIALS

by

T.C. Gregson and S.D. Gehman

The Goodyear Tire & Rubber Company
Akron, Ohio

SUMMARY

An airplane tire is a relatively complex, highly stressed structure. Radiation damage effects are unusually complicated in this case because of the number of materials involved and the cooperative effort required of each. Damage to tire components typical of present production was studied with cobalt-60 gamma radiation. The influence of various environmental factors was also investigated. Tire fabric and fabric-rubber adhesion are far more susceptible to radiation damage than are the rubber compounds in general use. Damage to the fabric is especially critical, in terms of tire performance, since it bears the brunt of the stresses. Cord fatigue and dynamic adhesion are the most serious aspects of radiation damage to tires. Various types of nylon tire cords possess significant differences in their ability to withstand irradiation. Presence of a nitrogen atmosphere was found to be very efficacious for reducing radiolysis in nylon cords. It was thus conceived that nitrogen inflation would provide a practical means of raising the damage threshold of tubeless airplane tires. Several nitrogen inflated tires were exposed to a dose of 10^7 rad, a level above the damage threshold for nylon cords when irradiated in air. Their performance in laboratory tests confirmed the protective benefits of nitrogen inflation.

INTRODUCTION

An airplane tire is the end result of the skillful blending together of rubber, adhesive, textile, and wire into the integrated type of structure shown in Figure 1. Its relatively complex structure is subjected to high stresses and repeated thermal shocks during operation. Its performance will depend upon the degree to which all constituents mutually cooperate in absorbing these mechanical and thermal stresses.

Since tires have provided the only workable means to date for takeoff and landing of high speed land based airplanes, we quite naturally assume they will also be essential to a nuclear propelled plane. In anticipation of the need for information on the performance of airplane tires operating in a radiation environment, The Goodyear Tire & Rubber Company initiated in its Research Division, late in 1956, a study of radiation damage to typical present day tire production materials.

This work has been carried out in Akron where we have a versatile facility containing 3800 curies of cobalt-60. Our arrangement combines the desirable features of irradiations in air with the ease of handling and storage of the source in a water shield. Any predetermined environmental and temperature conditions can be maintained during exposure.

RADIATION DAMAGE - - - - - GENERAL

It is well known that all organic materials are affected adversely sooner or later if given a sufficient exposure to radiation. This impairment of a material's ability to perform its specified functions, i.e., a foreshortening of its useful lifetime, is called radiation damage. The minimum cumulative exposure which will produce a detectable degree of damage in a property essential to an article's normal service life is spoken of as the threshold damage dose. Likewise, a dose which will cause a 25% loss in such a property is termed the 25% threshold level.

Radiation damage to tire materials takes the form of lowered resistance toward abrasion, tensile or compressive forces and flexure. Severe damage obviously leads to premature failure in service. Threshold levels for readily detectable damage vary for these constituents from perhaps 10^5 rad for textiles[2] and adhesives to 2X 10^6 rad for rubber compounds.[2] Similarly, 25% damage levels might be 10^6 rad and 2.5×10^7 rad, respectively.

RADIATION DAMAGE - - - - - RUBBER COMPOUNDS

Several investigators have published results of radiation damage studies on rubber.[2,-15] After receiving a dose of about 2 megarads typical rubber compounds begin to show decreased tensile strength and elongation and increased modulus and hardness. Such changes in the physical properties of a tread compound are shown in Figure 2 for both a natural rubber and a GR-S type. This behavior is quite similar to normal deterioration in use, though obviously accelerated, as shown by Figure 3.[16]

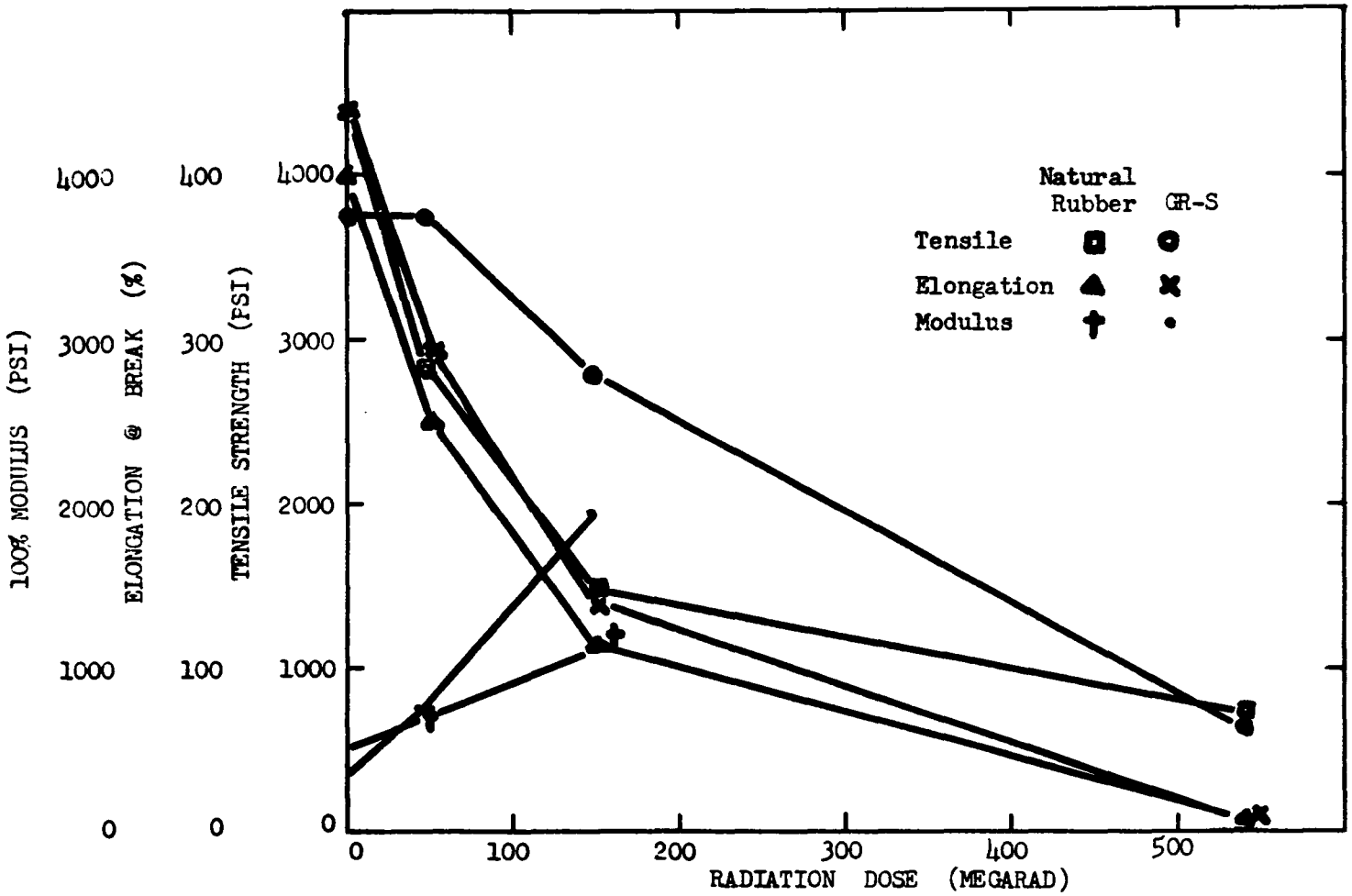

Fig. 2. Effect of irradiation in air at 75°F on stress-strain properties of rubber vulcanizates.

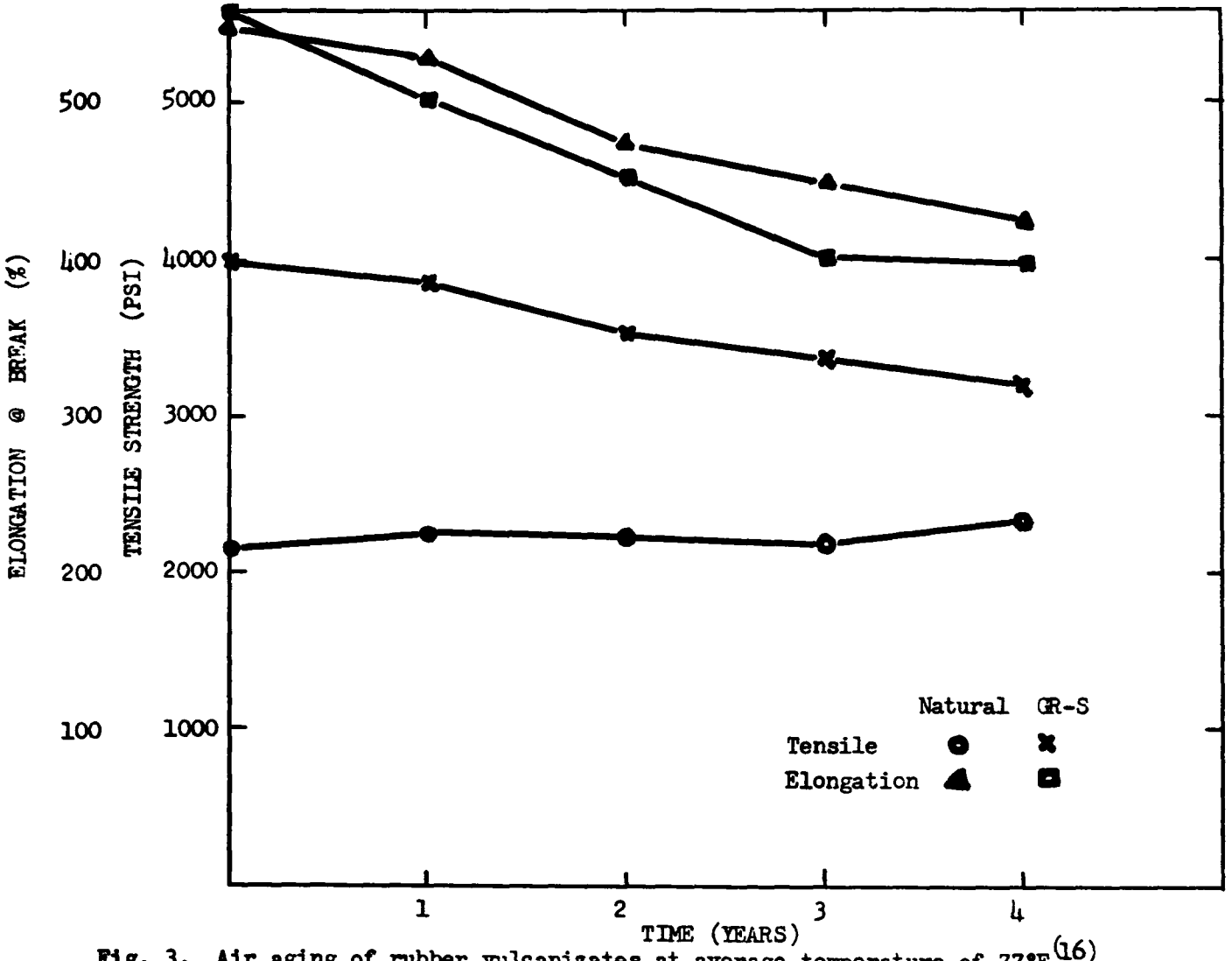

Fig. 3. Air aging of rubber vulcanizates at average temperature of 77°F (16)

The fundamental reaction responsible for ageing of rubber is thought to be oxidation of the rubber hydrocarbon by air.[17] The rate at which ageing progresses depends on the presence of such accelerators as heat, light, moisture, and ozone.

There are five variables to be recognized in any ageing study: (1) type of rubber, (2) degree of cure, (3) presence of antioxidant, (4) temperature, and (5) environment. Each of these can exert a pronounced effect on the rate of ageing. These same variables must be considered in any radiation damage study.

The type of rubber compound is an important factor in radiation damage. Natural rubber and GR-S tend to harden under exposure, whereas butyl becomes progressively softer. The precipitous drop in tensile strength of butyl, Figure 4, admirably illustrates this point. For this reason, when choosing tubeless airplane tires which might be subject to irradiation, one must be careful to select those whose satisfactory functioning do not depend upon butyl rubber. Static tests on an irradiated tire containing a butyl gas barrier might prove quite misleading because the sticky damaged butyl might still act as a gas barrier under this particular condition. The tire would certainly fail, however, when tested under conditions simulating actual operation.

The degree to which a rubber compound is vulcanized prior to irradiation also governs the degree of damage it will sustain after a given dose. Note, in Figure 5, how the same natural rubber gum compound appears more radiation resistant when undercured and less resistant when overcured in comparison with the best cure. The undercured sample actually continues essentially to cure or cross-link during the early exposure period, reaching its peak tensile after 50 megarad. Because of this, comparisons between compounds may be more difficult than one would normally think.

The presence of an antioxidant or antiozonant in the compound under study may have a significant bearing on its ability to withstand irradiation. Such damage inhibitors have been the subject of a continuing investigation by Born and coworkers. [8,9,10] We are inclined to think that chemicals which act as radiation damage inhibitors conform to the normal mechanism of protection offered by antioxidants or antiozonants since they usually belong to those classes of chemical structures known to possess such properties.

Radiation damage to most rubbers is quite temperature dependent. Note in Figure 6 how damage to a natural rubber tread stock increases rapidly in severity as the temperature during exposure is increased. This response has also been noted with nitrile and chloroprene rubbers. A new type of rubber developed by Goodyear, called Adduct rubber, Figure 7, however, appears to possess an improved resistance toward radiation damage at room temperature and a surprisingly lack of any particular tendency toward temperature dependence throughout the range of -120°F to 200°F.

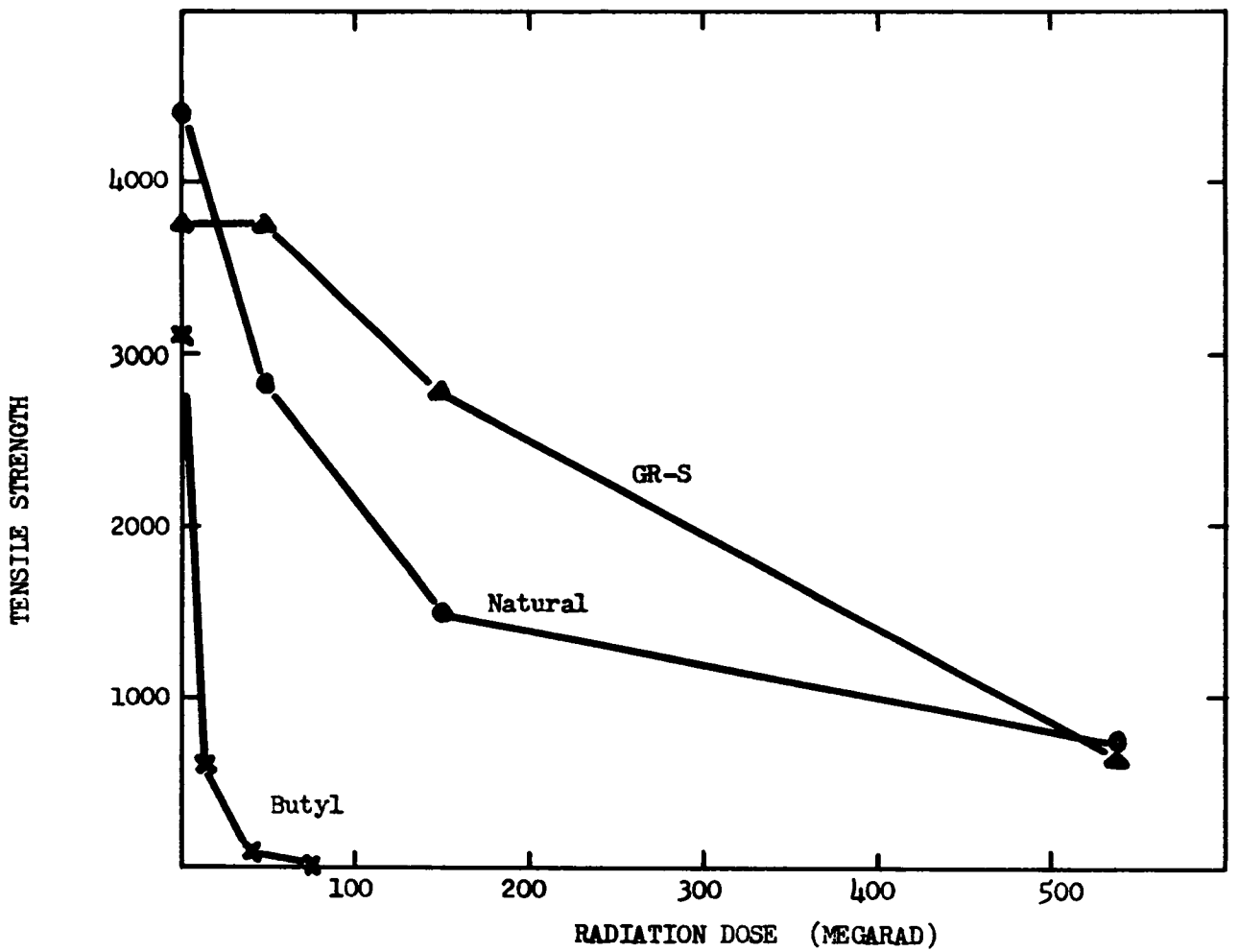

Fig. 4. Dependence of degree of radiolysis on type of rubber compound exposed in air.

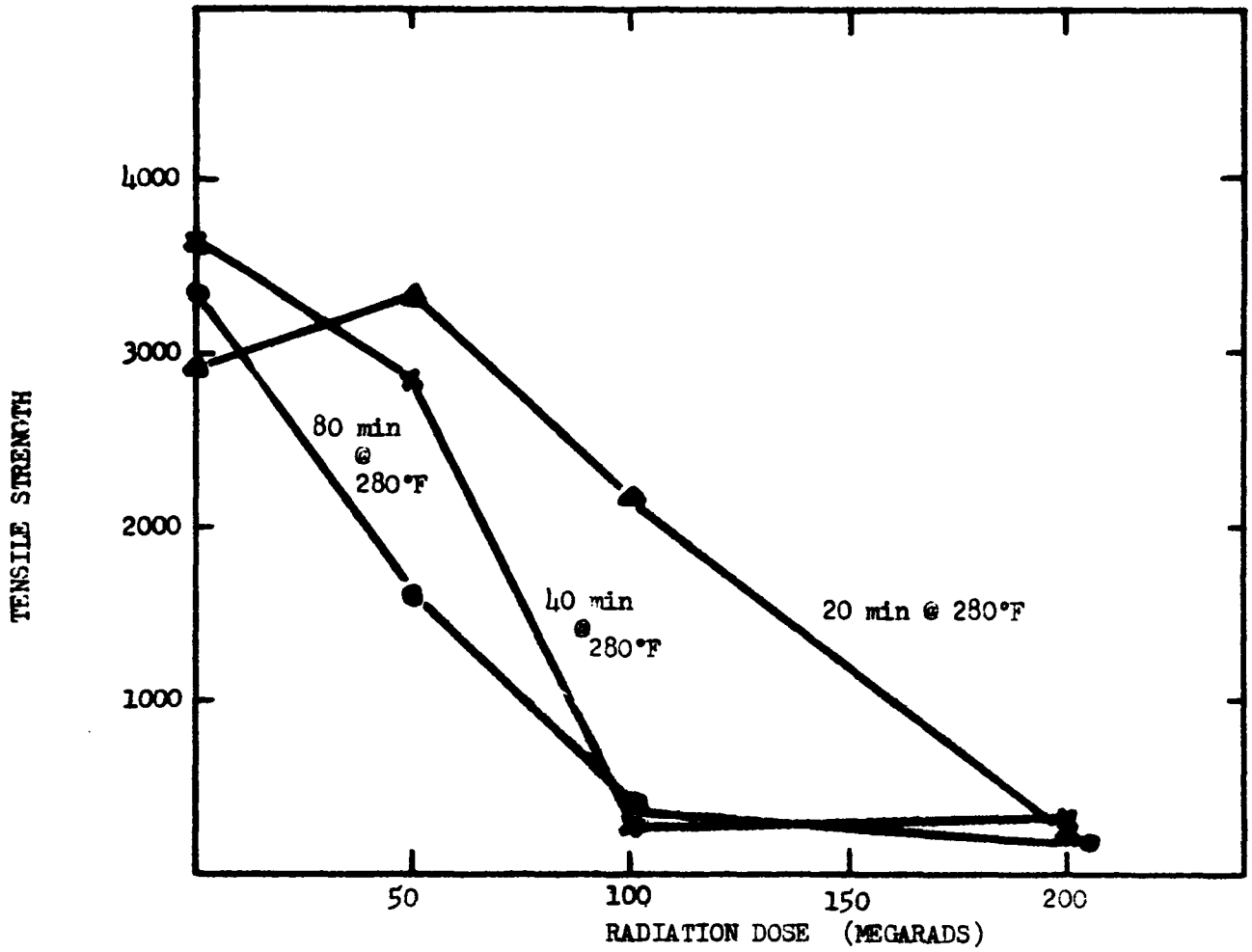

Fig. 5 Effect of state of cure on radiation damage to gum rubber vulcanizates exposed in air at 75°F.

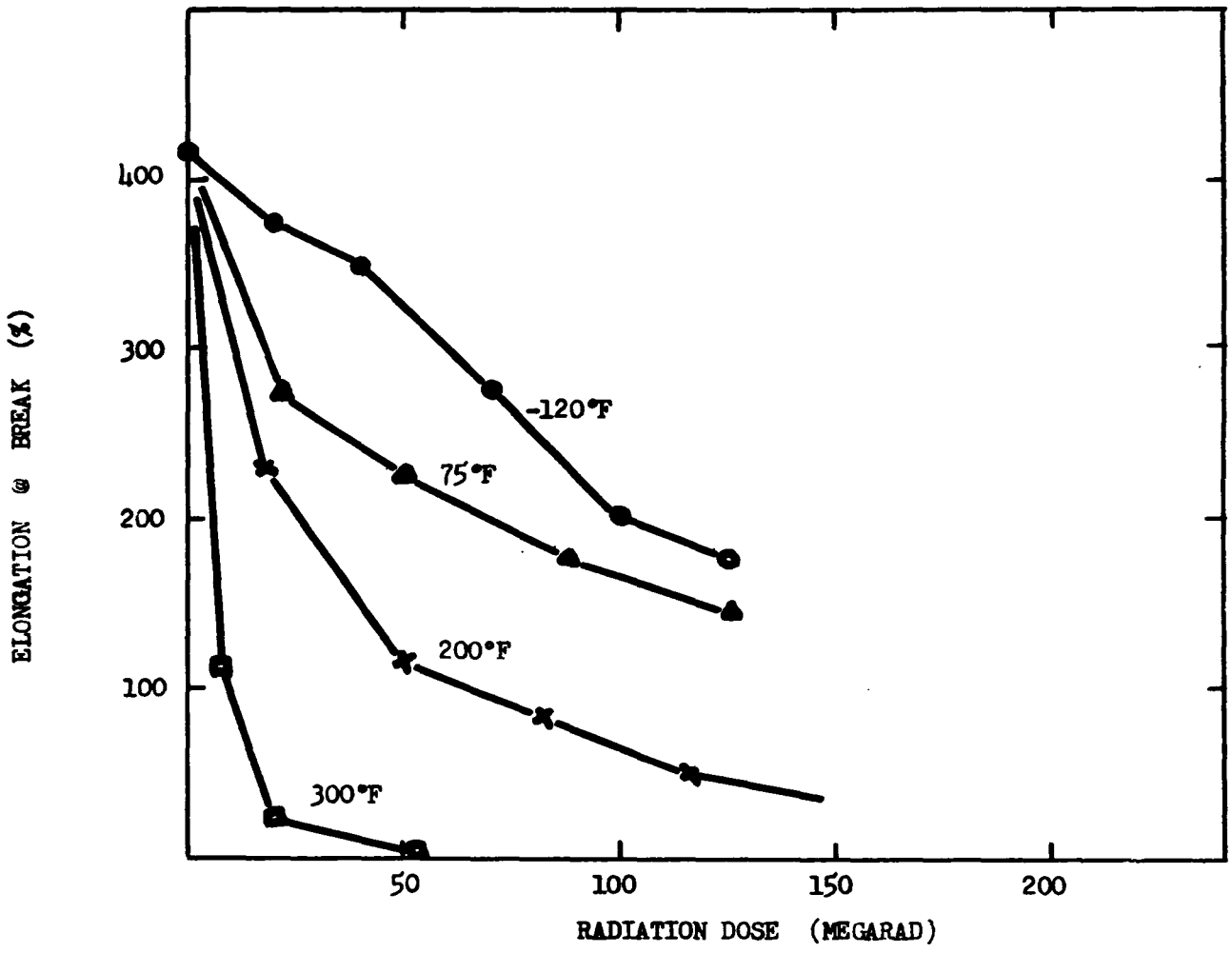

Fig. 6. Temperature dependence of radiation damage to a natural rubber compound exposed in air.

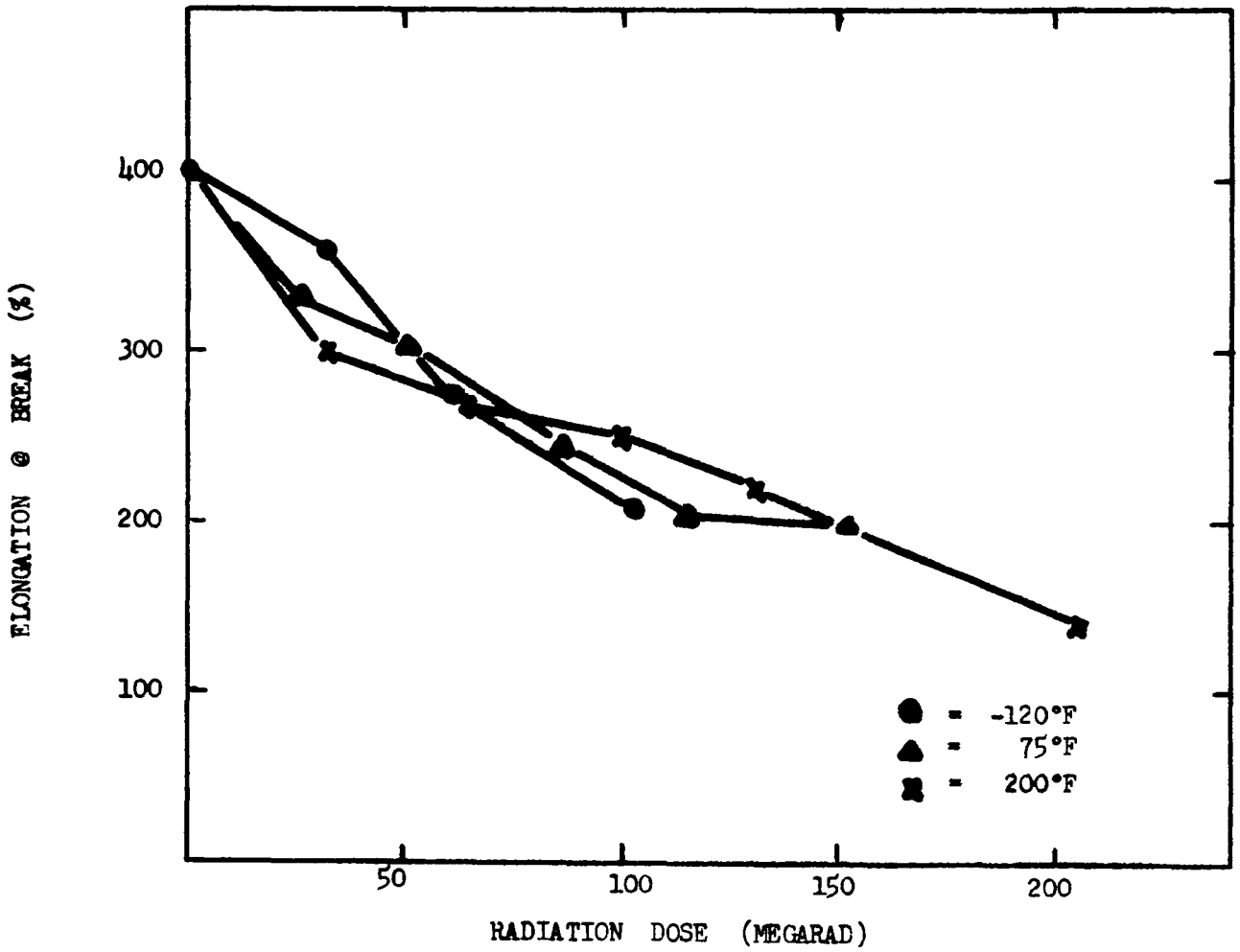

Fig. 7. Effect of temperature on radiation stability of an Adduct rubber compound during exposure in air.

The environment in which a rubber is exposed can also be influential in the matter of radiation damage. Gamma radiation produces ozone in air and this reactive gas is perhaps rubber's worst enemy. It is especially damaging when the compound is under stress. We have found that this type of surface attack can be prevented by flushing with an inert gas prior to irradiation and holding the sample in such a protective atmosphere during exposure. Figure 8 indicates the degree of protection one can obtain with this method when irradiating a natural rubber tread stock.

Rubber's dynamic properties also suffer during irradiation. Johnson, et. al.,[15] found the flex life of a natural rubber vulcanizate to decrease by 14% affer a 50 megarep dose and that of a GR-S vulcanizate to drop by 86%.

RADIATION DAMAGE - - - - - FABRIC-RUBBER ADHESIVE

Radiation damage to adhesives of the type employed in bonding textiles to rubber offers a virgin field of exploration. At least, one must so conclude from the paucity of literature on the subject. The adhesive which bonds rubber to cord performs a very critical function in a tire. As such, its susceptibility to radiation damage must not be overlooked.

We have a few preliminary tests on two proprietary adhesives coded A and B. Table I illustrates how the dynamic adhesions between rubber and various tire cords behave after irradiation. Data in the second and third columns were obtained from test pieces which had been built and then irradiated, whereas those in columns four and five resulted from specimens in which the adhesive coated cord was exposed before the test pieces were made up. The greater damage shown by the latter type treatment must be due to radiation induced oxygen attack during the exposure in air. After a 14 megarad dose nylon shows a high loss in adhesion, rayon shows a small loss, and Dacron, with poor initial adhesion, retains virtually none after exposure. Table II illustrates what happens when a similar approach is followed in studying the loss of adhesion through hot static tests. Here again the samples made up from exposed cords showed greater damage. The degree of damage again increases in the order Dacron, rayon and nylon.

In summarizing the data in these two tables we can say that after a dose of the order of 15 megarad, (1) rayon retains most of its adhesion strength,[2] nylon shows a large loss in adhesion but may still be in the "get by" range, and (3) Dacron, which is difficult to bond to rubber, retains virtually no adhesion. Also, dynamic properties are more sensitive to radiation damage than are static properties.

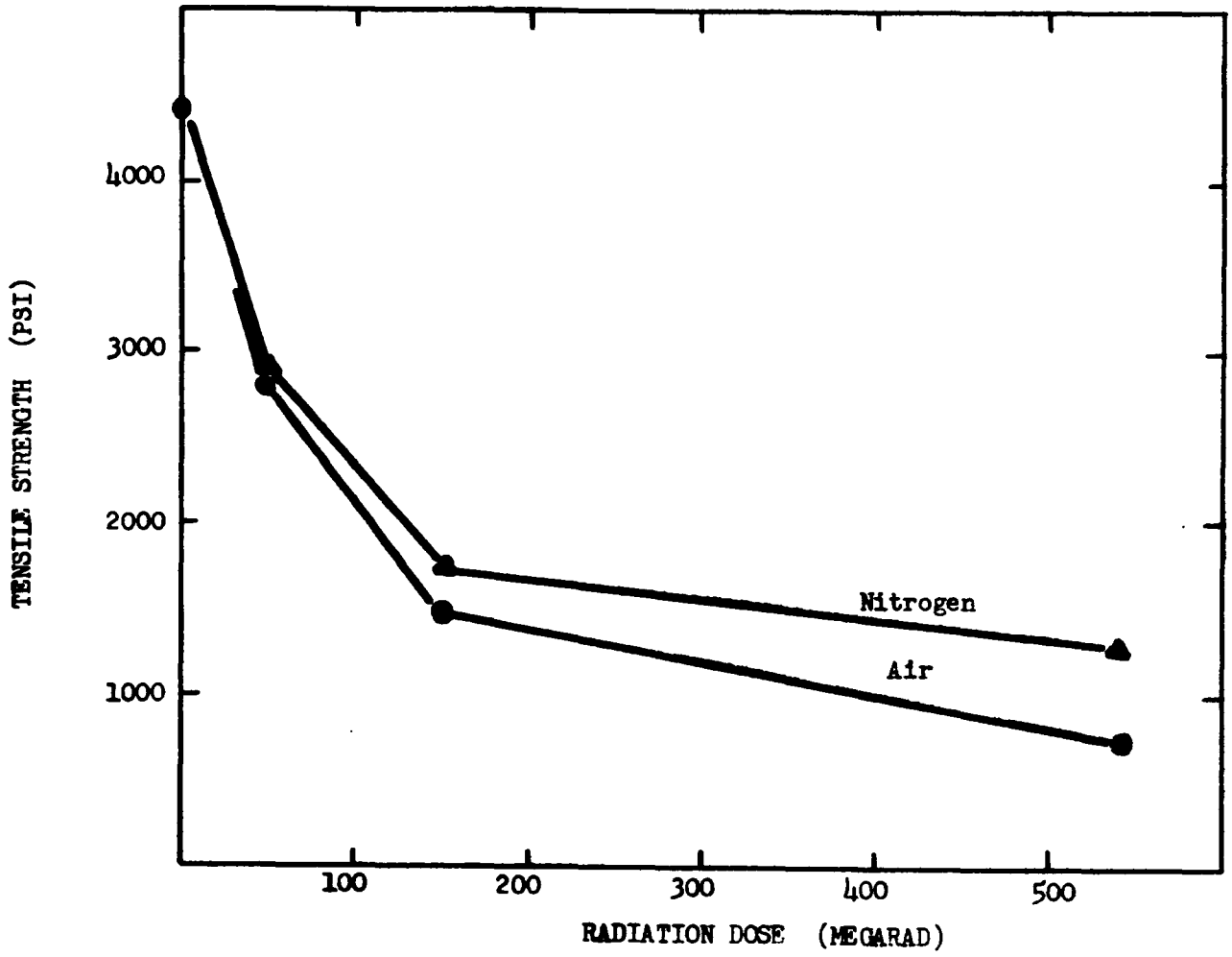

Fig. 8. Effect of environment on radiation damage to a natural rubber tread vulcanizate during exposure at 75°F.

TABLE I.

Effect of 14 Megarad Gamma Ray Exposure
on Dynamic Strip Adhesions of Tire Cords

$(\text{Rate of Separation}^{*})^{-1}$

Type Cord	Type Adhesive	Control	Exposed**	Separation Rate Increase %	Exposed***	Separation Rate Increase %
Nylon 700 L	A	5.55	2.12	161	0.72	672
Nylon 700	A	5.55	2.12	161	0.55	555
Rayon T258	A	5.55	5.00	11	4.55	22
Rayon T258	B	1.39	1.16	18	1.39	0
Dacron 5100	A	0.645	virtually no adhesion			

* subjected to 3 lbs. @ 250°F

** test pieces built before irradiation

*** test pieces built after irradiating dipped cords

TABLE II.

Effect of 14 Megarad Gamma Ray Exposure
on Hot Static Adhesion of Tire Cords

Type Cord	Type Adhesive	Hot Static Adhesion, lbs @ 250°F Control	Exposed*	Adhesion Loss %	Exposed**	Adhesion Loss %
Nylon 700L	A	11.0	9.3	15.4	7.5	31.8
Nylon 700	A	13.1	9.0	31.5	3.0	77.0
Rayon T258	A	17.1	15.1	11.8	14.5	15.2
Rayon T258	B	18.3	15.5	15.3	13.5	26.2
Dacron 5100	A	4.0	4.1	0	5.5	+37.5

* test pieces built before irradiation

** test pieces built after irradiating dipped cords

RADIATION DAMAGE - - - - - TIRE FABRIC

Radiation damage to tire fabric is especially critical, in terms of performance, since this material bears the brunt of all stresses to which the tire is subjected. We believe this to be the factor which limits a tire's usefulness when operating in a radiation environment. This is the weak link in the chain. Currently used textiles may turn out to be inadequate because of poor radiation resistance. Other cord-type materials better able to withstand irradiation have never been used successfully in tires due to poor tension-compression fatigue and/or poor adhesion. Therefore the major emphasis at this time should be placed on improving the radiation resistance of tire fabric rather than tire compounds.

Quite a few publications have dealt with effects of radiation on textiles, some of which are used in tire fabrics(1, 18, 19, 20). When estimating radiation damage to a synthetic textile, one must be cautioned against assuming that data obtained from molded or pressed samples of the polymer will be the equivalent of data gathered on fiberous type specimens. The large surface to volume ratio of fibers, the highly oriented condition in which they are drawn, and the twisted state in which cords are normally used all contribute to an increased sensitivity to radiation damage. Figure 9 demonstrates the differences one can expect in stress-strain properties of nylon cords and nylon molded sheets. Note how the two cases in many respects show exactly opposite trends.

There are also five variables which should be investigated in a thorough analysis of radiation damage to tire fabrics: (1) type of fabric, (2) environment, (3) stress, (4) temperature, and (5) effect of antioxidants and antiozonants. We have a study underway to evaluate the separate and combined effects which these variables play during irradiation of tire fabrics.

Different fabrics possess varying resistances to radiolysis. Even different types of the same fabric show this phenomenon. Note in Figure 10 how the relative resistance varies with fabric material and with type of nylon as well. Since an airplane tire may have to withstand a cumulative dose somewhat greater than 10^7 rad, we have exposed these cords to doses in the range of 4 to 400 megarads. Cotton and nylon are virtually destroyed by a 100 megarad dose whereas Dacron suffers only a 14% loss at twice this dose. Since types 66, 300, and 700 nylon are the same chemically and vary only in such respects as molecular weight, crystallinity, surface finish, and antioxidant type and concentration, the significant differences in their radiation sensitivity is most interesting. This subject will be considered shortly.

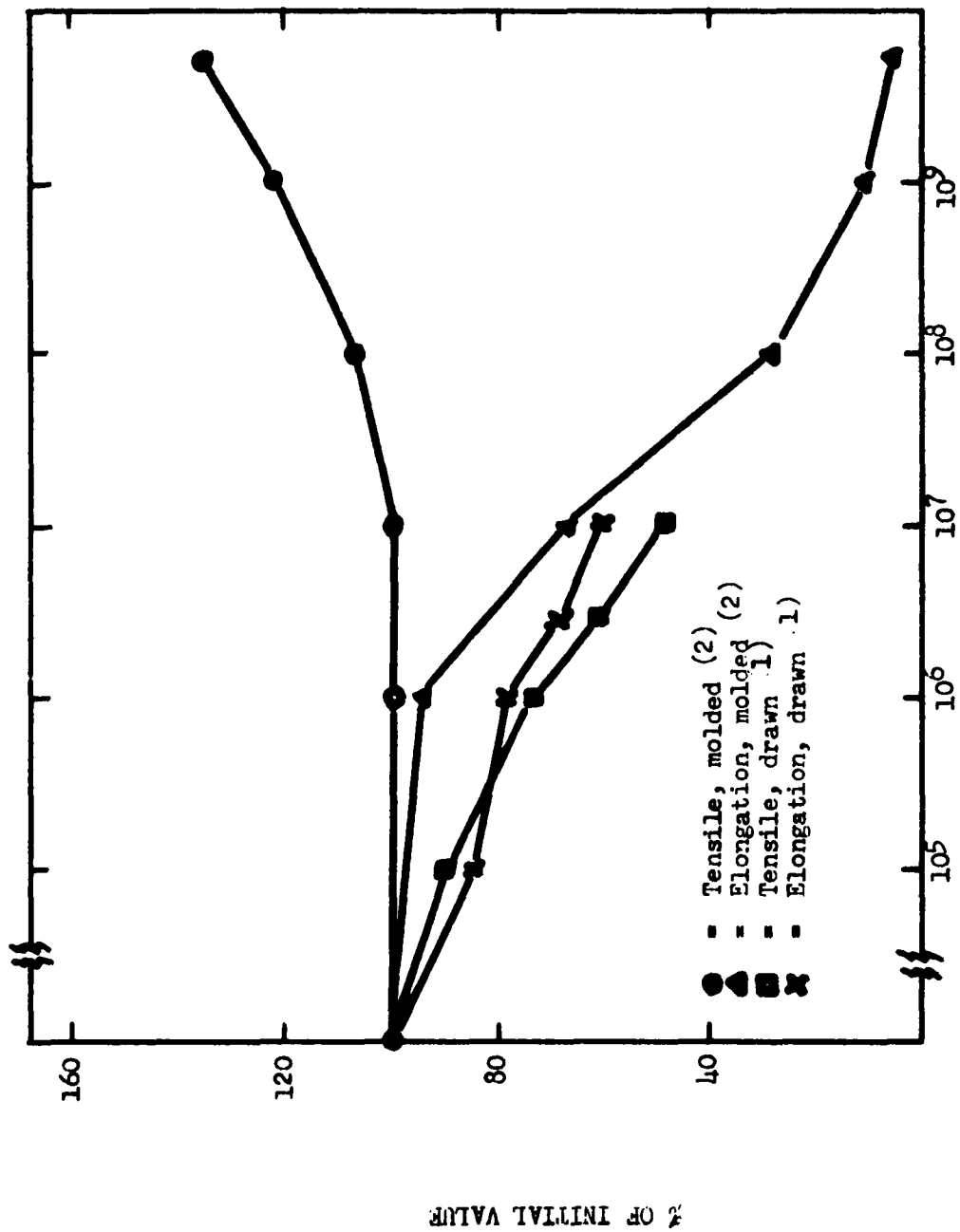

Fig. 9. Dependence of radiation damage to nylon 66 on the polymer's prior history.

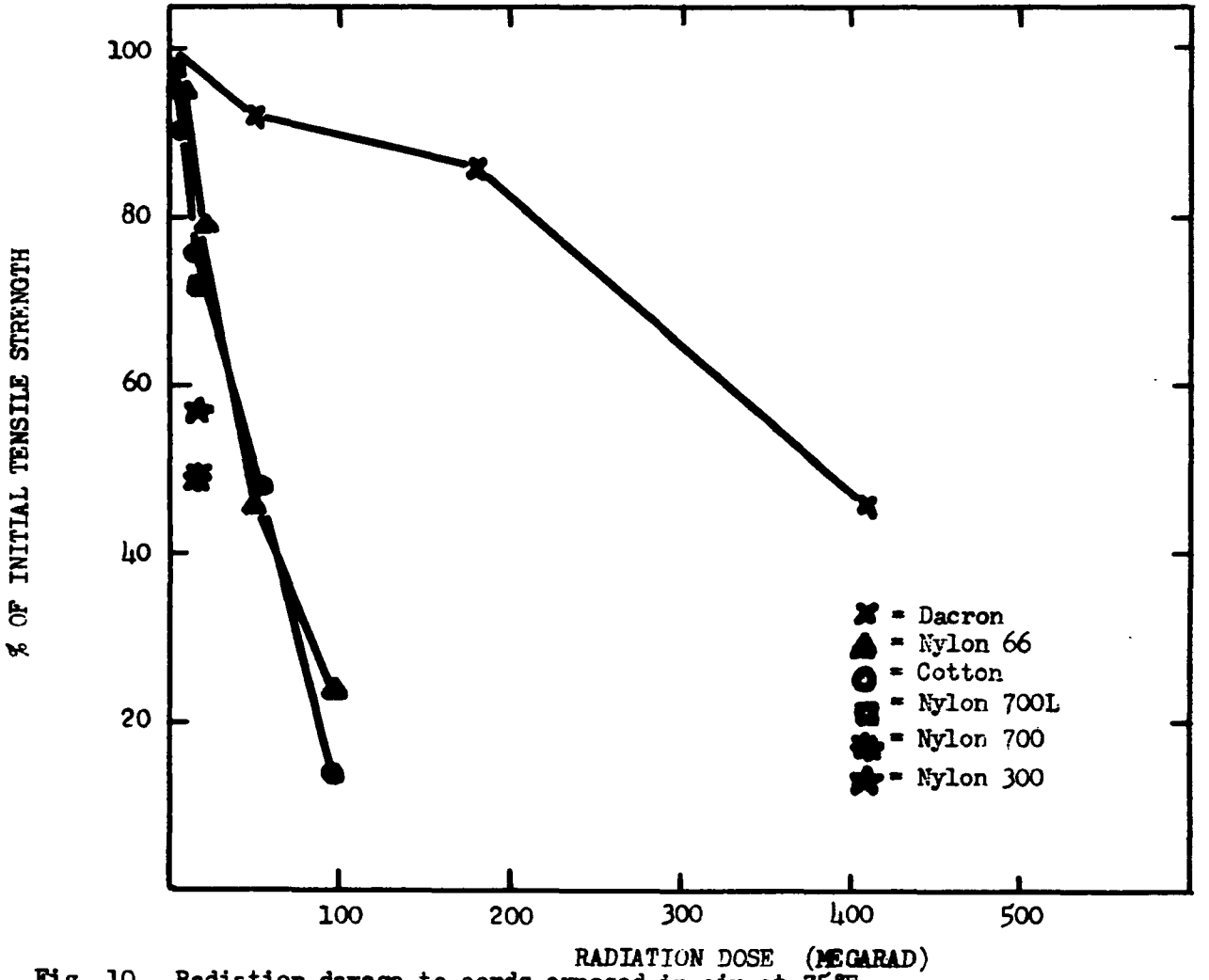

Fig. 10. Radiation damage to cords exposed in air at 75°F.

The most serious aspect of radiation damage to tire fabric lies in cord fatigue. Table III shows that nylon and rayon suffer virtually a complete loss in ability to withstand repetitive tension-compression stresses. A cord which will stand about 1 million cycles is considered acceptable in this respect. Note that Dacron is poorer initially than nylon after a dose of 16 megarads. These data are in substantial agreement with those published by Harmon[1].

The environment in which a cord is exposed is definitely related to the damage it suffers. Figure 11 compares damage to type 300 nylon in air to that when exposed in nitrogen. If a 30% loss in initial tensile and elongation can be tolerated, a tenfold increase in lifetime, dosagewise, can be gained by bathing nylon in nitrogen during irradiation. The superior retention of properties of fabrics exposed in vacuum over those treated in air has been reported in the literature[1]. Radiation induced oxidation is very detrimental, as shown by the data in Table IV. A 1-2% drop in stress-strain properties occurs in nylon type 300 exposed to 5 megarad in nitrogen, and a 3-5% drop occurs if the cords are under stress during this period. However, cords exposed in air, at relatively low dose rates in order to emphasize oxidative effects, show losses of 54-64% when unstressed and 69-71% if stressed.

The degree of radiation damage to tire cords depends very much on the magnitude of both temperature and stress during irradiation. We are currently investigating the combined effects of dose, temperature, stress, and environment. Some preliminary data are listed in Table V. Controls held in air showed some degradation, especially when stressed; but, samples exposed to 28 megarad were destroyed. A specimen held at 200°F under a stress of 2 kg per cord failed statically at a dose less than 28 megarad. These tests are being repeated in nitrogen to clarify the overall importance of oxygen in this damage.

If the previously mentioned ability of some nylons to resist damage is due to varying types or concentrations of antioxidants, either incorporated throughout the polymer or added only to the surface finish, it is conceivable that yet greater protection by this means is still possible. To test the validity of this hypothesis we surface coated nylon cords with several antioxidants prior to irradiation. These did not demonstrate any significant degree of protection. It may be necessary to actually innoculate nylon with an appropriate antioxidant during manufacture in order to get effective protection by this means.

Compounding rubber stock in which fabric is to be cured with a damage inhibitor of the antioxidant-antiozonant type did confer some protection to the fabric in some of our experiments. Figure 12 indicates the percent of initial tensile strength retained by adhesive dipped nylon 700P cords when subjected to irradiation while bare, while covered with a natural rubber vulcanizate lacking an antioxidant,

TABLE III.

Damaging Effect of 16 Megarad Gamma Ray Exposure on Fatigue Characteristics of Tire Cords

Type Cord	Type Adhesive	Number Test Cycles Required for Failure* Control	Exposed	Loss in Fatigue Resistance, %
Nylon 700 L	A	2,205,500	56,900	97.2
Nylon 700	A	2,672,600	58,867	97.7
Rayon T258	A	553,700	2,125	99.6
Rayon T258	B	1,186,550	1,975	99.8
Dacron 5100	A	20,825	22,450	+7.8

*Mallory Fatigue Tester operating at 850 RPM with 50 lbs. inflation.

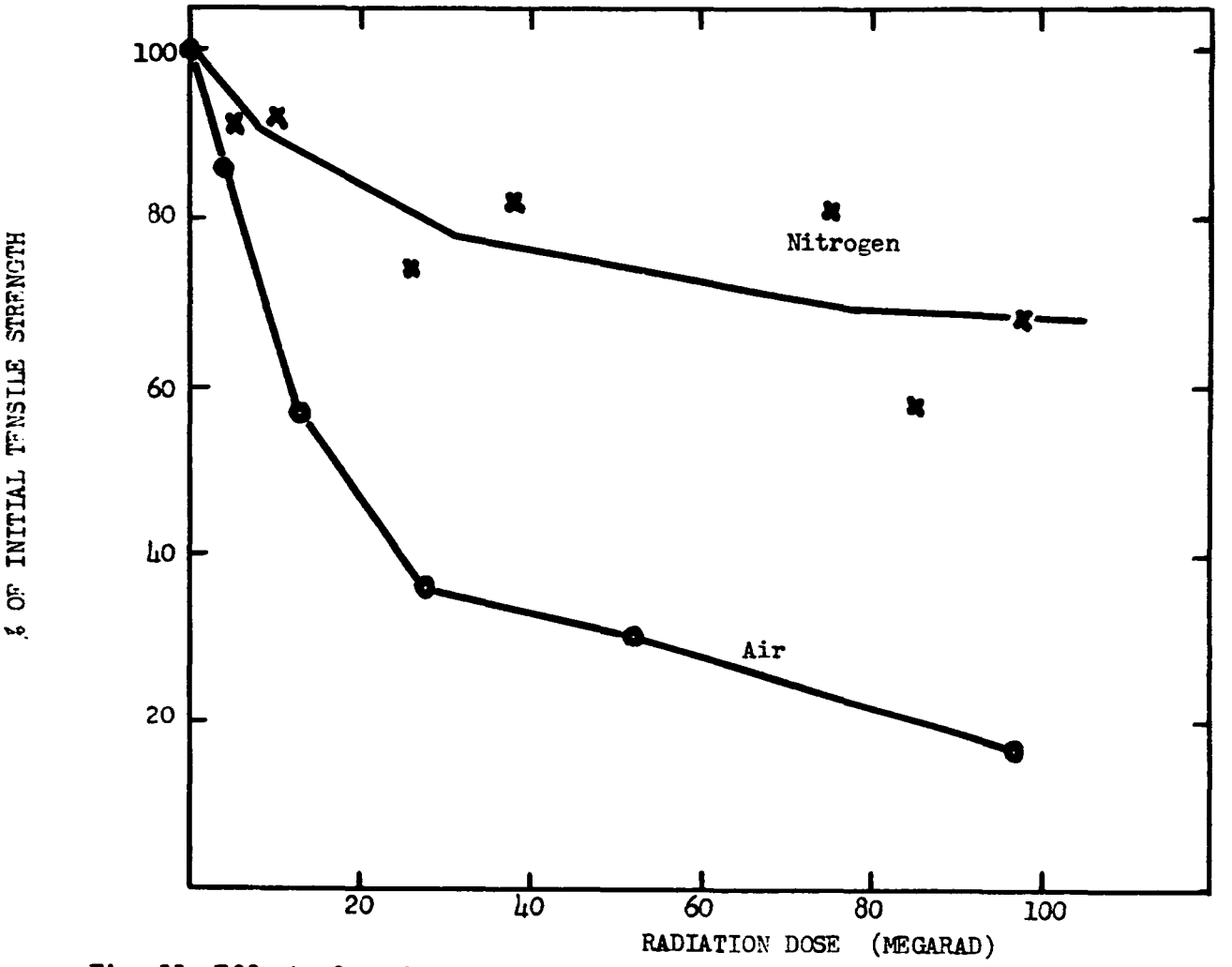

Fig. 11 Effect of environment on radiation damage to nylon cords exposed at 75°F.

TABLE IV.

Effect of Environment on Damage to Type 300 Nylon Tire Cords Induced by 5 Megarad exposure to Co-60 Gamma Rays at 75°F

Experimental Conditions			Stress-Strain Properties			
Time Required for Exposure days	Environment	Stress, gm/cord	Ultimate Tensile, psi.	% of Initial Tensile	Elongation at Break %	% of Initial Elongation
90 (control)	air	0	28.0	100	17.5	100
90 (control)	air	1600	28.7	102	17.9	102
90	air	0	10.1	36	8.1	46
90	air	1600	8.2	29	5.5	31
5	nitrogen	0	27.4	98	17.3	99
5	nitrogen	1600	26.5	95	17.0	97

TABLE V.

Effect of Temperature and Stress on Radiation Damage to Nylon 700M Exposed in Air

Experimental Conditions			Stress-Strain Properties			
Dose, megarad	Temperature °F	Stress kg per Cord	Ultimate Tensile psi.	% of Initial Tensile	Elongation at Break %	% of Initial Elongation
0	80	0	28.6	100	21.3	100
0	80	2	28.7	100	19.3	91
0	200	0	27.0	94	20.8	98
0	200	2	27.0	94	16.5	78
28	80	0	10.1	35	10.1	47
14	140	1	8,0	30	7.7	36
28	80	2	5.4	19	4.3	20
28	200	0	2.7	9	2.5	12
Less than 28	200	2	broke during exposure			

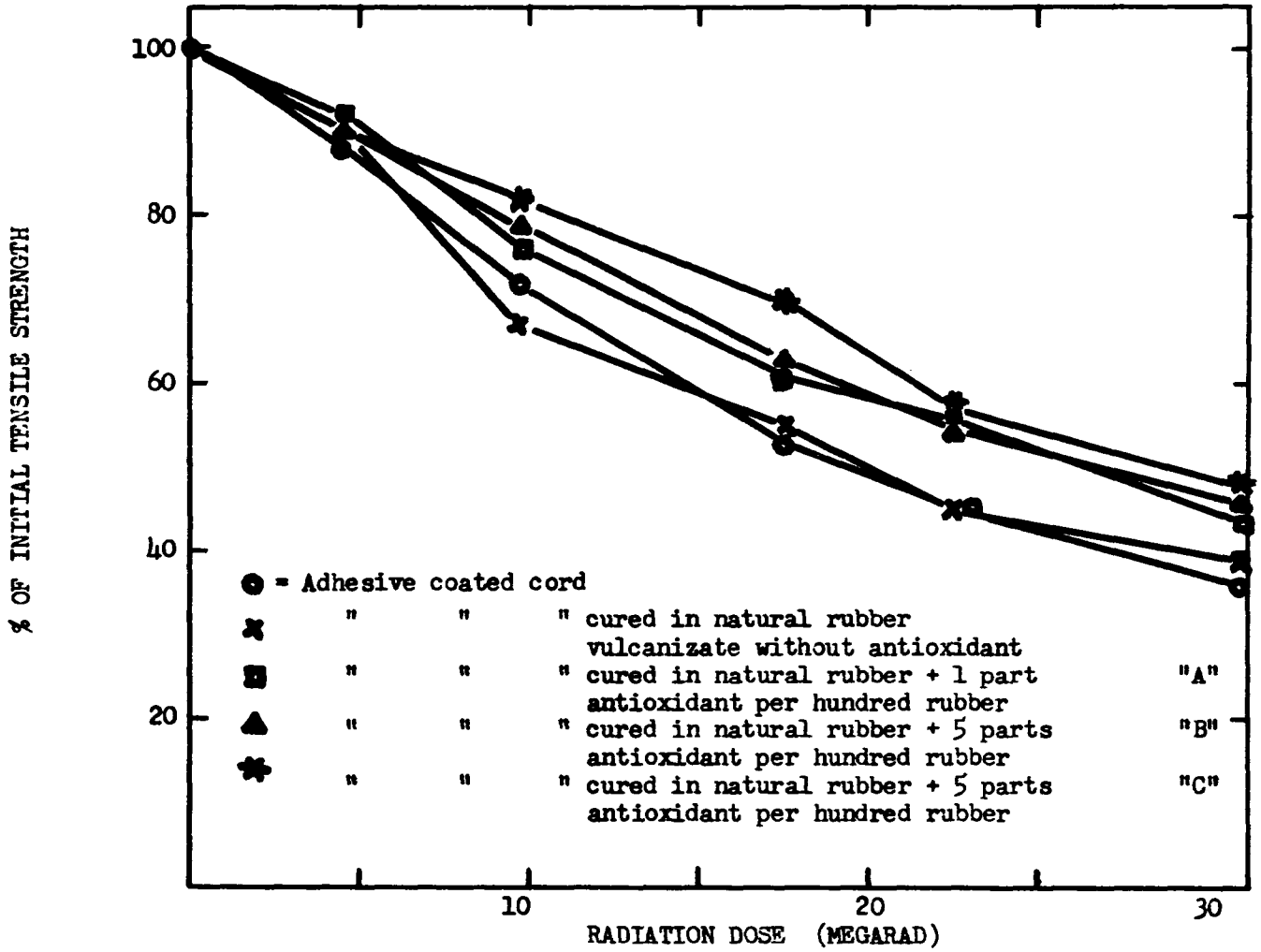

Fig. 12. Effect on radiation damage to nylon cords of antioxidant added to rubber compound used to coat fabric.

and while covered with similar rubber compounds containing different antioxidants. This method did not prove as effective in preventing damage to nylon cords as did the use of a nitrogen atmosphere, since with these antioxidants present a 50% loss in tensile still occurred whereas in a nitrogen environment only a 20% loss was detectable.

RADIATION DAMAGE - - - - TIRES

Having observed the efficacy of a nitrogen environment in reducing radiolysis in nylon cords, it was conceived that nitrogen inflation would provide a practical means of raising the damage threshold of tubeless airplane tires. The gas with which a tubeless tire is inflated normally diffuses to some extent through the gas barrier and into and through the fabric layers. Cords in a tire inflated with nitrogen should thus be bathed in nitrogen after a sufficient storage period.

On the assumption that doses of from 10 to 100 megarad may be realistic service requirements, we have been exposing nitrogen inflated tubeless airplane tires to levels within this range. Our experimental setup is shown in Figure 13. The tires are rotated during exposure in order to improve the uniformity of the dosage they accumulate.

Tires exposed to 10^7 rad, a level above the damage threshold for nylon cords when irradiated in air, made over 200 high speed landings and gave a normal static burst test. Their performance thus confirmed the protective benefits of nitrogen inflation during irradiation.

ACKNOWLEDGMENT

It is a pleasure to acknowledge the help of Messrs L B Bangs, G A Barber, N C Bletso, E H Manuel, and J K Phillips in preparing, irradiating, and testing many of the experimental specimens used in this study.

REFERENCES

(1) Harmon, D.J., Effects of Cobalt 60 Gamma Radiation on the Physical Properties of Textile Cords, Textile Research Journal 27, 318 (1957) Apr.

(2) Collins, C.G. and Calkins, V.P., Radiation Damage to Elastomers, Plastics, and Organic Fluids, APEX-261, 32, (1956).

(3) Sisman, O. and Bopp, C.D., Physical Properties of Irradiated Plastics, ORNL-928 (1951).

(4) Bopp, C.D. and Sisman, O., Radiation Stability of Plastics and Elastomers, ORNL-1373 (1954).

(5) Gehman, S.D. and Hobbs, L.M., Changes in Elastomers Due to Radiation from Cobalt-60, Rubber World 130, 643 (1954).

(6) Bopp, C.D. and Sisman, O., Radiation Stability of Plastics and Elastomers, Nucleonics 13, 28 (1955) July.

(7) Bopp, C.D. and Sisman, O., How Radiation Changes Polymer Mechanical Properties, Nucleonics 13, 51 (1955) Oct.

(8) Loughborough, D.L., Juve, A.E., Beatty, J.R., and Born, J.W., A Study of the Effects of Nuclear Radiations on Elastomeric Compounds and Compounding Materials, WADC TR 55-58 (1956) Aug.

(9) Born, J.W., A Study of the Effects of Nuclear Radiations on Elastomeric Compounds and Compounding Materials, WADC TR 55-58, Part II (1956) Sept.

(10) Born, J.W., Diller, D.E., and Rowe, E.H., A Study of the Effects of Nuclear Radiation on Elastomeric Compounds and Compounding Materials, WADC TR 55-58, Part III (1951).

(11) Harrington, R., Elastomers for Use in Radiation Fields, Rubber Age 81, 971 (1957).

(12) Harrington, R., Effects of Gamma Radiation on Heat Resistant Elastomers, Rubber Age 82, 461 (1957) Dec.

(13) Harrington, R., Effect of Gamma Radiation on Elastomers, Rubber Age 82, 1003 (1958) Mar.

(14) Harrington, R., Effects of Gamma Radiation on Miscellaneous Elastomers and Rubberlike Plastic Materials, Rubber Age 83, 472 (1958) June.

(15) Johnson, B.L., Adams, H.E., and Barzan, M., Radiation Effects in Elastomeric Vulcanizates, Rubber World 137, 73 (1957) Oct.

(16) Juve, A.E., and Schock, M.G., The Effect of Temperature on the Air Ageing of Rubber Vulcanizates, ASTM Bulletin 195, 54 (1954) Jan.

(17) Bruist, J.M., Ageing and Weathering of Rubber, Heffer & Sons, Ltd., Cambridge, England (1956).

(18) Teszler, O. and Rutherford, H.A., The Effect of Nuclear Radiation on Fibrous Materials, Part I, Textile Research Journal 26, 796 (1956) Oct.

(19) McGrath, J., and Johnson, R.H., The Effects of Gamma Radiation on Textile Materials, WADC TR 56-15 (1956) Feb.

(20) Gilfillan, E.S., and Linden, L., Effects of Nuclear Radiation on the Strength of Yarns, Textile Research Journal 25, 773 (1955) Sept.

RADIATION EFFECTS ON FLIGHT CONTROL SUBSYSTEM DESIGN

by

D O. Gunson

Lockheed Aircraft Corporation
Marietta, Georgia

Successful application of nuclear propulsion to aircraft requires the development of a high performance flight control subsystem that is not only more reliable, serviceable, and maintainable than the best flying today but is at least as efficient while operating in a radiation environment. The attainment of these aims demand close and continued cooperation between the radiation effects specialist and controls designer throughout the design, development, and testing of this subsystem. The basic problems considered are: the establishment of the important characteristics of a flight control subsystem, how radiation environment affects these characteristics and the type of radiation effects data required by the controls designer.

A practical control subsystem is as fundamental to a useful flying machine as the lifting surfaces and power plants. Upon its development has hinged the success of every advancement in aircraft performance. Its role will not diminish in the future, for a flying machine is of no value unless it can be controlled under all design flight conditions with sufficient accuracy to perform the desired mission. Thus, each advancement in aircraft impose increased requirements on the control system. During the past decade and a half, the requirements for dynamic performance have advanced at an ever increasing rate. Now an entirely new environment and increased flight times are being added to the already stringent requirements.

The successful application of nuclear propulsion to aircraft and its full utilization requires the development of a completely compatable flight control subsystem that is also tolerant of the radiation environment to which it will be subjected under operating conditions. This subsystem must have as high performance capabilities as any flying today and be more reliable, serviceable, and maintainable. This is a big order for the controls designer.

Since the radiation environment affects the physical configuration of the subsystem as well as the chemical and physical properties of the component materials, close and continued cooperation between the radiation

effects specialist and the controls designer is necessary. Each must have a thorough understanding in mutual areas and be conversant with the problems of the other. The controls designer must specify those characteristics and material properties that are important, specify the test programs, and evaluate the test results as to subsystem performance. The radiation effects specialist must, in turn, evaluate the subsystem under dynamic conditions in the radiation environment for changes in these characteristics and properties. He must also aid in the selection of materials and components and perform pre and post irradiation analyses.

Even though a considerable amount of radiation effects data on applicable materials and components is presently available, it is incomplete from an engineering view point. Most of these data were measured under static conditions. The amount of data taken under dynamic conditions is small and only sufficient to show that there is a great difference between the effect on materials and components alone under static conditions and the same items in a subsystem under dynamic conditions. In many cases the effects for the later case are much less severe. If a practical flight control subsystem for a nuclear powered airplane is to be developed, the actual changes in material properties and physical characteristics must be evaluated under realistic operating conditions which include other environments.

At the present time, some programs are being undertaken to determine certain effects under dynamic conditions on small representative subsystem test panels. Other and larger programs are being planned. If these programs are to produce the greatest possible gain in basic system knowledge, both the radiation effects specialist and controls designer must actively participate. Thus, it is appropriate to point out the more important characteristics of control subsystems, how a radiation environment affects these characteristics, the type of data needed by the controls designer and some possible methods of overcoming the problems.

The more important of control subsystem characteristics can be summarized as listed in Figure 1.

FIGURE 1

CHARACTERISTICS

1. Controllability
2. Stability
3. Reliability
4. Safety
5. Versitility
6. Serviceability
7. Maintainability

This list could be expanded greatly, but it is felt that the other pertinent characteristics can be suitably defined as an attribute of one or more of the basic seven.

Controllability is the measure of the pilot effort required for controlling the aircraft in the manner and with the accuracy required to perform the mission To free the pilot from giving continual attention to flying, stability is required. That is, the subsystem must respond only to the pilot's command. Reliability is an absolute necessity and requires no definition in view of the emphasis presently being placed on it The primary aim must be toward substantially failure free subsystems and components. Safety is an important characteristic which must be provided through "fail-safe" design techniques and elimination of materials that retain high levels of activation. This recognizes that due to damage, human errors, or material failures emergencies do occur, but they must be so controlled that safe flight can be maintained even after an emergency occurs Safety of ground personnel during service and maintenance periods must also be provided. Versatility is a measure of the ease with which additional features can be incorporated into a subsystem without undue duplication of functions and complexity of design and installation Serviceability and maintainability are measures of the time required by ground personnel for servicing and maintaining the subsystem. These last factors have assumed primary importance not only due to the desire for a maximum aircraft utilization, but because of the radiation environment in which most of the flight controls subsystem components are located. Most of the components will have residual activation after having been irradiated on the aircraft All of these characteristics must be attained by design, development, and tests of the subsystem and its components.

The accomplishment of these characteristics involve problems that can be categorized as shown in Figure 2

FIGURE 2

PROBLEM TYPES

1 Human Factors

2. Mechanical

3 Hydraulic

4. Electrical

5 Aerodynamic

6 Support Equipment

Human factors and aerodynamics establish the requirements for controllability and stability. Human factors and support equipment problems are predominant in obtaining serviceability and maintainability. Mechanical, hydraulic, and

electrical design problems are involved in accomplishing all the characteristics.

Existence of the radiation environment affects the characteristics and complicates the problems in the manner shown in Figure 3.

FIGURE 3

RADIATION EFFECTS

1. Changes in Material Properties
2. Requirements for Remote Handling
3. Increased Danger to Personnel and Equipment

Changes in certain of the chemical and physical properties of the mechanical, hydraulic, and electrical component materials affect the controllability, stability, and reliability characteristics of the subsystem. Changes in friction, hardness, rigidity, strength, and dimensions of the mechanical components are of primary importance to the dynamic performance of the subsystem. For the same reason, changes in the bulk modulus, visocity, and lubricity of the hydraulic fluid are important. Changes in such properties as flexibility, compliance, dimensions, and friction coefficient are important in hydraulic seals. Such properties of electrical components as resistance of insulation, conductivity of wires, magnetic characteristics of core materials, and certain operating characteristics of components are important. These lists can be greatly expanded by being more specific. The radiation effects engineer must determine the specific materials and significant properties through close cooperation with the controls designer. The important point to be made is that not all chemical and physical properties of any material are significant in a particular application

Reliability is of prime importance to the controls designer It can be achieved only through the assistance of the radiation specialist in selecting the materials whose significant properties are most tolerant to radiation for use in the control subsystem design, and through developmental and reliability testing under dynamic conditions in realistic environments.

Radiation from the power plants and activation of the component materials affect the safety, serviceability, and maintainability characteristics of the subsystem. The equipment must be serviced and maintained while on the aircraft as well as installed and removed by ground personnel whose safety must be assured at all times. Thus, the human factor establishes the requirements for remote checkout provisions and test equipment, remote servicing provisions and equipment, designs for quick installation and removal of the subsystem components, and for the remote handling equipment for the installation and removal of those components most susceptible to failures.

Safety of flight requirements are affected by the radiation environment through the effects on equipment reliability since they are met primarily through design. This considers the human factors as related to the flight crew. The aim is to provide safe control even after a primary failure in the subsystem.

From analyses of the available data, the apparent problem areas are as shown in Figure 4.

FIGURE 4

KNOWN PROBLEM AREAS

1. Piercing of Radiation Shields
2. Lubrication
3. Hydraulic Fluid
4. Hydraulic Seals
5. Electrical Insulation
6. Remote Checkout and Malfunction Detection
7. Activation

All of the above problem areas except activation and, to some extent, remote checkout and malfunction detection, are similar to those faced in the designs for very high temperature applications. In most cases the same solutions are applicable. Many of the techniques being employed by Lockheed were developed in experimental programs on high temperature hydraulic and pneumatic subsystems.

Crew shield penetration will be accomplished by the use of torque tubes and linkages as shown in Figure 5. With this method, a minimum of free path area for penetration of radiation can be provided. The free path area consists only of that occupied by the torque tube itself plus the clearance around the outside diameter of the tube. By the use of shield rings on each end of the tube, the clearance area can be effectively reduced to help maintain the level of radiation. This method also adds a minimum of friction to the controls subsystem.

FIGURE 5

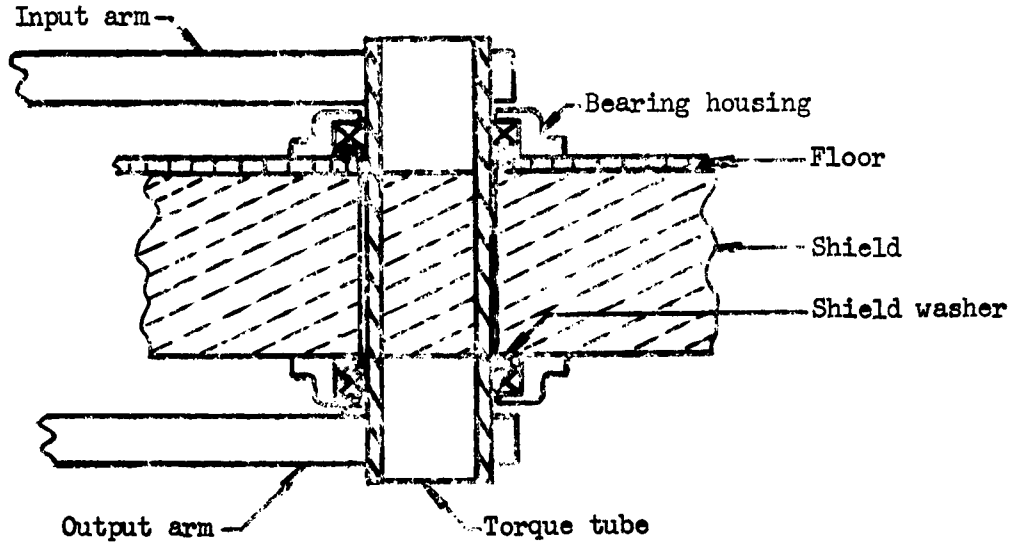

Friction always is an important problem in control subsystems. It increases the pilot effort required, decreases the sensitivity and positional accuracy obtainable, and has a destabilizing effect. Due to the long flight times allowable in nuclear powered aircraft, the pilot effort required for satisfactory control must be a minimum. Hence, adequate lubrication must be provided. To lessen the reliance on lubrication, the features shown in Figure 6 must be employed in the subsystem design.

FIGURE 6.

FRICTION REDUCTION FEATURES

1. Rotary Motion through Seals
2. Elimination of Cable Pulleys
3. Large Bellcranks and Quadrants
4. Straight Control Runs

All of these features employ the principle of increasing the mechanical advantage over the friction forces that cannot be eliminated.

Hydraulic fluid remains the best proven power transmitting media; therefore, the subsystems must be designed to give the required dynamic performance for conditions where the fluid properties vary under irradiation. The primary

effects anticipated are changes in bulk modulus, visocity, lubricity, and sludging. During recent tests on advanced fluids in dynamic subsystem test panels, the changes in these properties have been small, but the test conditions have not been entirely realistic. Therefore, some difficulty must be anticipated. The filters normally in the subsystem are expected to be adequate for removing any sludge that forms. Most of the gas generated in the fluid by radiation will remain entrained under working pressures, and will become separated in the return lines and reservoirs. This gas can be utilized in maintaining reservoir pressurization and be bled off to the atmosphere through pressure relief valves when an excessive quantity has collected.

Hydraulic seals remain one of the most troublesome problem areas because of the almost universal reliance on elastomeric seals, packings, and back-up rings in the past. Only with the recent interest in high temperature applications has development of other types of seals been undertaken on an intensive scale. Various types of metal and mineral seals are being developed for the high temperature application. These seals will be radiation tolerant by nature. It is felt that within the near future, complete subsystems having no elastomeric seals will be developed. This must be the aim for flight control subsystems of nuclear propelled aircraft. In the interim, some elastomeric seals must be used. At present, Buna-N seals are proposed as the best under irradiation.

The problem of electrical insulations fall in generally the same catagory as hydraulic seals. The materials found good for application in very high temperatures are generally inorganic; hence, they are also radiation tolerant. Some of the standard insulation materials are adequate in many regions of the aircraft due to low radiation levels. Therefore, the aircraft can be divided into zones and the types of insulation can vary by the zones in order to minimize the cost.

Since most of the high strength metal alloys, ball and roller bearings, and magnetic core materials contain percentages of the heavier elements, residual activation will be a hazard to the ground support personnel who must service and maintain these subsystems and components. This coupled with the residual activation of the aircraft requires that the component installation designs must allow quick installation and removal. In some cases remote handling techniques must be employed. Since it will not be practical to design all components for assembly and disassembly by remote handling equipment, the supply and overhaul logistics problem is also complicated. Provisions must be made at the using facility for storing repairable components until they cool off enough for manual overhaul, and for repairing these items. The non-repairable components must be disposed of in accordance with AEC requirements. The personnel utilization problem is complicated by the safe dose rate allowable.

The requirements for remote checkout and malfunction detection techniques and equipment are no less than those for the largest missiles.

Provisions must be made for checking the complete flight controls subsystem for function and malfunction from a central point located in the nose of the aircraft since this is the only position inside the shielded hangar. This equipment must be able to isolate a weak or malfunctioned part to the least removable component in order that a minimum of exposure time is required by the ground support personnel for service and maintenance. The problem is further complicated by the necessity for continued reliability of the test sensors. Failure of a sensor will cause at least as much work as an equipment failure.

As has been pointed out, if the development of nuclear propelled aircraft is to be successful, the radiation effects specialist and the controls designer are faced with problems requiring close cooperation and mutual support throughout the design, development, and testing phases of the flight controls subsystem development program. It is hoped that you who are responsible for the radiation effects now have a somewhat better appreciation of the problems and requirements for this particular subsystem.

PNEUMATICS - A TOOL FOR THE DESIGNER OF NUCLEAR POWERED AIRCRAFT

by

J. A. Osterman

Lockheed Aircraft Corporation
Marietta, Georgia

Pneumatics has been demonstrated to have promise in the field of high temperature aircraft system operation. Air has greater resistance to nuclear radiation and is capable of operating over a wider range and higher temperatures than any available hydraulic fluid. This paper gives the essential results of a program of study of a high temperature pneumatic system which offers a promising tool to the nuclear aircraft system designer.

The susceptibility of hydraulic fluids to radiation damage has been one of the most important problems facing the aircraft engineer who is charged with designing control systems for nuclear powered aircraft. It is only natural therefore, that considerable attention has been directed toward the possible use of pneumatics as providing a service fluid undamaged by nuclear radiation.

The same approach has been used to solve the high temperature problem in aircraft system design. The aircraft engineer is faced more and more by higher and higher temperatures which are beyond the operating limits of hydraulic fluids. Here again, pneumatics has been given an appraisal with the view of providing a working fluid compatible with high temperature.

For the past two years, Lockheed Aircraft Corporation, under contract with Wright Air Development Center, has been engaged in the field of high temperature pneumatics. Specifically this effort has been aimed at the design, development and test of a 5000 pound per square inch actuator for 1000°F operation. The purpose of this paper is to present the results of this program which adds a promising tool not only in the field of high temperature but in nuclear engineering design.

The initial effort was embodied in a study program to determine the feasibility of pneumatics and to design an aircraft speed brake servo system to operate in ambient temperatures up to 1000°F. Two basic points of philosophy were germane to the program right from the beginning. Since it was felt that much of the failure in other pneumatic programs arose because the "hardware" consisted of modified hydraulic components, it was decided that we should, in effect, "design for pneumatics". Secondly, with the high operating temperatures particularly in mind, it was decided

to use the best materials, finishes, and surface treatments available. This approach was taken because the number of critical design problems demanded the utmost care in dealing with each one so that all possible "weak links" could be eliminated.

Once the program philosophy had been established, the study began with a comparison of various gases. While the term pneumatics generally implies air in its gaseous state, it was defined here to include all likely gases. The properties and characteristics of thirteen condidates were studied and compared. The list included air, ammonia, argon, carbon dioxide, carbon monoxide, Freon, helium, hydrogen, neon, nitrogen, oxygen, steam, and sulphur dioxide. In addition to the physical properties of gases such as bulk modulus, boiling point, specific heat, and density, various other characteristics were studied and compared. Some of these were toxicity, corrosiveness, chemical stability, effect of nuclear radiation, and availability. As a result of this comparison, no one gas was found to be ideal; however, the greatest favor fell to air and to steam, with air being given first choice and steam appearing to merit study should air prove otherwise unattractive.

Concurrently with the study of gases, a preliminary design was made of an airplane of sufficient scope to support the study and be appropriate to the operational conditions spelled out in the contract with Wright Air Development Center. While details of the airframe configuration and the mission profiles are classified, it may be stated that a high speed aircraft was assumed. This airframe design was necessary in order to logically locate hardware, to determine the thermal history of the air as it passed through the system, and to establish appropriate tubing lengths for purposes of weight study.

Before going on with the history of the study program, it may be well to dwell a moment on one of the characteristics of gases which has been mainly responsible for the poor light in which pneumatics is so often considered. That characteristic is compressibility. The direct measure of compressibility of any fluid is bulk modulus, which is to fluids what modulus of elasticity is to solids. On theoretical grounds, the bulk modulus of a gas is the product of its specific heat ratio and the applied pressure.

If a graph is made of the bulk moduli of several fluids under 2000 and 4000 pounds per square inch pressure at various temperatures, a number of interesting circumstances will be noted. First, at ordinary temperatures a wide disparity exists between the bulk modulus of hydraulic fluid and air Secondly, and more to the point, it will be seen that as temperature goes up, the bulk moduli of the hydraulic fluids go down. In fact, at 1000°F, if these hydraulic fluids were sufficiently stable chemically to operate at that temperature, their bulk moduli would have fallen better than 90 percent and into the region of air at the same temperature.

On the other hand, air over this temperature range has a virtually constant bulk modulus. This then explains why many hydraulic servo systems,

otherwise stable at ordinary temperature levels, may go unstable when the temperature is increased In other words, temperature change can drop the bulk modulus out of the stability limits inherent in a given system design. If the system had been designed for pneumatics and for the appropriate bulk modulus however, no change in system stability would be expected. As will be pointed out later, the speed brake system designed for this program ran as stably at high temperature as it did at room temperature conditions.

Several types of pneumatic systems were studied in relation to the nature of the power source and power actuation components.

Classified by power source, the investigation covered engine-mounted compressors, ground charged reservoirs, and liquefied gas converters. The other pneumatic power sources (using the term in the broad sense) were a regenerative steam system and a solid propellant system. With regard to power actuation components, the pneumatic devices studied were air turbines and air motors as well as piston-cylinder actuators. For purposes of weight comparison, hydraulic and electrical systems were studied, assuming materials to exist which were not actually available.

On the basis of weight alone, the systems which proved the most favorable were the engine-mounted compressor and the regenerative steam system; however, those weights were so close to each other that a strong position in favor of one over the other in this regard was not warranted.

System stability investigations indicated strong likelihood that the system could be made stable. This, together with high temperature material studies, led to the conclusion that pneumatics was feasible for aircraft system operation in 1000°F ambients. To give the greatest margin of stability it was decided that the pressure of the system should go up from the 3000 pounds per square inch of conventional hydraulic systems to 5000 pounds per square inch supply pressure. Since no 5000 pound per square inch compressor was available which could operate at high temperature, a two-pronged attack was necessary.

Therefore, in early 1957, Lockheed proceeded with the Phase II program for the design, development, and test of a 5000 pound per square inch system assuming the successful development of a compressor was forthcoming. The compressor problem was not only one of designing for operation at high temperature in general, but included the problem of precooling, interstage cooling, and aftercooling at altitudes where the heat transfer correlations were scant or conflicting or both. Subsequently a contract for the development of a high temperature 5000 pound per square inch compressor was awarded to the Walter Kidde Company of Belleville, New Jersey.

The pneumatic speed brake system downstream of the compressor consisted generally of two parts. In the so-called accessory compartment are to be found the air reservoirs, filters, relief valves, mechanical moisture separator, chemical drier, pressure regulator, and shut-off valve for the necessary storage and handling of the compressor discharge air prior to speed brake operation. The definition of the system requirement established the maximum ambient temperature in this compartment at 400°F. The actuator

compartment, on the other hand, is where the temperature rises to 1000°F. In this compartment is located the actuator, servo valve, and coiled tubing connecting the two, in addition to rod-end bearings and associated linkage and fittings. Since this is the area of primary interest in this paper, we will continue with a discussion of these components.

As regards materials for 1000°F usages a wide range of materials, surface treatments, surface coatings and hardnesses were considered. Approximately seventy-five combinations were run off in a wear testing machine in an ambient temperature of 1000°F and at bearing loads up to 6150 pounds per square inch.

The materials tested included Inconel-X, Haynes Alloy No. 6B (both wrought and cast), alundum, and carbon graphite compacts. Protective coatings included flame platings of aluminum oxide and tungsten carbide, Electrolizing, electroless nickel, hard chrome plate, nitriding, chrome diffusion, and nickel oxide. Dry film lubricants included Electrofilm No. 1000 and No. 2006, Everlube, Surf-Kote, and Drilube. Where a particular combination showed promise, the test was repeated by inverting the materials of the wear block and running race.

As borne out by these tests and by the subsequent system testing, the so-called flame platings, particularly those of tungsten carbide, have exceptionally good wear characteristics at these temperatures. These platings are very hard coatings applied with high velocity to the surface of the part to be plated. The base material is in effect immersed in the flame resulting from the detonation which imparts the high velocity to the plating material. The resulting physical and chemical bond effects a coating which in the "as used" condition is machined to about .002 of an inch thickness. While the aluminum oxide has a lower coefficient of friction and can stand higher temperatures than the tungsten carbide, it is less dense and more brittle. In the various actuator assemblies tested, failures of the aluminum oxide coating occurred from time to time, whereas the tungsten carbide showed virtually no signs of visible wear or scoring.

Most parts of the actuator are Inconnel-X. The actuator cylinders were of two types. One was Inconnel-X Electrolized on the inside diameter, the other Inconel-X with a Haynes Alloy No. 6B liner. The pistons and piston rods were flame plated with either aluminum oxide or tungsten carbide on a base material of Inconel-X. The cylinder wall, which is approximately four inches on the inside diameter and accomodates an eleven inch piston stroke, has a wall thickness of one-half inch. Actually, from a pressure and structural point of view, the wall is twice as thick as necessary; but to prevent breathing under pressure the cylinder wall is one-half instead of one-quarter of an inch The bearing around the piston rod is Haynes Alloy No. 6.

Piston seals tested have been of two types, the conventional piston rings and a pack of segmented carbon base rings. The rod seals have been of four types, contracting piston rings, a pack of the segmented carbon base rings, stacked chevron packings made of asbestos contained in an

Inconel wire mesh, and the Boeing ring-spring seal. Of all of these, the Boeing ring-spring seal shows the most promise. While it seems to have more friction than the segmented carbon ring, for instance, it is by far the best, having shown virtually no leakage on bench test.

The servo valves tested were of two types, the rotary plate valve and the linear spool valve. The rotary plate valve utilized a plate made of Haynes Alloy No. 25 mounted on a flame plated base. Very high friction was experienced with the plate valve; therefore, the majority of the system testing was accomplished with the spool type.

To minimize the chance of differential expansion both sleeve and spool were made of the same material. With respect to materials, both tool steel and Haynes Alloy No. 25 were used. As it turned out, the bulk of the cycling was accomplished with tool steel valves which became blued with temperature, but showed no excessive corrosion and no evidence of erosion. The Haynes Alloy No. 25 valve, while softer, is basically of a high temperature material, which would be expected to exhibit no corrosion.

Since the servo valve was not mounted on the actuator, the two were connected by coiled tubing. Three-eighth inch Inconel-X tubes were wound into coils of four turns each with a mean diameter of four inches and allowed a relative rotation of twenty-five degrees of the actuator at its fixed pivot. These coils were trouble free throughout the program. Part of this is due to the fact that the tubes underwent virtually no flattening, when coiled, which is directly attributable to the manufacturing process. Before bending the coils the tubes were filled with Cerrobend, the zero coefficient of expansion alloy used for special inspection techniques and other purposes. This technique held flattening of the tubing to less than one percent of the tubing diameter, being on the order of one thousandth of an inch on an outside diameter of three-eighths of an inch.

System testing was accomplished in two phases, stability and endurance. Stability testing was run initially at room temperature. Various stabilizing techniques were employed, such as adding velocity feedback to the mechanical displacement feedback signal. Provisions were also made for varying the gain of the feedback signal. Initally, the system was run under a torsion bar load to simulate the aerodynamic forces. Each torsion bar was four inches square in section and had an effective length of about 43 feet. At full speed brake actuation this represents approximately 60,000 foot-pounds of torque, with an actuator force of 38,000 pounds. Later the load was removed. In all cases the system operation was stable, not only at room temperature, but also at the maximum ambient temperature which was in excess of 1050°F.

The system endurance testing was largely accomplished at elevated temperature. Except for stability testing, system check-out runs, and some cycling at intermediate points, endurance running was accomplished in a 1000°F ambient. In general, the endurance testing verified the results of the wear tests run off early in the program. The tungsten carbide flame plating stood up very well, as did the Haynes Alloy No. 6B and the Electrolized Inconel-X.

It is believed that the aluminum oxide flame plating would have also made a good showing if failure of it had not been aggraveted by a seizure of the rod-end bearing. When this occurred, the aluminum oxide failed locally. Then, by virture of its highly abrasive nature, mating surfaces became heavily scored, causing further failure of the aluminum oxide. On the other hand, a rod-end bearing failure had little effect on the tungsten carbide flame plate.

A case in point to the credit of the tungsten carbide flame plate was demonstrated when a rod packing backup ring shrunk more than the design allowance in operation. The ring was bound so tightly on the piston rod that it could only be removed by cutting it off. As would be expected, the ring was severely scored; however, the flame plate on the rod showed practically no effect.

In conclusion, it may be stated that pneumatic systems can be made to operate stably. Each system must be carefully designed recognizing the limitations which air imposes when used as the service fluid. With some allowance for friction, the way to successful sealing of the piston rod is becoming manifest. Sealing of the piston remains as one of the problem areas, but application of the rod seal technique to the piston may have considerable merit. Until the sealing problem has been ironed out, broad conclusions are yet forthcoming, but it has been demonstrated that pneumatic systems can be made stable.

Materials and surface finishes are available which indicate that operation in ambients as high as 1000°F are possible for aircraft usage. Generally, the metals tested are fairly high on the stategic materials list or often involve processes which border on the exotic. A logical next step, of course, is to go to more commonly used materials. In any event, the program shows high temperature operation to be entirely possible.

In summary, it is felt that this program has not only demonstrated the feasibility of pneumatics but has pointed the way to a successful solution of the radiation problem in aircraft actuation systems.

AIRCRAFT RADOME DESIGN PROBLEMS ASSOCIATED WITH A NUCLEAR ENVIRONMENT

by

Frank W. Thomas

Lockheed Nuclear Products
Lockheed Aircraft Corporation
Georgia Division, Marietta, Georgia

The effects of nuclear radiations in relation to microwave transmission through a dielectric lens, or radome, presents a number of design problems associated with nuclear-powered aircraft. A mathematical prediction technique was used to estimate the effect of radiation on multilayer dielectric flat panels.

The results show how radiation effects data may be interpreted in the design of a radome test panel.

RADOMES IN THE ANP PROGRAM

The advent of nuclear power has introduced many special technical problems into aircraft radome design. Some of these problems concern only effects of radiation on matter; but others concern also additional aircraft environments, such as temperature. The design of radome dielectric lens for a nuclear aircraft is considerably more complex than would be the case with chemically powered aircraft. This paper is concerned with the analysis and the effects of nuclear radiation on radome wall materials and especially with the transmissivity of a radome wall composed of these materials.

Electrical parameters of a radome wall are changed as a result of nuclear radiation. Extensive changes can limit radome performance; therefore the scope of such effects must be established. Simple changes in electrical properties can best be interpreted as total effects on transmission through a particular radome wall, so some means must be employed to interpret radiation induced electrical changes in materials in terms of actual radome wall performance. The primary object of this paper is to show the application of a predictability technique in analyzing typical radome wall flat panel sections that are exposed to radiation. The proper use of the predictability technique can reduce drastically the environmental testing requirements that would otherwise be needed to test full-scale microwave lenses in a nuclear radiation environment.

Following are listed radome properties that are affected by radiation and related aircraft environmental factors:

Temperature coefficient of dielectric constant and loss tangent

Electrical thickness equivalent skin or core

Insertion phase difference

Boresight error

Total transmissivity

Radioactivation of materials

Phase effects of incident and reflected waves

Changes in electrical constants of dielectric arrays

Antenna near field patterns

Far field energy distribution

Dielectric anisotrophy of radome wall materials

Beam shift

Polarization of transmitted waves

Incidence angle of beam

Relaxation effects

Anisotrophy

Reflection coefficient

Insertion phase shift

RADIATION AND RADOME DESIGN

It is first necessary to describe briefly some of the more fundamental aspects of the problem of correlating radiation effects with the design of a dielectric lens. Radomes are conventionally used for gun laying, fire control, bombing, and navigation. They

must meet stringent mechanical and structural specifications, which may also be affected by nuclear radiations. High strength, electrical stability, and physical serviceability over a wide range of temperatures and microwave frequencies are necessary. Furthermore, the shape of a radome must conform to aerodynamic and microwave optical design criteria. For these reasons, a tool for the interpretation of radiation effects is needed in the preliminary design of any nuclear aircraft microwave dielectric lens device.

The effects of the various kinds of nuclear radiation are briefly considered in selecting materials for a radome wall. Numerous tests have been conducted on unirradiated materials, and Wright Air Development Center has conducted an extensive study of effects of gamma radiation on radome materials. However, relatively little work has been done on pertinent electrical parameters of radome material during and after neutron irradiation. Wave guide, or cavity, measurements made on materials being irradiated in a nuclear environment at microwave frequencies are not fully adequate to assess actual radome wall performance.

Tests made before and after irradiation do not show the transient effects on transmission that may occur in a radome wall. Little, therefore, has been determined on what happens during nuclear irradiation of an entire radome module. Actually, transient effects may be of particular importance, since irradiation and transmission must take place simultaneously.

RADOME RADIATION ENVIRONMENT

Various processes for the interaction of particle and electromagnetic radiation in radome wall materials are covered only briefly in this paper.

Interactions produce two main effects: absorption of the photon and scattering or reflection from either the atomic nucleus or atomic electron cloud. Of the atoms within the dielectric, at least a dozen combinations of interactions and effects are possible; but for dielectric lens design purposes only the following need be considered:

Compton Effect: The electrical properties of a radome dielectric are changed by the Compton process. This is caused by ionization resulting from Compton scatter electrons and their interaction with other atoms.

Photoelectric Effect: The photoelectric and Compton processes are competitive, the latter is perhaps the more important in its effect on dielectrics for the lower photon energy ranges encountered.

Pair Production: The effect of the pair production process is to augment the Compton process damage in radome dielectric materials, since the 0.51-mev photons from positron annihilation are largely absorbed in radome materials. The pair process is not likely to affect radome materials unless photon energies are adequate.

Neutron Radiation: Many radome materials contain hydrogen and nitrogen. A reaction with hydrogen produces a gamma photon. Reaction with nitrogen can yield a proton and carbon-14. Neutron alpha reactions cause short but intense ionization tracks in the dielectric. Scattering of fast neutrons can produce nucleus and proton recoil.

RADIATION ON RADOME MATERIALS

Greatest concern in the selection of materials suitable for radome walls is with the photoelectric, Compton, and neutron interactions.

Organic radome materials such as resin fiberglas laminate skins; foam plastic cores; and resin fabric or fiberglas honeycombs composed of carbon, hydrogen, oxygen, and nitrogen may be particularly affected.

Recoil protons derived from fast neutron collisions in organic materials lose their energies by interaction with orbital electrons, resulting in ionized atoms or molecular fragments. This can effect dielectric changes and result in molecular fragment recombinations, yielding new molecular species with resultant change in electrical properties of the radome materials.

Final degradation of thermal energy of a neutron and its resultant capture by a hydrogen atom will produce a gamma ray of 2.11 mev, thus increasing the original gamma ray flux reactions. The use of lithium, boron, or excessive nitrogen in radome materials may be undesirable because of thermal neutron capture and resultant intense ionization caused by the secondary radiations. Elements that yield high energy beta radiation may also be undesirable in radome design. Complex dielectric properties may be especially sensitive to flux rate.

DATA ANALYSIS BY MEANS OF THE PREDICTABILITY TECHNIQUE

Transient and post-irradiation test data on basic radome materials alone do not show the ultimate effect of nuclear radiation on radome performance. The net effect of changes in loss tangent and dielectric constant must be stated in terms of power transmission for a specific wavelength through a specific wall. Such a wall may be symmetrical or unsymmetrical and composed of a mono layer or multi-dielectric layers. Three-layer unsymmetrical walls were selected as possible examples for analysis of radiation effects.

The complex parameter changes resulting from radiation were related and presented in final form as power transmission through the dielectric lens.

For the analysis of typical radome wall flat panel sections, the use of a predictability computer program, developed by William Schroder, Lockheed Aircraft Corporation,

California Division , is employed.

An IBM 704 computer, which prints transmission coefficients in tabular form, can be readily programmed to accept as input data the loss tangent, dielectric constant of each sheet, and thickness and number of dielectric layers.

Output data will then be the power transmission coefficient as a function of the indicent angle and polarization of the beam. Details of the actual IBM routine and the equations used to establish the IBM program employ Maxwell's relations and related expressions for energy absorption, reflectance, and transmission in terms of complex electrical parameters. Manual computation is not practical because of the time required. Theoretical estimates of the results of nuclear radiation on radome dielectric sandwich panels were made by the use of this program. Changes of +10% and -10% in dielectric constant and loss tangent of the skin and core of the panel were considered equivalent to those induced by radiation, and power transmission was calculated for three unsymmetrical radome flat well panels.

The theoretical analysis of three typical panels is presented in Figures 1 through 8. Each flat panel consists of a core and two skins or faces. The electrical and physical properties of the core and each skin are defined in these figures.

Figures 1, 2, and 3 show that power transmission for the test panels is changed about plus or minus 3% when a change of initial parameters is $\pm$ 10%. This may not be too significant for systems where normal efficiencies are high, but it could be critical for those with marginal design level as regards range and sensitivity and energy reflection.

Figures 4, 5, and 6 show that transmission is less affected by induced changes for parallel polarization.

Figures 3 and 6 show that a tapered panel optimized as to core thickness and incidence angle provides increased transmissivity and that changes that might result from radiation would be less significant.

Figures 7 and 8 show that polarization influences transmission more at high incidence angles.

Although emphasis was placed on assumed changes in electrical properties and the span of these changes was arbitrarily chosen, the predictions indicate the ultimate results of radiation on a dielectric lens assembly when actual changes are used instead of simulated ones.

Advanced mathematical routines for the IBM 704 are being devised to analyze radomes of complex shape or contour. Such programs will permit rapid analysis of proposed radome designs, allowing faster correlation of aerodynamic, structural, nuclear, and microwave design requirements.

Ultimate prediction capability of the program for any shape radome as a function of radiation would include the following:

Beam shift

Phase front shift

Transmission

Bore sight error

Far field pattern

CONCLUSIONS

1. Radome parametric studies involve such a number of variables that direct measurement of all parameters simultaneously in a nuclear environment for an actual radome is difficult.

2. Mathematical routines using known perturbation of dielectric wall properties as a function of nuclear radiation integrated dose can predict radome performance.

3. Estimates using these techniques indicate that the overall effect of radiation may not be too great on actual radome performance for a $\pm$ 10% variation of electrical properties within the limits of the design cases studied.

4. Correlation of radiation effects in dielectric materials with actual performance in a dielectric lens can best be made using a computer program.

5. Correlation of dose and change in transmission to any design panel can be performed.

BIBLIOGRAPHY

1. The Atomic Nucleus, R. D. Evans, Ph. D., McGraw Hill Book Co., 1955

2. "Radiation Damage to Non-Metallic Materials," V. P. Calkins, APEX 167 August 1954

3. "Measurement of the Complex Dielectric Constant of Very High Dielectric Constant Materials at Microwave Frequencies," Signal Corps Eng. Lab., N. J. Memo #M-1569, April 1954.

4. "Radome-Antenna Beam Pattern Efficiency and Beam Shift: IBM 704 Computer Program," William Schroder, Lockheed Aircraft Corporation, California Engr. Report #LR-12356, June, 1957.

5. "Microwave Electrical Characteristics of Radome Materials at 8.5 KMC per Second During Exposure to Gamma Radiation," B. Noe, WADC TN 56-87

6. "Nuclear Radiation of Plastic Radome Materials," R. C. Tomashot, D. G. Harvey WADC TR 56-296

7. "Effects of Radiation of Dielectric Materials," NRL, Washington, D. C., December 14, 1954

8. "Lockheed Aircraft Corporation Math Analysis Memo N. 031," Supplement 3, William Schroder, 1956

9. Communication, J. M. Googe to F. W. Thomas

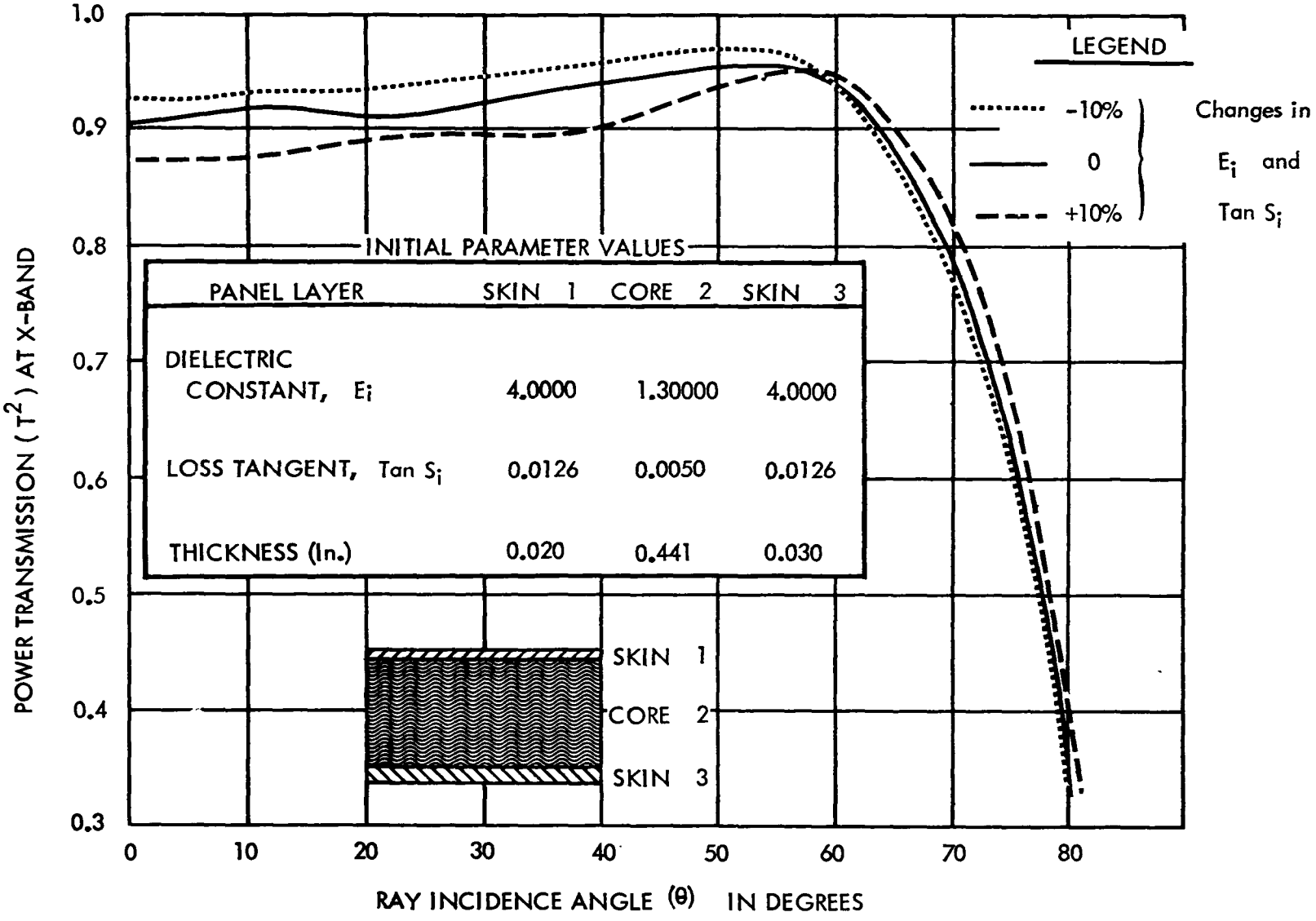

FIG. 1 - CONVENTIONAL UNSYMMETRICAL WALL ELECTRIC PARAMETERS
(PERPENDICULAR POLARIZATION)

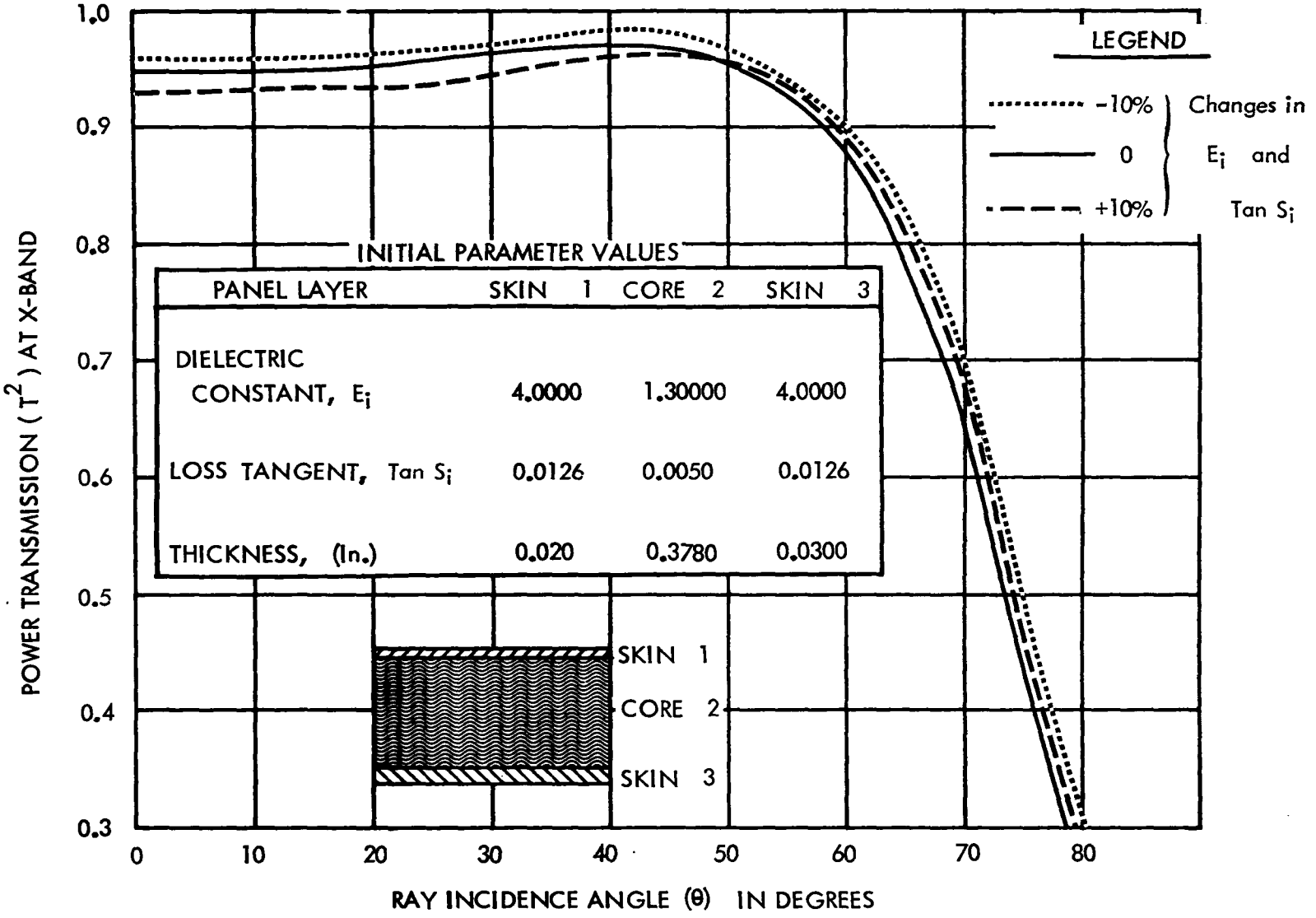

FIG. 2 - CONVENTIONAL UNSYMMETRICAL WALL CORE OPTIMIZED FOR MAXIMUM LOW INCIDENCE ANGLE TRANSMISSION (PERPENDICULAR POLARIZATION)

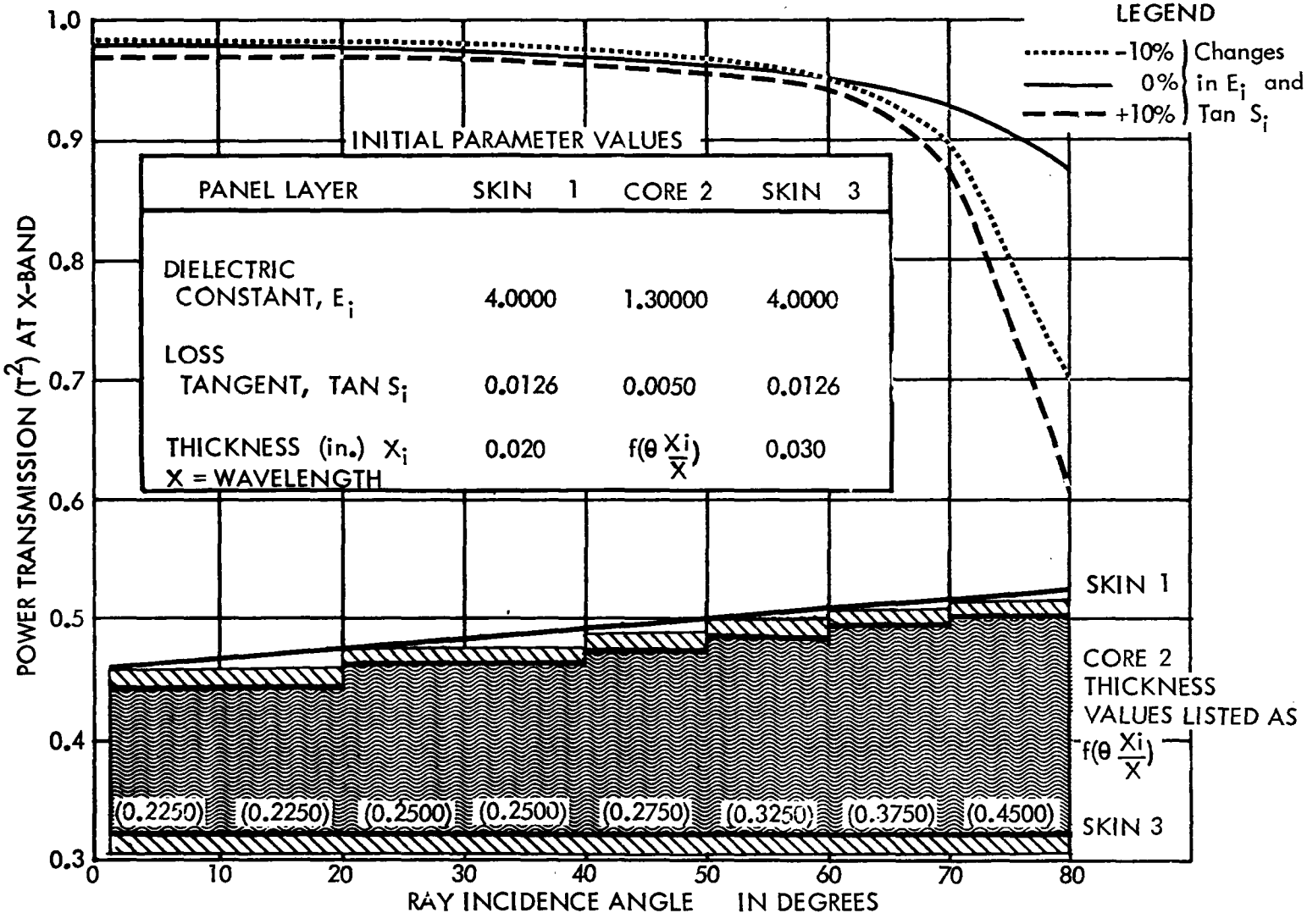

FIG. 3 - UNSYMMETRICAL TAPERED PANEL WALL OPTIMIZED FOR EACH INCIDENCE ANGLE (PERPENDICULAR POLARIZATION)

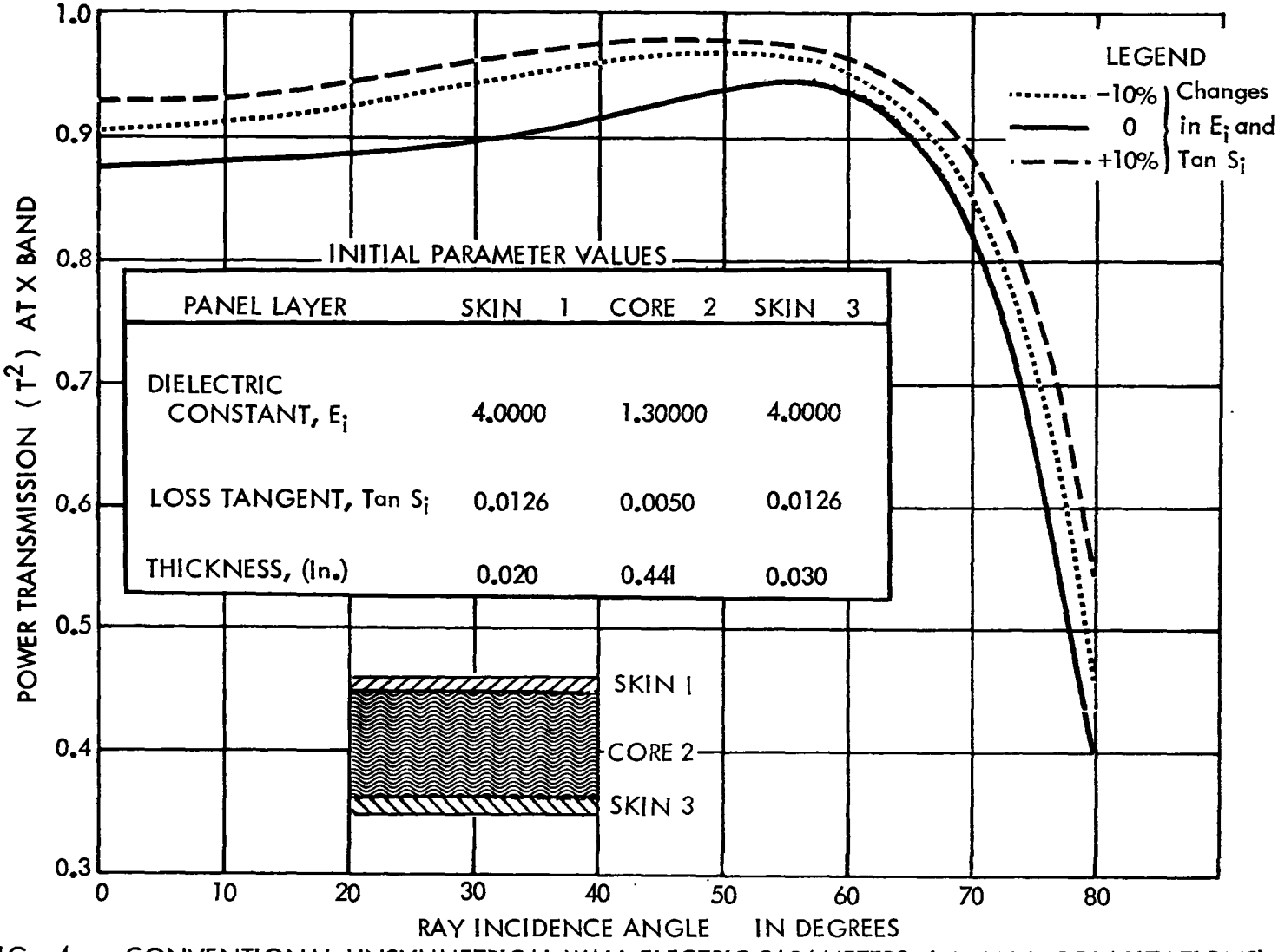

FIG. 4 - CONVENTIONAL UNSYMMETRICAL WALL ELECTRIC PARAMETERS (PARALLEL POLARIZATIONS)

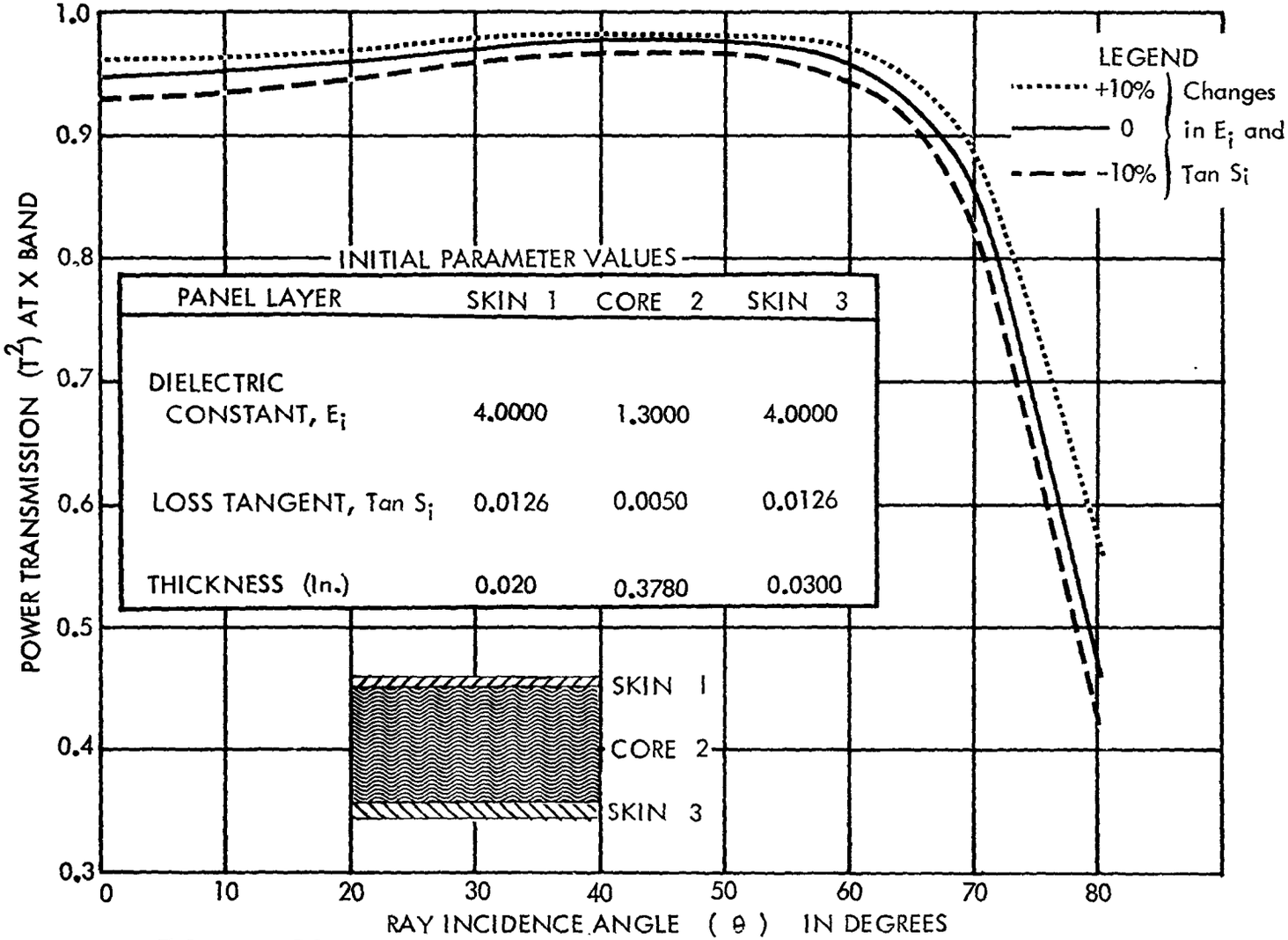

FIG. 5 CONVENTIONAL UNSYMMETRICAL WALL CORE OPTIMIZED FOR MAXIMUM LOW INCIDENCE ANGLE TRANSMISSION (PARALLEL POLARIZATION)

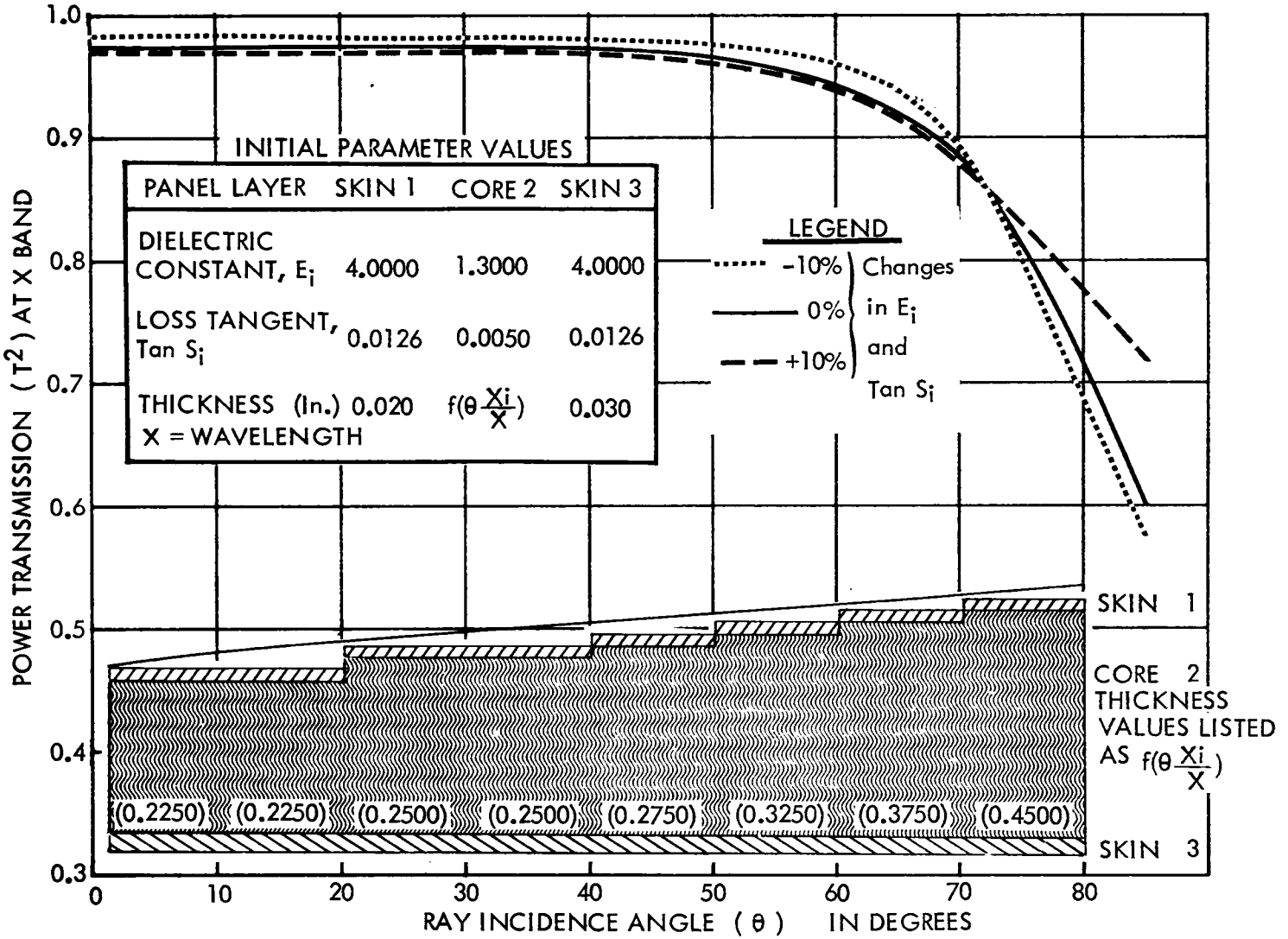

FIG. 6 UNSYMMETRICAL TAPERED PANEL WALL OPTIMIZED FOR EACH INCIDENCE ANGLE (PARALLEL POLARIZATION)

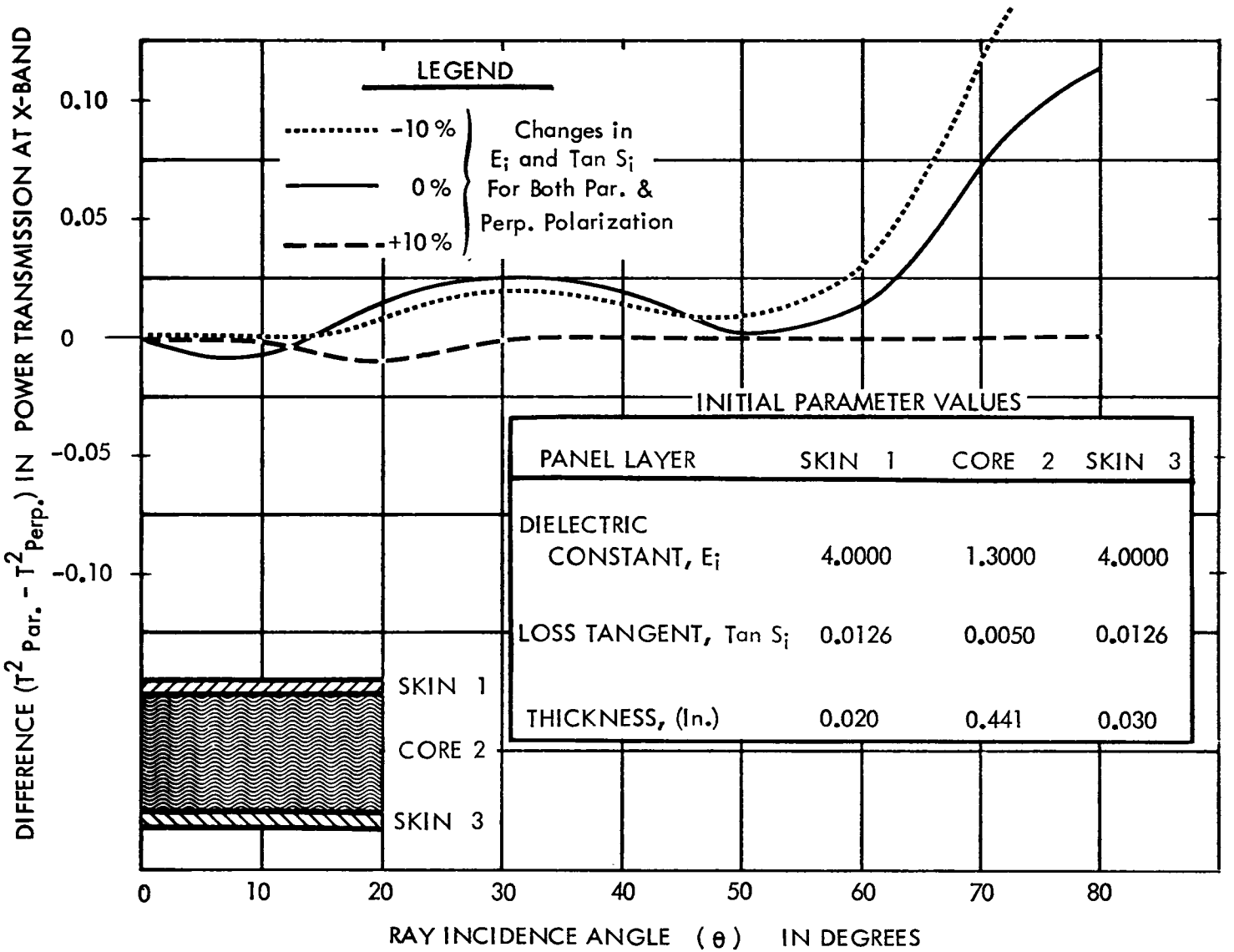

FIG. 7 CONVENTIONAL UNSYMMETRICAL WALL ELECTRIC PARAMETERS (PERPENDICULAR & PARALLEL POLARIZATION)

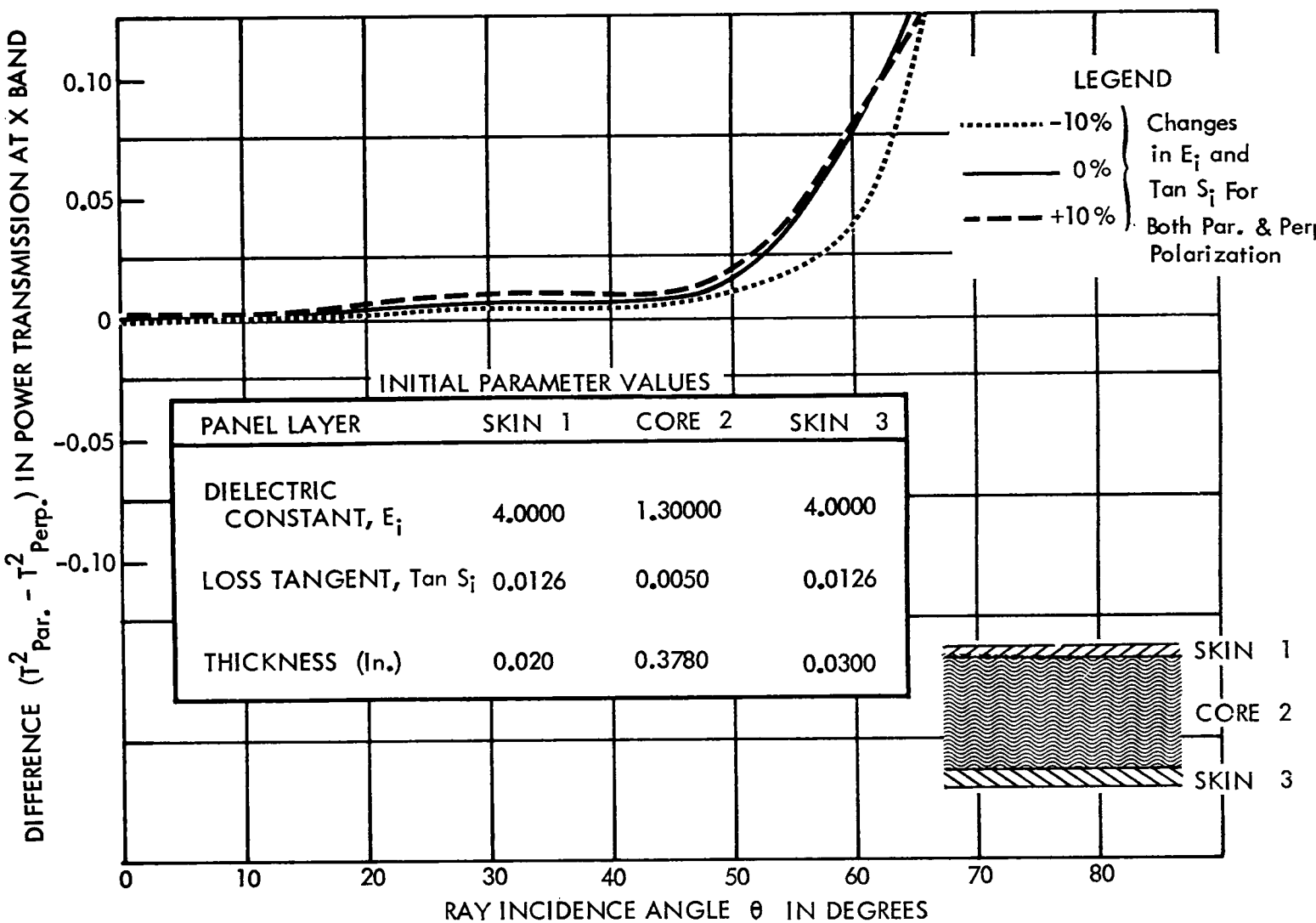

FIG. 8 - CONVENTIONAL UNSYMMETRICAL WALL CORE OPTIMIZED FOR MAXIMUM LOW INCIDENCE ANGLE TRANSMISSION (PERPENDICULAR & PARALLEL POLARIZATION)

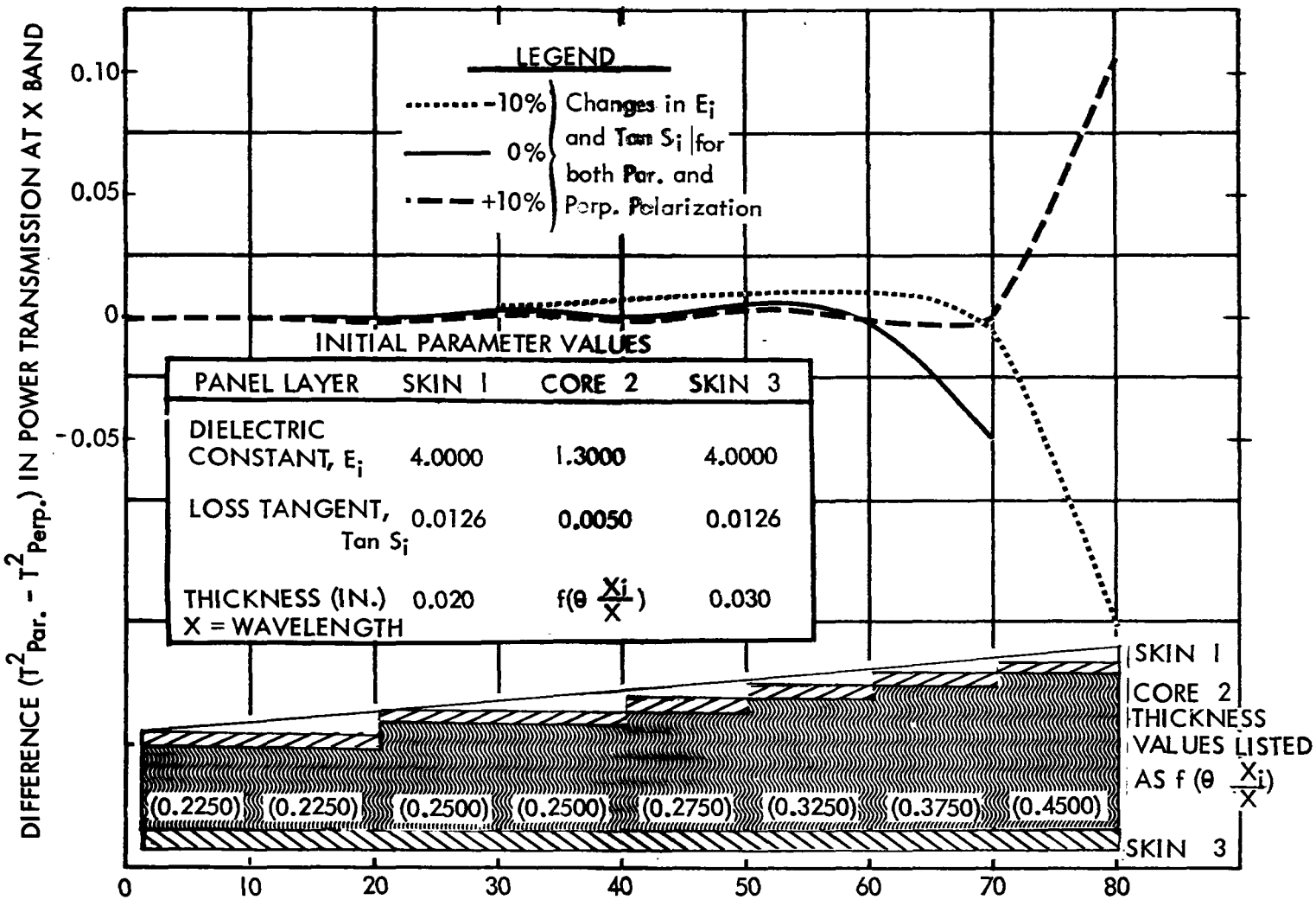

FIG. 9 - UNSYMMETRICAL TAPERED PANEL WALL OPTIMIZED FOR EACH INCIDENCE ANGLE (PERPENDICULAR AND PARALLEL POLARIZATION)

EFFECTS OF HIGH ALTITUDE NUCLEAR DETONATIONS ON PROPAGATION OF ELECTROMAGNETIC WAVES

by

SAMUEL HOROWITZ and LT. RICHARD SUGARMAN
U. S. Air Force Cambridge Research Center
Bedford, Massachusetts

This paper is classified and is bound in Volume Six.

THE EFFECTS OF GAMMA RAY AND REACTOR IRRADIATIONS ON THE SENSITIVITY OF EXPLOSIVES

by

PAUL W. LEVY
Brookhaven National Laboratory
Upton, Long Island, New York

and

J. V. R. KAUFMAN and JAMES E. ABEL
Explosives Research Section, Picatinny Arsenal
Dover, New Jersey

This paper is classified and is bound in Volume Six.

ON THE ENERGY LEVELS IN NEUTRON-IRRADIATED P-TYPE SILICON

by
C. A. Klein and W. D. Straub
Research Division, Raytheon Manufacturing Company
Waltham, Massachusetts

High resistivity p-type silicon samples were irradiated in the Brookhaven pile for short periods of time resulting in integrated fast neutron fluxes of the order of a few 10^{14} n/cm.^{2} Hall coefficient and conductivity measurements were then performed over extended temperature ranges. A detailed analytical investigation of these data provides evidence for at least two bombardment-induced hole trap levels in the lower half of the energy gap. The deep trap, at 0.29 ev from the valence band, is introduced at a rate which appears to be proportional to the integrated flux. Moreover, it has been established that for this level the product of the statistical weight factor by the temperature shift factor, as defined below, is practically equal to one. The shallow trap, at 0.16 ev from the valence band, is not yet as fully describable. The work is still in progress, and only the established results at the time of this writing (August 1958) are given here. The whole approach is of a "phenomenological" nature, in the sense that no attempts were made to correlate the presently available data with possible types of defects or defect models.

I. INTRODUCTION

The electrical and optical properties of semiconducting materials are known to be extremely sensitive to any high-energy nuclear radiation. It has been recognized that this sensitivity is primarily due to the introduction of new energy states in the forbidden band, as a result of the disorder induced in the lattice structure during the bombardment. Considerable effort has been spent on the determination of the position and characteristics of the "defect states" produced in germanium by a wide variety of energetic particles[1,2,3]. Much less extensive work has been done on the radiation effects in high-purity silicon, mainly because single-crystal specimens have only recently become generally available, and also because it was felt that the position of the defect states in the forbidden band of silicon is such that it is more difficult to locate them[4].

The present paper is concerned with the nature of defect states introduced in the lower half of the energy gap of silicon by pile-neutron irradiation. The samples studied were cut from a high-resistivity undoped single crystal (K-121) and of the standard "bridge" form. Hall coefficient measurements performed before irradiation showed that they were all p-type with a net impurity concentration of about 2×10^{14} cm^{-3} with boron as majority impurity. These samples were packed in dry ice and irradiated in the BNL graphite reactor for short periods of time (a few minutes or less), using one of the pneumatic tube facilities[a]. Hall coefficient and conductivity have then been measured as a function of temperature after room-temperature storage periods extending from several days to more than a year. The observed

---

[a] The exposure times were determined by L. Davis, Jr. of Raytheon's Research Division, on the basis of results obtained at the Oak Ridge National Laboratory indicating that under similar conditions the number of defects per fast incident neutron is approximately 1.6 in germanium, and chosen so that the concentration of bombardment-induced defects should be comparable to the net chemical impurity density.

effects, therefore, should be practically identical with those produced by a fast-neutron bombardment at or near room temperature.

The purpose of this paper is to present information on the defect states in irradiated silicon. This information could be gained by a detailed quantitative analysis of some of our data. It was not attempted to correlate our results with existing ideas or models concerning the properties of the energy states associated with Frenkel defects or any defect expected to result from irradiation. Theoretical fits of the charge carrier concentration in bombarded samples, from about 100°K up to 450°K, based on well-established laws and obvious assumptions, permitted us to locate and partly describe two of the defect states in the lower half of the energy gap of neutron-bombarded p-type silicon.

II. EXPERIMENTAL RESULTS

For two of the irradiated samples (6a and 8b), the charge carrier concentration as a function of the reciprocal temperature is given in Fig. 1. The same figure also exhibits typical carrier concentration data for an unbombarded sample cut from crystal K-121. These concentrations were obtained from the Hall coefficient measurements and the ratio of Hall mobility to drift mobility according to the formula[5]

$$p = \frac{1}{Re} \cdot \frac{\mu_H}{\mu_d} \quad . \tag{1}$$

The value of the mobility ratio at a given temperature above 100°K was estimated on the basis of the results of Morin and Maita for high-purity p-type silicon[6,b]. It can be seen from the carrier concentration data of

---

[b]Recent experiments by Long seem to indicate that the linear negative temperature dependence of Hall to conductivity mobility and the result that μ_H/μ_d is less than unity at 300°K are truly intrinsic properties of p-type silicon, which may be due to the warping of the constant-energy surfaces.[7]

the unbombarded sample that such a mobility ratio correction leads to the expected absence of any temperature dependence in the hole density above 150°K, where all the chemical impurities are ionized. On the other hand, the ratio is believed to change very little with bombardment, as long as impurity scattering is not too important[8,9]. It was felt, therefore, that above 100 or 150°K, the hole concentration in bombarded samples should be as given by Eq. (1) with the pre-bombardment mobility ratio values. The marked temperature dependence of the charge carrier concentration in irradiated samples, especially the very large removal observed at low temperatures, implies the existence of bombardment-induced hole trapping centers which manifest themselves by a rapid "freezing out" of free carriers, as the temperature is lowered. A quantitative analysis of this trapping process was the main object of our investigation, and will be presented in part III of this report.

As mentioned in the introduction, the irradiations were performed in a pneumatic tube facility (PN-6) of the Brookhaven reactor. Sample 6a was bombarded for two minutes in May 1957, and the "damaging dosage" was estimated of the order of 1.2×10^{14} n/cm^2. In view of the difficulties in determining the effective dose and the general confusion which exists in this matter, it might be of interest to report how this number was obtained. According to Primak, the fast-neutron damage produced in a nuclear reactor has to be related to the uppermost two decades of energy below the energy at which the pile neutron spectrum begins to fall greatly from a "resonance" distribution[10]. The damaging dosage $(nvt)_d$ is therefore defined as the time integral of the resonance flux over a two-decade range of energies at the upper end of the abundant part of the pile neutron spectrum. Assuming a cadmium-ratio of 33,[c] the resonance flux in any energy decade is known to be just one seventh of the thermal neutron flux[11]. In May 1957, the thermal flux in PN-6 was given as 3.5×10^{12} cm^{-2} sec^{-1}. The resonance flux in this facility

---

[c] This value was generally quoted for the BNL-reactor lattice before the recent fuel element conversion[11].

was then 5×10^{11} $cm^{-2} sec^{-1}$ per energy decade, so that a two-minute exposure probably resulted in a damaging dosage of about 1.2×10^{14} n/cm^2. Sample 8b was irradiated in November 1957 under similar conditions, but for four minutes. At that time the fuel element conversion process was already started, and accurate neutron-flux data were not available. Nevertheless, the Brookhaven staff felt that the resonance flux in PN-6 should not have significantly changed, so that the damaging dosage received by sample 8b was tentatively assumed to be twice the damaging dosage of sample 6a, i.e., 2.4×10^{14} n/cm^2.

In connection with sample 8b, it will be noted (Fig. 1) that two temperature runs were performed, the first in December 1957, about a month after irradiation, and the second in April 1958. At first glance it might appear that the post-bombardment carrier concentration was practically not affected by five months of room-temperature aging, and this seems to confirm the exceptional stability of radiation-induced defects in silicon already noticed in electron-bombarded specimens[12]. Closer examination, however, reveals that at low temperatures the hole concentration slightly recovered, possibly as a result of an energy level shift in the bombardment-induced traps. This point will be examined in detail later on.

Attempts to fit the charge carrier concentration data made it clear that a reliable analysis had to be based on a thorough understanding of the Fermi-level behavior in the studied specimens, before and after irradiation. This behavior is illustrated in Fig. 2, which gives the Fermi-energy as a function of temperature for the three investigated samples. The Fermi-energies were computed from the carrier concentration data using the standard expression for the hole density

in a non-degenerate semiconductor [5],

$$p = 2\left(\frac{2\pi m_p kT}{h^2}\right)^{3/2} \exp\left(\frac{E_v - E_f}{kT}\right) \quad , \tag{2}$$

where $E_v - E_f$ is the energy interval between the Fermi-level and the edge of the valence band, and m_p the density-of-states mass for the valence band. This density-of-states mass is given by the following relationship:

$$(m_p)^{3/2} = (m_{pL})^{3/2} + (m_{pH})^{3/2} \quad , \tag{3}$$

where the subscript L refers to the light holes and the subscript H to the heavy holes[13]. With $m_{pL} = 0.14\, m_o$ and $m_{pH} = 0.53\, m_o$, as calculated for silicon by Lax and Mavroides from cyclotron resonance data at 4.2°K, one obtains

$$\left(\frac{2\pi m_p kT}{h^2}\right)^{3/2} = 5.50 \times 10^{18} \left(\frac{T}{300}\right)^{3/2} \text{cm}^{-3} \quad , \tag{4}$$

an approximation we use throughout this paper. The resulting Fermi-energies, if plotted versus temperature on a linear scale, as in Fig. 2, strongly indicate that the main effect of radiation damage in silicon is the introduction of new energy levels in the forbidden gap. These new energy levels manifest themselves either by anchoring the Fermi-level high above the valence band, as in sample 8b, or by an appreciable slowing down of the level's movement, as in sample 6a.

II. THEORETICAL ANALYSIS

A. SAMPLE 8 B

The carefully measured carrier concentrations in sample 8b, as yielded by the second temperature run (Fig. 3), were the first to be submitted to an analytical treatment. More specifically, it was attempted

to interpret these data in terms of a single discrete bombardment-induced hole trap level possibly affected by a temperature dependence. According to this assumption, and in the investigated temperature range (150-400°K), the charge carrier concentration should be given by

$$p = N_c - N_{t\bullet}(T) \quad , \tag{5}$$

where N_c is the net chemical impurity density ($N_c = N_a - N_d = 2.02 \times 10^{14}$ cm^{-3}, as indicated by pre-irradiation measurements), and $N_{t\bullet}$ the density of the filled hole traps. The law of mass action shows that

$$N_{t\bullet}(T) = \frac{N_t}{1 + K(T)/p} \quad , \tag{6}$$

where N_t is the total trap concentration, and K(T) the equilibrium constant for this trapping process. If the free carriers are non-degenerate, one can write

$$K(T) = \frac{Q_p Q_{t\circ}}{Q_{t\bullet}} \quad , \tag{7}$$

the Q's representing the respective partition functions of free holes, empty and filled traps. Therefore,

$$K(T) = \frac{2\Omega_{t\bullet}}{\Omega_{t\bullet}} \left(\frac{2\pi m_p kT}{h^2}\right)^{3/2} \exp\left(-\frac{E_t}{kT}\right) \quad , \tag{8}$$

if $\Omega_{t\circ}/\Omega_{t\bullet}$ is the ratio of the statistical weight of the empty trap to that of the full one, and E_t the energy level of the trap measured from the top of the valence band. It is usual to assume a linear temperature variation for such an energy level:

$$E_t(T) = E_t(O) + \alpha T \quad . \tag{9}$$

If this is correct in the case of a bombardment-induced level, we find that the equilibrium constant can be written as

$$K(T) = \Gamma\ C(T) \exp\left(-\frac{E_t}{kT}\right) \quad , \tag{10}$$

where Γ is the product of the statistical weight factor $\gamma = 2\Omega_{t\circ}/\Omega_{t\bullet}$ by the temperature-shift factor $\tau = \exp(\alpha/k)$ of the level, a level whose zero-temperature position is at an energy E_t from the valence band. $C(T) = 5.50 \times 10^{18} (T/300)^{3/2}$ cm^{-3} as previously calculated for holes in silicon (Eq. 4).

After bombardment, and at temperatures below 250°K, the charge carrier concentration in sample 8b is seen (Fig. 3) to be exceedingly small, if compared to the initial concentraion N_c. We may, therefore, write

$$N_{t\bullet} = \frac{N_t}{1 + K(T)/p} = N_c \tag{11}$$

for $1000/T > 4.5$, or

$$p = \frac{N_c}{N_t - N_c}\ K(T) \quad . \tag{12}$$

Substitution of Eq. (10) in Eq. (12) yields

$$p(T/300)^{-3/2} = \frac{5.50 \times 10^{18}}{\eta} \exp\left(-\frac{E_t}{kT}\right) \text{ cm}^{-3} \, , \tag{13}$$

where

$$\eta = \frac{N_t/N_c - 1}{\Gamma} \tag{14}$$

is a dimensionless quantity critically dependent on the ratio of the radiation-induced trap density to that of the net chemical impurities.

The experimental values of $\log [p(T/300)^{3/2}]$ at low temperatures are plotted versus the reciprocal temperature in Fig. 3; they exhibit a characteristic slope corresponding to an activation energy of 0.287 ev. On the basis of Eq. (13), this activation energy may be considered as the zero-temperature energy level of a bombardment-induced hole trap in our p-type silicon sample 8b at the time the measurements were performed (about six months after irradiation). The associated value of the parameter η is then determined as equal to 0.350 ± 0.005.

A single level approach has to be substantiated by proving that, with the parameters obtained from the low-temperature slope, the model provides correct carrier concentrations in the higher temperature range. According to Eqs. (5) and (6), the hole density in an irradiated sample is given by

$$p = N_c - \frac{N_t}{1 + K(T)/p} \quad , \tag{15}$$

a quadratic equation in p, the solution of which is

$$p = -\frac{1}{2}[K(T) + N_t - N_c] + \sqrt{\frac{1}{4}[K(T) + N_t - N_c]^2 + N_c K(T)} \tag{16a}$$

or

$$p = -\frac{1}{2}[K(T) + \Gamma \eta N_c] + \sqrt{\frac{1}{4}[K(T) + \Gamma \eta N_c]^2 + N_c K(T)} \tag{16b}$$

if we introduce the parameter η. Let us define the function $K(T)$ as follows

$$K(T) = \frac{1}{N_c} C(T) \exp\left(-\frac{E_t}{kT}\right) \quad . \tag{17}$$

Then p is given by

$$p = \frac{N_c \Gamma}{2} \left\{ - \left[K(T) + \eta \right] + \sqrt{\left[K(T) + \eta \right]^2 + \frac{4K(T)}{\Gamma}} \right\} , \tag{18}$$

and this expression may be used to test the single-level model at high temperatures, since the only adjustable parameter is Γ. Results of some of the computations are illustrated in Fig. 3. They strongly suggest that our 8b data (run 2) are correctly described by a single discrete hole trapping level at 0.287 ev above the valence band. Moreover, this bombardment-induced level is characterized by a Γ practically equal to one; in other words, the trap is such that

$$\gamma \cdot \exp\left(\frac{a}{k}\right) \simeq 1 , \tag{19}$$

where γ refers to the spin situation of its quantum state and exp (a/k) to the temperature dependence of its energy level.

As recently emphasized by Wertheim in connection with electron-bombardment damage studies, carrier concentration measurements can only serve to determine the combined effect of the statistical weight ratio and the energy-level shift[9]. This is strikingly demonstrated by the present analysis, but the knowledge of Γ allows an accurate evaluation of N_t, the total density of those defect centers leading to localized states at an energy E_t above the valence band. This solves one of the main problems the present investigation was considering. $\Gamma = 1$ means $N_t = 1.35 N_c$ on the basis of Eq. (14), if $\eta = 0.35$. In other words, this means that the four-minute exposure of sample 8b ($N_c = 2.02 \times 10^{14}$ cm^{-3}) in the BNL reactor has resulted in the introduction of 2.73×10^{14} defect centers per cm^3, which all act as hole traps with the same zero-temperature

depth of 0.287 ev[d].

The carrier concentrations measured in sample 8b about one month after irradiation are shown in Fig. 4. The previous treatment again yields an excellent fit, if Γ is taken as equal to one. It should, nevertheless, be noted that the low-temperature data now points towards an activation energy of 0.291 ev instead of 0.287 ev, with $\eta = 0.30 \pm 0.01$. The implications of this result are not clear at the present time, since the observed discrepancies may possibly be due to a small systematic error during one of the runs. Yet the overall quality of the data leads us to believe that either the first temperature run (though limited to 350°K) or the room-temperature aging process actually resulted in a small increase in the density of the detected traps coupled with an apparent decrease in the trap depth. Similar phenomena, but much more pronounced, have been reported by Cleland et al. for neutron-bombarded germanium[2,3].

At this point it might be of interest to consider the behavior of the Fermi-level in sample 8b, as exhibited in Fig. 5. The Fermi-energies determined from the two sets of carrier concentration data, if plotted versus the reciprocal temperature, seem to indicate that, after crossing the expected trap level at about 0.29 ev from the valence band, the Fermi-level moves up again with decreasing temperature. It will be shown that this remarkable behavior can be very well explained on the basis of a single-level model with the previously determined characteristics.

By taking Eqs. (2) and (10) into account, Eq. (15) becomes

$$2\,C(T)\,\exp\left(-\frac{E_f}{kT}\right) = N_c - \frac{N_t}{1 + \frac{\Gamma}{2}\,\exp\left(\frac{E_f - E_t}{kT}\right)}, \qquad (20)$$

where E_f is the Fermi-energy and E_t the zero-temperature level of the

---

[d] Evidently, this statement does not imply that the totality of the radiation-induced defect states are located on this unique level. It only refers to that part of the forbidden gap that could be reasonably explored by the carrier concentration analysis.

hole trap, both measured from the valence band edge. Eq. (20) yields a quadratic equation in exp (E_f/kT), the solution of which provides the following expression for the Fermi-energy as a function of temperature:

$$E_f = E_t + kT \ln \{ K(T) + \eta + \sqrt{[K(T) + \eta]^2 + \frac{4K(T)}{\Gamma}} \}, \quad (21)$$

if $K(T)$ and η are defined according to Eqs. (14) and (17). At low temperatures the function $K(T)$ becomes exceedingly small. The behavior of the Fermi-energy is, therefore, essentially fixed by the value of the parameter η. It is then easy to realize that a rise of the Fermi-level by lowering the temperature can only be brought about, if $0 < \eta < 0.5$. (or $\ln(2\eta) < 0$). Curves obtained with $\eta = 0.2$, 0.3, and 0.4, assuming $\Gamma = 1$, are drawn in Fig. 5. For each of these, the trap depth was chosen in such a manner as to fit the Fermi-energy at 300°K ($E_f = 0.308$ ev), in order to get a kind of "normalization" making a selection of the correct parameter possible. Clearly, an acceptable overall fit is provided by $\eta \sim 0.3$, a value which corresponds to an energy level at 0.289 ev above the valence band. This appears to be in excellent agreement with the results we gained from the straightforward analysis of the carrier concentration data, taking into consideration the fact that the Fermi-level analysis was performed simultaneously on both sets of data. It should also be mentioned that fitting attempts with $\Gamma \neq 1$ were unsuccessful, and in this respect the Fermi-level analysis reveals itself as an especially sensitive technique.

B. SAMPLE 6A

The two-minute exposure of sample 6a resulted in an estimated damaging dosage of 1.2×10^{14} n/cm^2, or half the dosage given to sample 8b. We may, therefore, expect to find in sample 8b about half as many defect states per unit volume, especially half as many hole traps of the type detected in 8b. More specifically, if we assume that

the density of each bombardment-induced defect goes linearly with the integrated flux, we expect the irradiation of sample 6a to result in the introduction of about 1.4×10^{14} cm^{-3} of those defect centers, which the foregoing analysis has shown to give rise to a hole trapping process characterized by a zero-temperature energy level at 0.29 ev from the valence band and a Γ -factor of one. Before exposure, the net impurity content N_c of sample 6a was found equal to 1.88×10^{14} cm^{-3}. Hence we expect a parameter η of about -0.25, and on the basis of Eq. (21) the Fermi level should cross the trap level and move monotonically towards the valence band, as the temperature is lowered. This is precisely the kind of behavior exhibited by sample 6a in Fig. 2.

The successful Fermi-level analysis of sample 8b (Fig. 5) strongly suggests that, at least in that part of the forbidden gap between 0.28 and 0.36 ev above the valence band, the situation is correctly described by Eq. (21) with $\Gamma = 1$, i.e.

$$E_f = E_t + kT \ln \{ K(T) + \eta + \sqrt{[K(T) + \eta]^2 + 4K(T)} \}, \tag{22}$$

where E_t is the zero-temperature hole-trap level, a level which is approximately at 0.29 ev but whose exact position might depend upon the density of defect centers, density which is characterized by the parameter $\eta \cdot K(T)$ is, of course, related to the equilibrium constant and the initial carrier concentration according to Eq. (17).

A close examination of the measured Fermi-energies in sample 6a (Fig. 6) reveals that, in the region around 300°K, the Fermi level moves linearly with temperature. This circumstance allows a rather accurate determination of the Fermi-level slope at 300°K, a temperature at which $E_f = 0.300$ ev and should, therefore, be determined by Eq. (22). The slope yields $dE_f/d(kT)\,|_{300°K} = 9.90$. On the other hand, if

we write

$$\chi(T,\eta) = K(T) + \eta + \sqrt{[K(T) + \eta]^2 + 4K(T)}\,, \qquad (23)$$

it will be seen that

$$\frac{dE_f}{d(kT)} = \ln[\chi(T,\eta)] + K(T)\left[\frac{E_t}{kT} + \frac{3}{2}\right] \frac{\chi(T,\eta) + 2}{\chi(T,\eta)\sqrt{[K(T) + \eta]^2 + 4K(T)}}\,. \qquad (24)$$

Thus, the knowledge of E_f and $dE_f/d(kT)$ at 300°K can supply the parameters E_t and η of sample 6a, independently of any previous determination, as a result of the simultaneous consideration of Eqs. (22) and (24). A numerical treatment of the system gave $E_t = 0.293$ ev and $\eta = -0.23$, in satisfactory agreement with what is expected: an energy level at about 0.29 ev from the valence band and a defect density apparently proportional to the damaging dosage[e]. If we accept the quoted values and put them into Eq. (22), the resulting curve should

a) fit the measured Fermi energies between 0.28 and 0.36 ev, if the conclusions of the 8b analysis are of general significance, and
b) fit all the measured Fermi-energies, if our 6a data admit of an interpretation in terms of a single-level model.

---

[e] It should be realized, however, that the foregoing procedure cannot be considered as a reliable one. It implies exceedingly accurate measurements in a temperature range where they are known to be difficult. Moreover, it implies that with a Fermi level at about 0.30 ev and temperatures near 300°K the trapping process is strictly due to a single discrete level. In any case, an accurate determination of E_t can only be made on the basis of a "true" carrier concentration slope. This requires the Fermi level to be pinned down on the level, in other words, requires a parameter η which is positive (see Eq. 13), and this condition is not fulfilled in sample 6a.

In fact, Fig. 6 clearly answers yes to test a and no to test b. A discrete energy-level at 0.293 ev provides an excellent description of the situation up to 0.42 ev from the valence band, but fails as soon as the Fermi level falls below 0.28 ev. Repeated calculations performed with somewhat different, but still acceptable (E_t, η) combinations only helped to corroborate this evidence.

The carrier concentrations which result from a single-level approach with $E_t = 0.293$ ev, $\eta = -0.23$, and $\Gamma = 1$ are plotted as curve 1 in Fig. 7. 1.45×10^{14} cm^{-3} hole traps are available and they will all be filled at 200°K. At temperatures below 200°K we expect, therefore, the bombardment-induced deep traps to manifest themselves simply by increasing the compensation. In other words, at temperatures below 200°K sample 6a should behave like a p-type specimen with a net impurity content

$$N'_c = N_c - N_t = - \eta N_c \quad , \tag{25}$$

if there were no other active defect states in the lower part of the energy gap. We already know that this is not the case. At low temperatures we are faced with a new trapping process, and this fact is strikingly borne out by plotting the experimental $\log [p(T/300)^{-3/2}]$ values versus the reciprocal temperature for $1000/T > 7$ (Fig. 7). The straight line yields an activation energy of 0.159 ev. In other words, our 6a data imply the existence of a discrete hole trapping level at 0.159 ev (zero-temperature position) from the valence band. In the temperature range, where all the deep traps are filled, and N'_c can be considered as an "initial carrier concentration", we are then obviously tempted to describe the situation according to the single-level model, that is, to write

$$p = N'_c - \frac{N'_t}{1 + K'(T)/p} \quad . \tag{15'}$$

The primed symbols now refer to the shallow level and the fraction of the initial charge carrier concentration which was not frozen out by the deep traps. For $p << N_c'$, that is $1000/T > 7$, Eq. (15') leads to

$$p(T/300)^{-3/2} = \frac{5.50 \times 10^{18}}{\eta'} \exp\left(-\frac{E_t'}{kT}\right) cm^{-3} , \qquad (13')$$

from which the parameter η' for the second level is then determined as equal to 10.5 ± 0.1, if $E_t' = 0.159$ ev.

Repeating the procedure adopted for sample 8b, we may then try to determine the Γ-factor of the shallow level, or Γ', by calculating

$$p = \frac{N_c' \Gamma'}{2} \left\{ -[K'(T) + \eta'] + \sqrt{[K'(T) + \eta']^2 + \frac{4K'(T)}{\Gamma'}} \right\} \qquad (18')$$

for different values of Γ' and confronting with the experimental points in the temperature range where Eq. (15') might be meaningful. Computations performed with $\Gamma' = 1$ and $\Gamma' = 4$ resulted both in virtually the same curve, the curve 2 of Fig. 7[f]. Thus it became apparent that our "Ansatz" should be correct, but any hope to determine the Γ-factor for the 0.16 level on the basis of our 6a data alone had to be abandoned. This unfortunate state of affairs is due to the large value of η' for this sample, since with $\eta' \sim 10$ we have always

$$[K'(T) + \eta']^2 >> \frac{4K'(T)}{\Gamma'} \qquad (26)$$

---

[f] Why $\Gamma' = 1$ or 4? If we do not take into consideration the problematic temperature-shift of the bombardment-induced energy levels, the Γ-factor is given by the statistical weight factor γ defined as the ratio of the statistical weights of the reactants to that of the product of the trapping process.[14] It is probably reasonable, but by no means obvious, to assume that γ can take a value of either unity of four depending on whether the state occupied by the hole has a residual electronic spin or not. This question and its implications in respect of a $\Gamma = 1$, as found for the deep trap, will be discussed in a forthcoming paper.

for any reasonable value of Γ', and, therefore,

$$p \simeq \frac{N_c' K'(T)}{K'(T) + \eta'} \quad , \tag{27}$$

i.e., the charge carrier concentration is practically independent of the Γ-factor if the parameter η becomes much larger than unity[g].

Under those circumstances, it is easy to understand why even very careful fitting attempts performed on the basis of a simultaneous consideration of the trapping by both levels (two-level model!), and with the help of an IBM-650 digital computer, failed to yield the true Γ-factor of the shallow trap. Nevertheless, such attempts have led to a very accurate determination of E_t, the zero-temperature level of the deep trap in 6a. The question will be discussed in detail elsewhere, but it can be seen in Fig. 8 that, with $E_t = 0.289$ ev (a surprising agreement with what was inferred from the Fermi-level analysis of sample 8b!), the theoretical fit provides an exact reproduction of the experimental data at all temperatures. A general discussion, an evaluation of the results, and a discussion of their implications for future work will also be postponed to a later paper.

---

[g] By the same token a large η' entails, even at relatively high temperatures, $K'(T) << \eta'$ and $p \sim K'(T)/\eta'$, as in Eq. (13') which provides us with the activation energy. There is no need to emphasize that the detection of the energy level is appreciably facilitated by a straight slope covering an extended temperature range.

IV. ACKNOWLEGMENTS

The Radiation Effects program was established and initiated at Raytheon by Dr. L. Davis, Jr. Assistant Manager of the Research Division. Without his help and advice this investigation could not have been completed. The authors enjoyed many enlightening discussions with Drs. M. Holland and L. Neuringer. They benefited from stimulating questions by Dr. H. Statz. Mrs. J. Newell skillfully performed the machine calculations. Mrs. G. Klein helped a great deal in the handling of numerical data, the preparation of drawings, and the writing of this report.

V. BIBLIOGRAPHIC REFERENCES

1. Fan, H. Y. and Lark-Horovitz, K., Fast Particle Irradiation of Germanium Semiconductors, Defects in Crystalline Solids, p. 232, The Physical Society, London (1955).

2. Cleland, J. W., Crawford, J. H., and Pigg, J. C., Fast-Neutron Bombardment of n-Type Ge, Phys. Rev., 98, 1742 (June 15, 1955).

3. Cleland, J. W., Crawford, J. H., and Pigg, J. C., Fast-Neutron Bombardment of p-Type Germanium, Phys. Rev., 99, 1170 (August 15, 1955).

4. Crawford, J. H. and Cleland, J. W., Radiation Effects in Semiconductors, Progress in Semiconductors, 2, 69 (1957).

5. Conwell, E. M., Properties of Silicon and Germanium II, Proc. I.R.E., 46, 1281 (June, 1958).

6. Morin, F. J. and Maita, J. P., Electrical Properties of Silicon Containing Arsenic and Boron, Phys. Rev., 96, 28 (October 1, 1954).

7. Long, D., Galvanomagnetic Effects in p-Type Silicon, Phys. Rev., 107, 672 (August 1, 1957).

8. Fan, H. Y., Valence Semiconductors, Germanium and Silicon, Solid State Physics, 1, 283 (1955).

9. Wertheim, G. K., Electron-Bombardment Damage in Silicon, Phys. Rev., 110, 1272 (June 15, 1958).

10. Primak, W., Fast-Neutron Damaging in Nuclear Reactors: its Kinetics and the Carbon Atom Displacement Rate, Phys. Rev., 103, 1681 (1956)

11. Hughes, D. J., Pile Neutron Research, Addison-Wesley Publishing Company, Cambridge (1953).

12. Bemski, G. and Augustyniak, W. M., Annealing of Electron Bombardment Damage in Silicon Crystals, Phys. Rev., 108, 645 (November 1, 1957).

13. Lax, B. and Mavroides, J. G., Statistics and Galvonomagnetic Effects in Germanium and Silicon with Warped Energy Surfaces, Phys. Rev., 100, 1650 (December 15, 1955).

14. Crawford, J. H. and Holmes, D. K., A Chemical Approach to the Treatment of Electronic Spin in Semiconductors, Proc. Phys. Soc. 67A, 294 (March, 1954).

VI. FIGURE CAPTIONS

Fig. 1: Charge carrier concentration vs. reciprocal temperature before and after pile exposure for three samples cut from a 60 Ohm-cm p-type silicon crystal.

Fig. 2: Fermi-energy measured from the top of the valence band vs. temperature before and after pile exposure for three samples cut from a 60 Ohm-cm p-type silicon crystal.

Fig. 3: Charge carrier concentration vs. reciprocal temperature for a p-type silicon sample with an initial hole density of 2.0×10^{14} cm^{-3} after a 2.4×10^{14} n/cm^2 exposure and six months room-temperature aging. The dotted straight line fits the $p(T/300)^{-3/2}$ values at low temperatures and yields the activation energy. The theoretical curves in the high temperature range indicate that the level has a Γ -factor practically equal to one.

Fig. 4: Charge carrier concentration vs. reciprocal temperature for a p-type silicon sample with an initial hole density of 2.0×10^{14} cm^{-3} after a 2.4×10^{14} n/cm^2 exposure and one month room-temperature aging. The dotted straight line fits the $p(T/300)^{-3/2}$ values and yields the activation energy. The curve was calculated assuming that the level has a Γ -factor equal to one.

Fig. 5: Fermi-energy measured from the top of the valence band vs. reciprocal temperature for a p-type silicon sample with an initial hole density of 2.0×10^{14} cm^{-3} after a 2.4×10^{14} n/cm^2 exposure. For each theoretical curve the trap depth and trap density were adjusted so as to fit the Fermi-energy at 300°K (matching point). The Γ -factor was always taken equal to one.

Fig. 6: Fermi-energy measured from the top of the valence band vs. temperature for a p-type silicon sample with an initial hole density of 1.9×10^{14} cm^{-3} after a 1.2×10^{14} n/cm^2 exposure. The theoretical curve was obtained by fitting the Fermi-energy and its temperature derivative at 300°K.

Fig. 7: Charge carrier concentration vs. reciprocal temperature for a p-type silicon sample with an initial hole density of 1.9×10^{14} cm^{-3} after 1.2×10^{14} n/cm^2 exposure. The dotted straight line fits the $p(T/300)^{-3/2}$ values at low temperatures and yields the activation energy of the shallow trap. Curve 1 corresponds to the theoretical Fermi energies of Fig. 6, and curve 2 was calculated according to Eq. (27) with $\eta' = 10.5$.

Fig. 8: Charge carrier concentration vs. reciprocal temperature for a p-type silicon sample with an initial hole density of 1.9×10^{14} cm^{-3} after a 1.2×10^{14} n/cm^2 exposure. The theoretical curve is an EDP solution of a cubic equation in p resulting from two uncorrelated hole trapping centers. The deep trap is characterized by $E_t' = 0.289$ ev $\eta = -0.21$ and $\Gamma = 1$; the shallow one by $E_t' = 0.159$ ev and $\eta' = 10.5$.

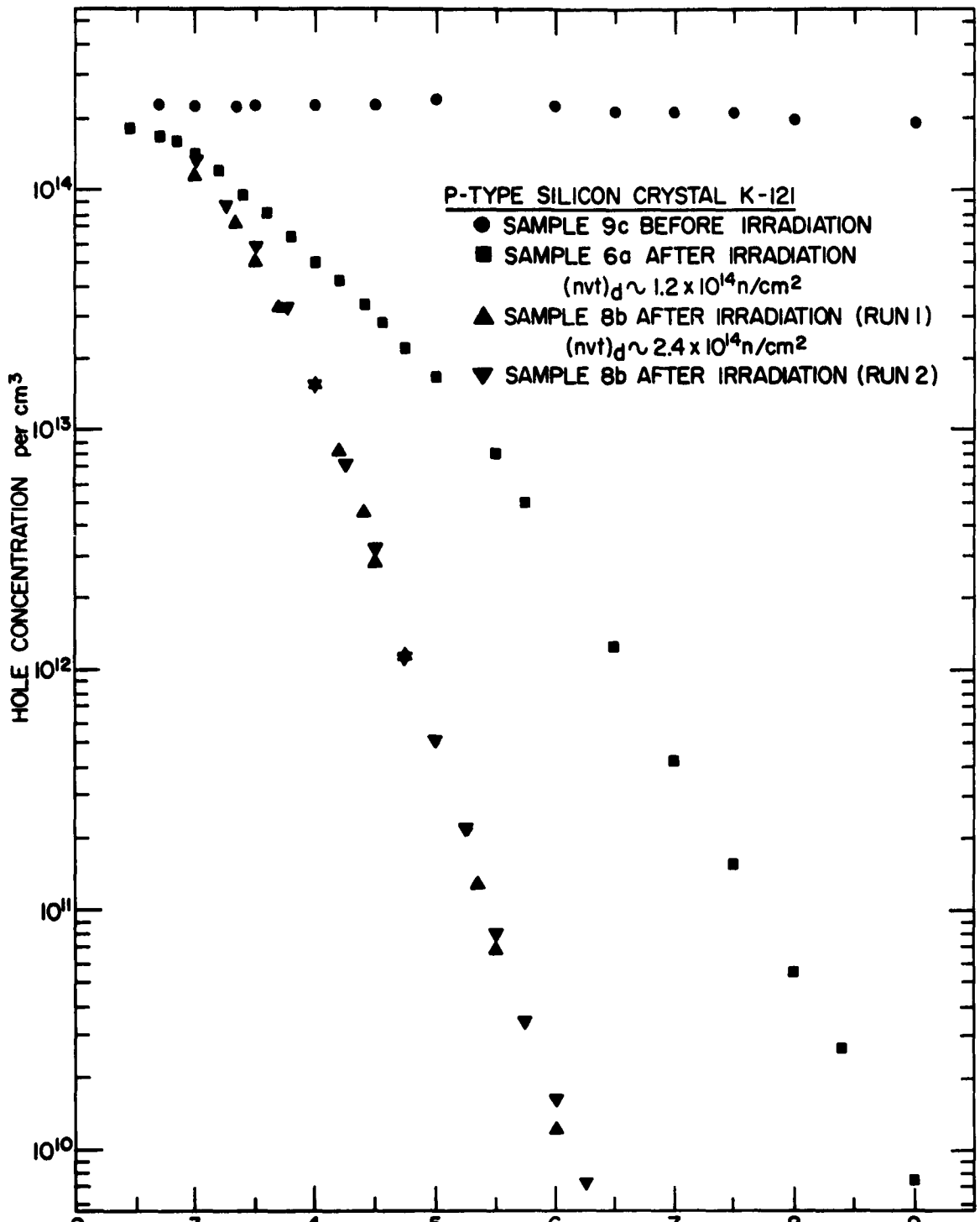
P-TYPE SILICON CRYSTAL K-121
SAMPLE 9c BEFORE IRRADIATION
SAMPLE 6a AFTER IRRADIATION
$(nvt)_d \sim 1.2 \times 10^{14} n/cm^2$
SAMPLE 8b AFTER IRRADIATION (RUN 1)
$(nvt)_d \sim 2.4 \times 10^{14} n/cm^2$
SAMPLE 8b AFTER IRRADIATION (RUN 2)
HOLE CONCENTRATION per cm³
10^{14}
10^{13}
10^{12}
10^{11}
10^{10}
2
3
4
5
6
7
8
9
x10⁻³
RECIPROCAL TEMPERATURE IN (°K)⁻¹

FIGURE 1

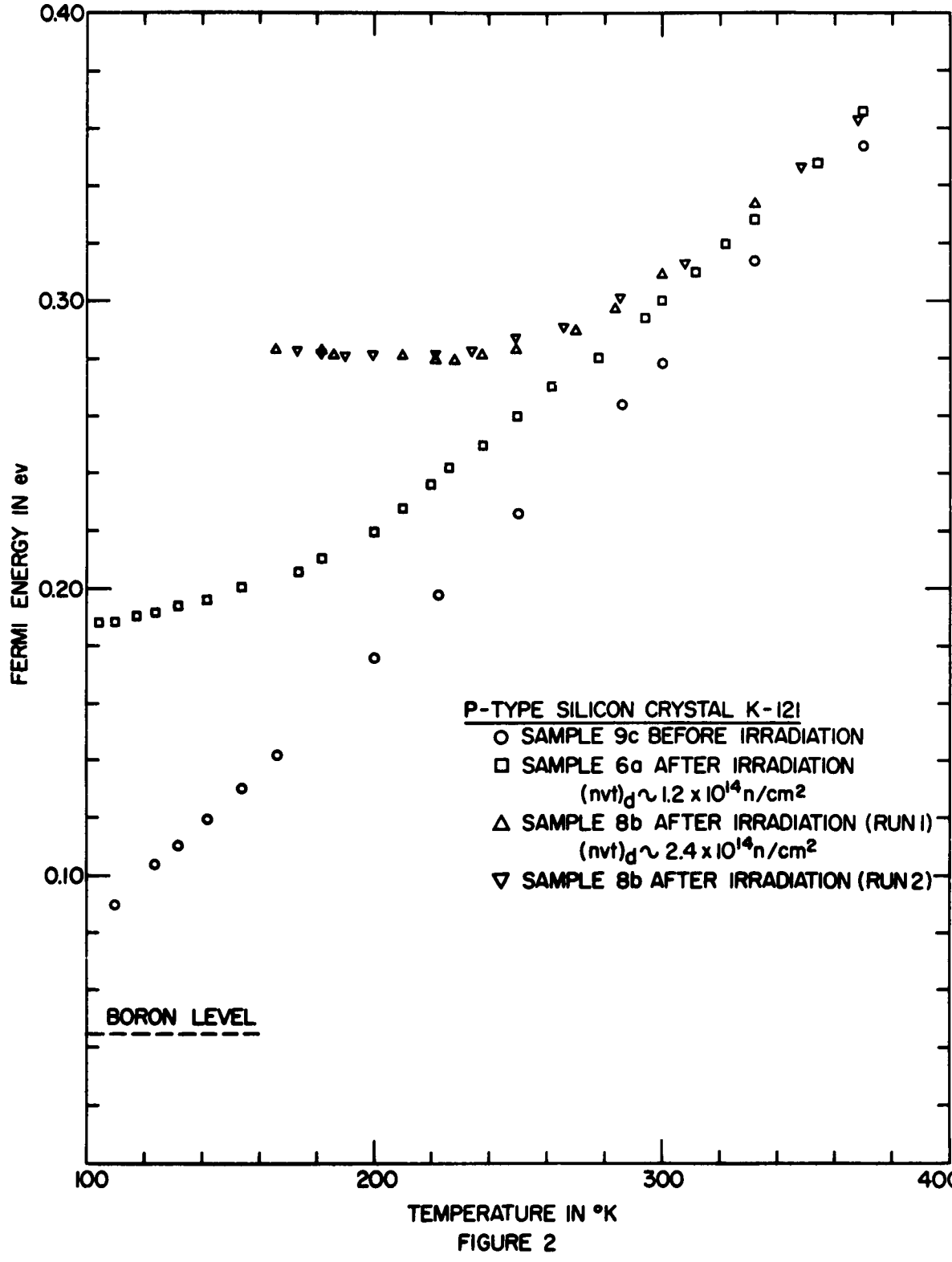
0.40
0.30
0.20
0.10
FERMI ENERGY IN ev
100
200
300
400
TEMPERATURE IN °K
P-TYPE SILICON CRYSTAL K-121
SAMPLE 9c BEFORE IRRADIATION
SAMPLE 6a AFTER IRRADIATION
(nvt)d ~ 1.2 x 10^14 n/cm^2
SAMPLE 8b AFTER IRRADIATION (RUN 1)
(nvt)d ~ 2.4 x 10^14 n/cm^2
SAMPLE 8b AFTER IRRADIATION (RUN 2)
BORON LEVEL

FIGURE 2

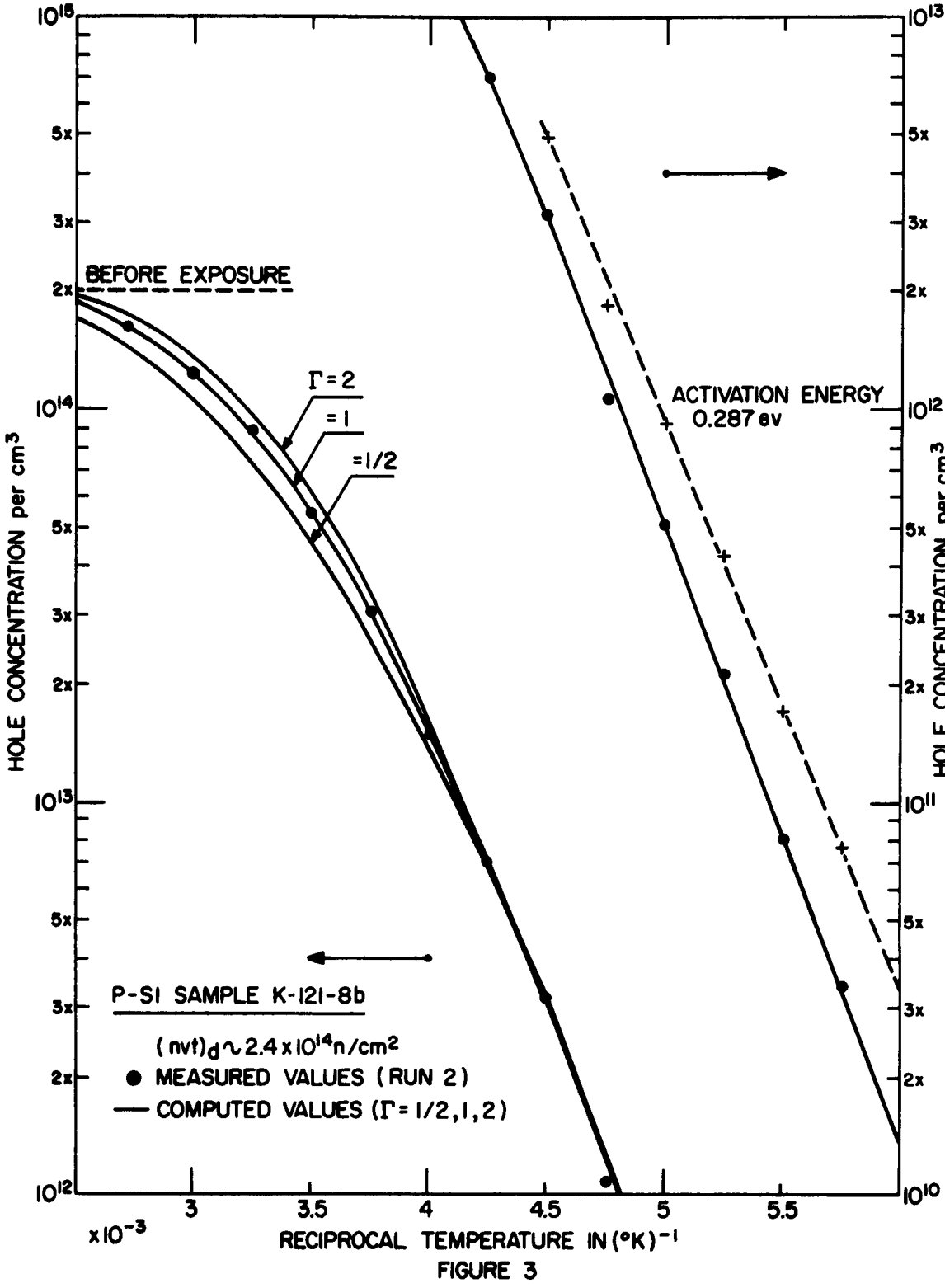
BEFORE EXPOSURE
Γ=2
=1
=1/2
ACTIVATION ENERGY
0.287 ev
P-SI SAMPLE K-121-8b
(nvt)d ~ 2.4 x 10^14 n/cm^2
MEASURED VALUES (RUN 2)
COMPUTED VALUES (Γ= 1/2, 1, 2)
HOLE CONCENTRATION per cm^3
HOLE CONCENTRATION per cm^3
x10^-3
RECIPROCAL TEMPERATURE IN (°K)^-1

FIGURE 3

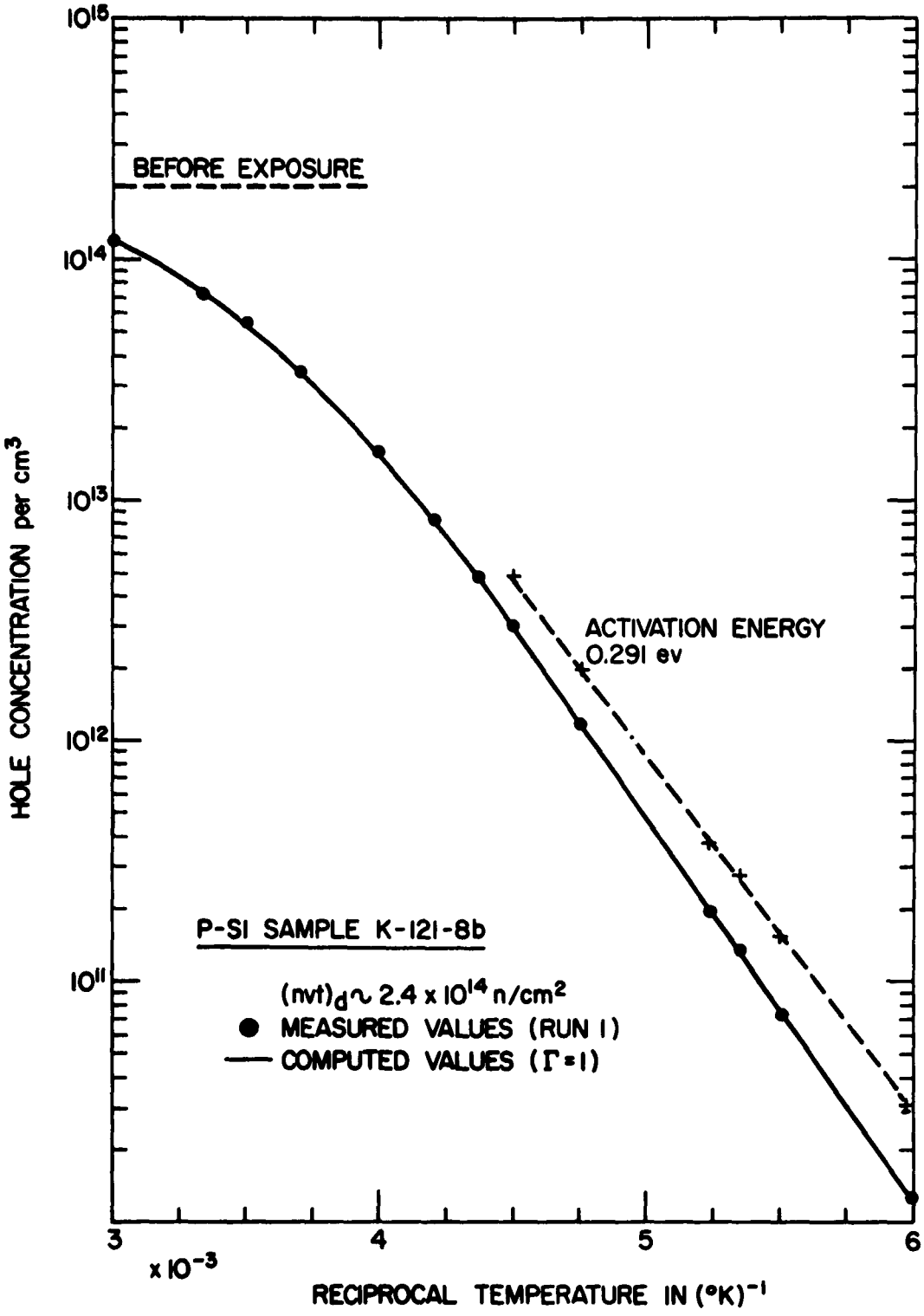
BEFORE EXPOSURE
ACTIVATION ENERGY
0.291 ev
P-SI SAMPLE K-121-8b
$(nvt)_d \sim 2.4 \times 10^{14}$ n/cm²
MEASURED VALUES (RUN 1)
COMPUTED VALUES (Γ=1)
HOLE CONCENTRATION per cm³
10^{15}
10^{14}
10^{13}
10^{12}
10^{11}
3
4
5
6
x 10^{-3}
RECIPROCAL TEMPERATURE IN (°K)⁻¹

FIGURE 4

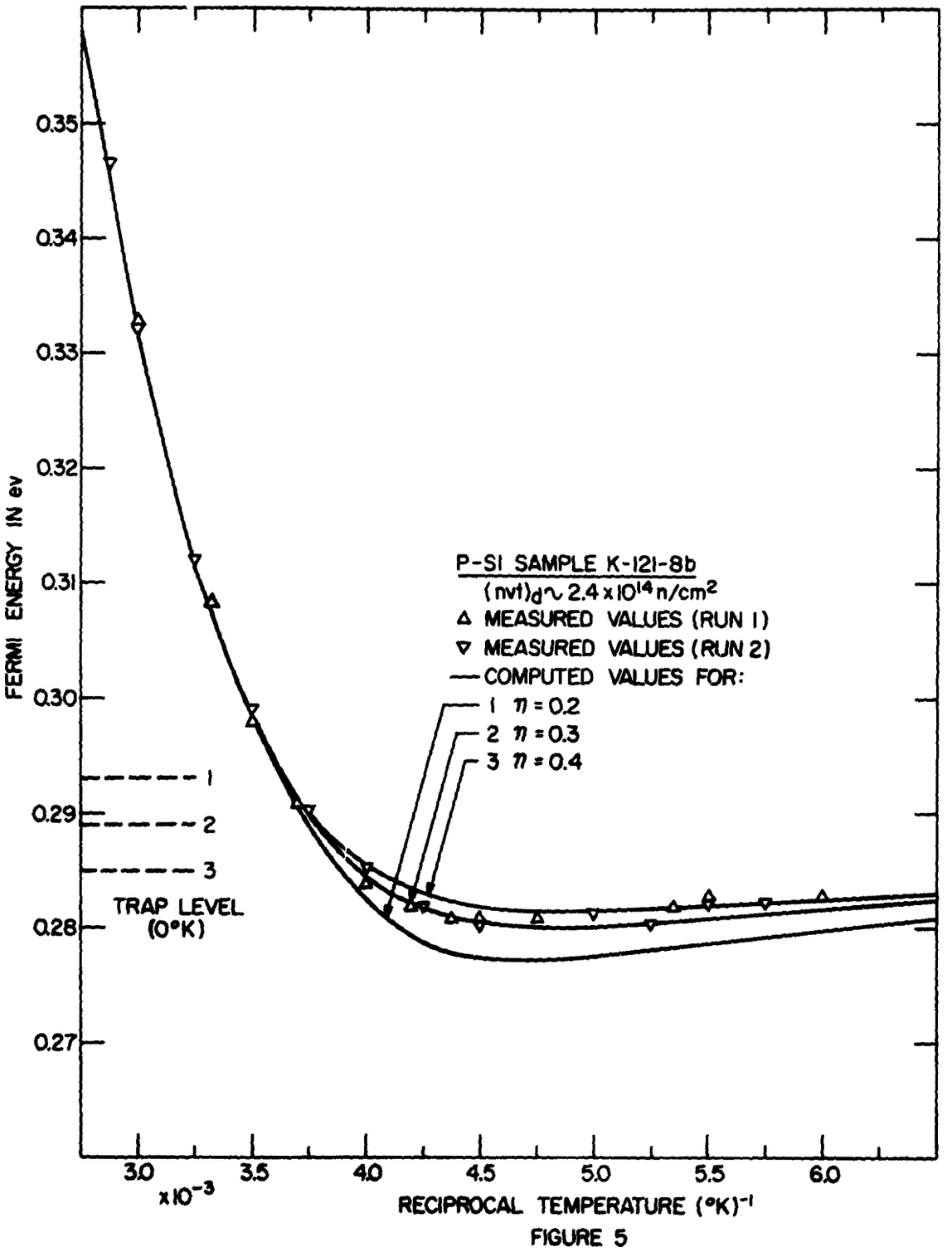
FERMI ENERGY IN ev
0.35
0.34
0.33
0.32
0.31
0.30
0.29
0.28
0.27
P-SI SAMPLE K-121-8b
(nvt)d ~ 2.4 x 10^14 n/cm^2
△ MEASURED VALUES (RUN 1)
▽ MEASURED VALUES (RUN 2)
— COMPUTED VALUES FOR:
1 η = 0.2
2 η = 0.3
3 η = 0.4
1
2
3
TRAP LEVEL (0°K)
3.0
3.5
4.0
4.5
5.0
5.5
6.0
x10^-3
RECIPROCAL TEMPERATURE (°K)^-1

FIGURE 5

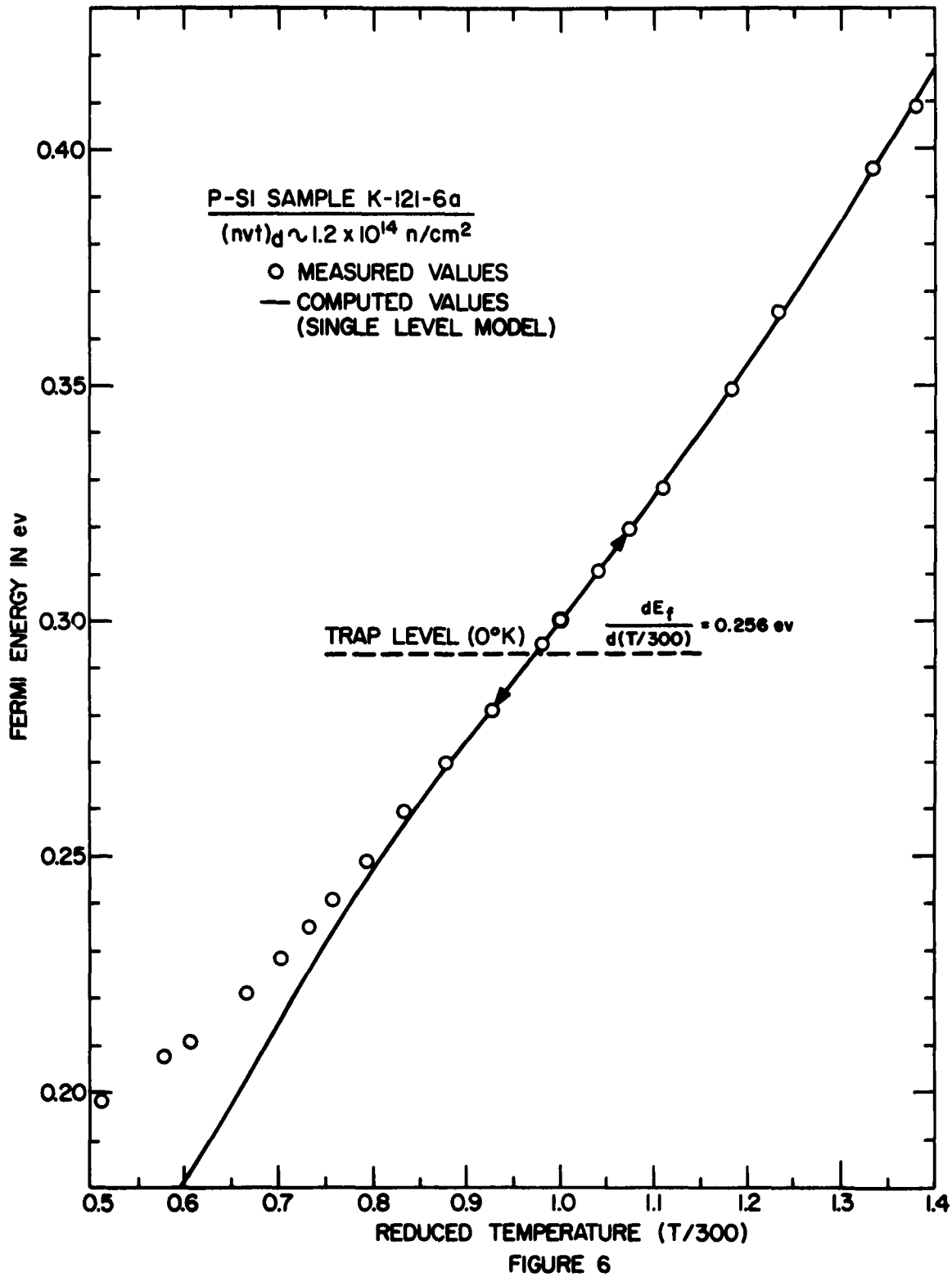
P-SI SAMPLE K-121-6a
$(nvt)_d \sim 1.2 \times 10^{14}$ n/cm²
O MEASURED VALUES
— COMPUTED VALUES
(SINGLE LEVEL MODEL)
TRAP LEVEL (0°K)
$\frac{dE_f}{d(T/300)} = 0.256$ ev
FERMI ENERGY IN ev
0.40
0.35
0.30
0.25
0.20
0.5
0.6
0.7
0.8
0.9
1.0
1.1
1.2
1.3
1.4
REDUCED TEMPERATURE (T/300)

FIGURE 6

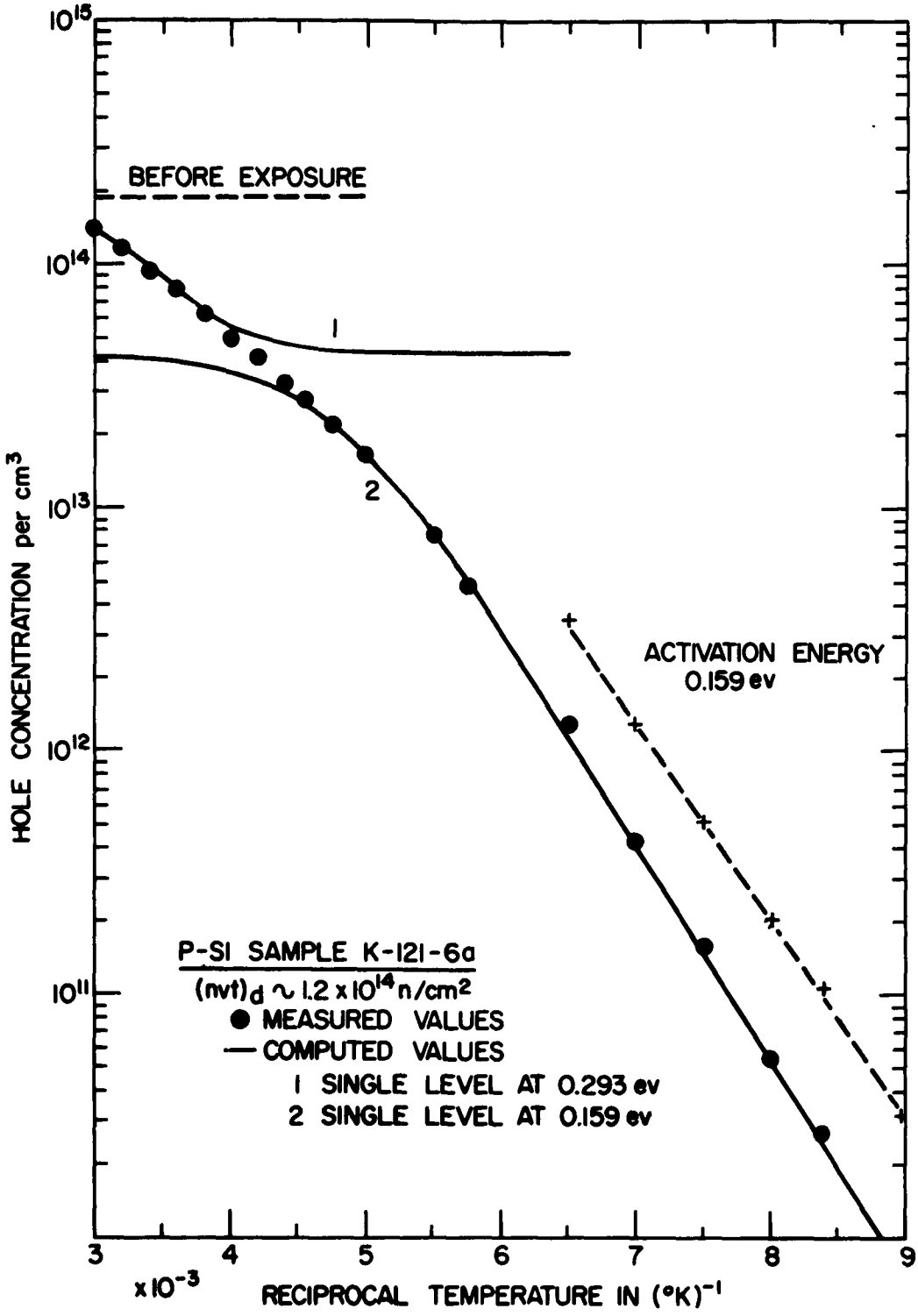
BEFORE EXPOSURE
1
2
ACTIVATION ENERGY
0.159 ev
P-SI SAMPLE K-121-6a
(nvt)d ~ 1.2 x 10^14 n/cm^2
● MEASURED VALUES
— COMPUTED VALUES
1 SINGLE LEVEL AT 0.293 ev
2 SINGLE LEVEL AT 0.159 ev
HOLE CONCENTRATION per cm^3
10^15
10^14
10^13
10^12
10^11
3
4
5
6
7
8
9
x10^-3
RECIPROCAL TEMPERATURE IN (°K)^-1

FIGURE 7

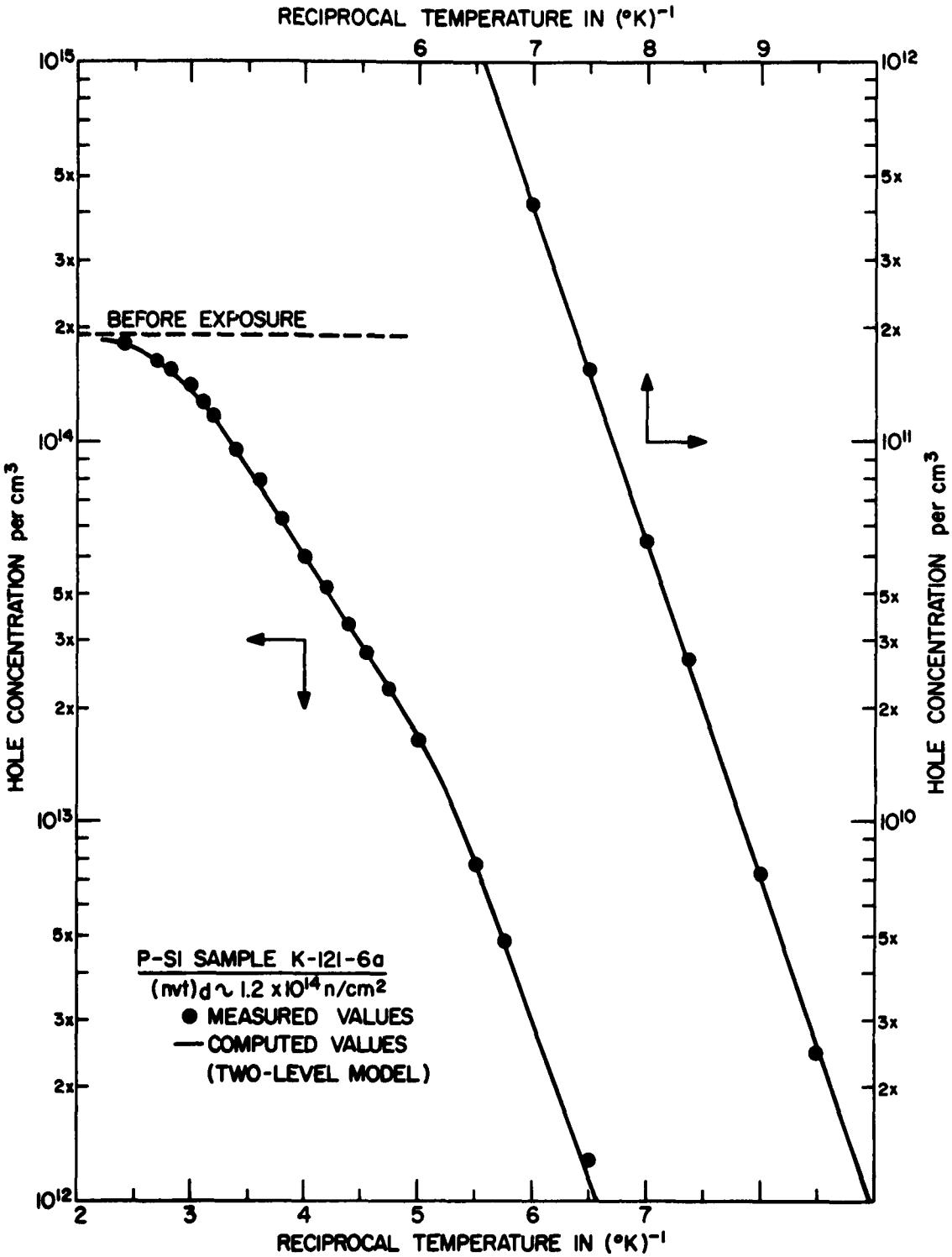
RECIPROCAL TEMPERATURE IN (°K)⁻¹
6
7
8
9
10¹⁵
10¹²
5x
3x
2x
BEFORE EXPOSURE
10¹⁴
10¹¹
5x
3x
2x
10¹³
10¹⁰
5x
3x
2x
10¹²
HOLE CONCENTRATION per cm³
HOLE CONCENTRATION per cm³
P-SI SAMPLE K-121-6a
(nvt)d ~ 1.2 x 10¹⁴ n/cm²
● MEASURED VALUES
— COMPUTED VALUES
(TWO-LEVEL MODEL)
2
3
4
5
6
7
RECIPROCAL TEMPERATURE IN (°K)⁻¹

FIGURE 8

EFFECT OF RADIATION ON THE CRITICAL SHEAR STRESS OF A METAL SINGLE CRYSTAL

by

C. E. Morgan

Convair
A Division of General Dynamics Corporation
Fort Worth, Texas

A mechanism is postulated to account for the radiation hardening of a metal single crystal. The mechanism is based on a lattice defect consisting of interlocking dislocation rings. According to this model, the critical shear stress of a metal single crystal varies as the cube root of the integrated fast neutron flux. This agrees well with the results of experiments by Blewitt et al on irradiated high-purity copper crystals.

INTRODUCTION

The critical shear stress of a metal single crystal is greatly increased under certain conditions by irradiation with neutrons. Such an effect arises from structural defects introduced into the lattice of the metal by the irradiation. The structural defects that supposedly result from bombardment of a metal with neutrons and that might conceivably harden the metal are: (1) Frenkel defects, (2) clumps of vacancies produced directly by the irradiation, (3) dislocation rings produced by the high stresses around thermal and displacement spikes, (4) small misoriented regions left behind by displacement spikes, and (5) clustered vacancies or interstitials formed by diffusion of the Frenkel defects. It is of interest to determine, if possible, which of these defects cause the increase in critical shear stress of an irradiated metal.

DISCUSSION OF PREVIOUS WORK

Frenkel defects would have to be extremely effective in interacting with the glide dislocations to produce the large amount of hardening that is observed for irradiated metals. For example, it is apparent that the Frenkel defects begin to anneal in copper at temperatures very low compared to the temperature at which the radiation-induced increase in critical shear stress anneals. In copper the interstitials begin to anneal rapidly at 30°K and the vacancies anneal at about 290°K. The increase in critical shear stress does not anneal until a temperature of about 550°K is reached. Quenching experiments[1] show that randomly dispersed vacancies do not appreciably harden a metal; hardening occurs only when the specimen has been warmed up to a temperature at which the vacancies can migrate to dislocations or else cluster to form voids. Therefore, it appears that randomly dispersed Frenkel defects cannot be the chief cause of the radiation-hardening.

If the Frenkel defects form jogs on the glide dislocations, hardening of the metal would be expected, since the jogs effectively increase the Peierls force for the dislocation. There are a number of objections to this view, however. Since the activation energy due to the increased Peierls force is not likely to be very large, even when the applied stress is zero, the jogged slip dislocations should be practically unrestrained at any but the lowest temperatures. Thompson and Holmes[2] have observed that the internal friction of copper single crystals decreases after reactor irradiation and that this decrease saturates at the very low dose of $4(10^{12})$nvt. Barnes and Hancock[3] find that the internal friction of copper single crystals remains unaffected by a short neutron bombardment at 78°K, if no warming is allowed before measurement. Successive pulse annealings produce no marked change until 300°K is reached, when the internal friction is greatly reduced. Since randomly dispersed Frenkel defects should have little effect on the damping, the decrease of internal friction is undoubtedly caused by pinning of the dislocations by the Frenkel defects. In view of the fact that the decrease of internal friction and the change in elastic constants are completely saturated at 10^{15} nvt, and that Blewitt[4] observes no radiation annealing or saturation of the increase in critical shear stress for integrated fluxes up to 10^{20} nvt, the radiation-hardening cannot be due to pinning of dislocations by point defects.

That the Frenkel defects cluster by diffusion to form aggregates of interstitials or to form voids, however, remains a possibility. Such clusters could be formed on dislocations or at random throughout the lattice. In either case, they would be very effective barriers to the movement of slip dislocations, provided that they are larger than a few atoms. There are a number of important difficulties, however. For example, if copper is irradiated at a temperature at which the point defects are mobile, it hardens at the maximum rate consistent with the bombarding flux, provided no self-diffusion takes place. This indicates that, since the point defects can easily reach the dislocations and disappear at jogs on the dislocation line, the metal is hardened even when a high steady-state concentration of point defects necessary to nucleate aggregates cannot be built up. Quenching experiments[5] on nickel and aluminum show that during annealing of the quenched-in vacancies the volume of the metal decreases simultaneously with its resistivity, indicating that the vacancies are actually disappearing and not merely aggregating into voids. Finally, Blewitt[1] has found that a single crystal copper specimen bombarded at 20°K with neutrons and immediately tested at 20°K has the same critical shear stress as specimens bombarded at 20°K, then pulse annealed to temperatures as high as 250°K, and at last tested at 20°K. It will be recalled that no diffusion of structural defects takes place in copper until a temperature somewhat above 20°K is reached; in fact, the interstitials anneal rapidly between 30°K and 40°K. Thus, the point defects cannot aggregate at 20°K, and yet the copper specimen is fully hardened by the irradiation.

Hence, one is led to the conclusion that radiation-hardening can only be caused by a defect formed directly by the irradiation. A hardening mechanism based on the Frenkel defects is unsatisfactory for the reasons which have been mentioned.

Brinkman[6] has suggested that small misoriented regions similar to small grains may be left behind when a displacement spike resolidifies. Since the freezing of the molten core of the displacement spike proceeds from the outside in with the surrounding lattice as a site for nucleation, the resolidified region should have the same orientation as the remainder of the lattice. Thus, one would not expect very many such misoriented regions to be formed by irradiation.

It is difficult to see how neutron bombardment could directly produce clusters of interstitial atoms merely by displacing lattice atoms. On the other hand, it is quite likely that small, stable, multiple vacancies might be produced directly by neutron bombardment. According to Brinkman[6], a primary knock-on will produce stable multiple vacancies in copper when its kinetic energy is 400 ev or less. Multiple vacancies produced by knock-ons with higher energy than this will be unstable and collapse to form a displacement spike. Snyder and Neufeld[7] have shown that the average total number of displaced atoms including the primary knock-on is approximately $\frac{E}{2E_0}$ where E is the energy of the knock-on and E_0 is the average threshold displacement energy. The threshold displacement energy is about 25 ev. Therefore, the largest stable multiple vacancy that can be produced directly by bombardment of copper is about eight atomic volumes. There is some question whether or not such small cavities can cause much hardening, because they are too small to exert a sizeable image force on a glide dislocation. If they did, the resulting hardening should be practically insensitive to temperature, in contrast to experimental results. The strain field around the multiple vacancy is probably not large. That means, there should be practically no interaction between glide dislocations and multiple vacancies except when they are separated by only a few interatomic distances. If an edge dislocation passes through a multiple vacancy, a jog will be formed on it. These jogs may not seriously impede edge dislocations. Jogs are probably not formed on screw dislocations by the multiple vacancies. Moreover, in this case it may not be necessary for the partial dislocations of an extended edge dislocation to come together to cut through the multiple vacancy, since complex stacking faults may not necessarily be formed by individual climbing of the partials. If they are formed, they will be only about 4 atoms in size. If multiple vacancies are effective barriers for the glide dislocations, they might well be the cause of radiation-hardening. Holmes[4] at Oak Ridge has advanced a theory that radiation hardening is caused by clumps of point defects. It appears to be difficult to explain, on the basis of clustered point defects, the fact that work-hardened metals are not hardened nearly as much as annealed metals by irradiation.

THE THEORY

The possibility that small shear or prismatic dislocation rings produced by the high stresses around thermal and displacement spikes might be the cause of hardening seems to have been overlooked so far. According to Seitz and Koehler[8], the atoms in the heated zone of a spike exert a pressure on the rest of the lattice of

the order of the shear modulus. These investigators show that the probability of a dislocation lying in the region about the spike, where the stress is high enough to move dislocations, is negligible for well-annealed metals. Therefore, this stress will probably not be relieved by gliding of the dislocations already present in the metal. Consequently, small dislocation rings should be formed spontaneously. If shear dislocation rings are formed by irreversible slip on intersecting glide planes so that the rings interlock, the ring may not collapse completely after dissipation of the spike. In fact, it seems probable that multiple slip occurs on nonparallel glide planes even for h.c.p. metals because of the exceedingly large stresses around the spike. As a result of intersection of the dislocation rings, jogs will be on opposite sides of the dislocation rings. When the temperature of the metal is below that required for rapid self-diffusion, the jogs prevent the collapse of the dislocation rings. Since jogs on the dislocation rings are edge dislocations and since there is a force of attraction between opposite sides of the dislocation rings, diffusion of vacancies to or from the jogs on the dislocation rings will cause these jogs to climb. The dislocation rings will then disappear from the lattice at temperatures in the self-diffusion range. An alternative is that prismatic dislocations are produced by the spike instead of shear dislocation rings. Each of these will probably consist of an extra half-sheet of material which is roughly circular in shape and have an edge dislocation all the way around the edge of the extra half-sheet. This prismatic dislocation ring will also be removed from the lattice by climb. Thus, the recovery of the critical shear stress of an irradiated metal will take place by self-diffusion.

From the phenomenon of work-hardening, we know that the presence of other dislocations in the lattice can seriously impede the glide dislocations and thereby cause a large amount of hardening. (This is not to suggest that radiation-hardening is like work-hardening.) The jogs on the shear dislocation rings should prevent collapse or expansion of the dislocation rings. At any rate, in order to expand a small dislocation ring with no jogs on it, the applied stress will have to oppose a very large stress acting to collapse the ring. For example, in the case of a shear dislocation ring in copper with a radius of 20 interatomic distances, a stress of about 200 kg/mm^2 is needed to expand it. Prismatic dislocation rings of this size should be practically immobile. Therefore, it seems likely that the dislocation rings will be immobile during deformation of the metal.

Now, consider an irradiated metal in which the density of dislocation ring groups is N. Two ways by means of which the principal glide dislocations interact with these groups may be envisioned. First, the strain field around the dislocation ring groups may hold up the glide dislocations so that they do not cut through the dislocation rings at the stress level during deformation. Since the dislocation rings are small and their strain field does not extend beyond a distance of the order of magnitude of the radius of the dislocation ring, the glide dislocations can bow out between them in the manner suggested by Orowan[9] for overaged alloys. In this case the critical shear stress will be inversely proportional to the average distance between dislocation ring groups, or directly proportional to $N^{1/3}$. The critical shear stress for this case is given by:

$$\sigma = \frac{Gb}{L}$$

or

$$\sigma = GbN^{1/3}, \tag{1}$$

where G is the shear modulus and b is the Burgers vector. This type of hardening, however, is not considered to be very sensitive to temperature.

The second kind of interaction would occur if the glide dislocations cut through the dislocation rings. When the glide dislocations cut through the dislocation rings, jogs will be formed on them. The energy required to form a jog will be $\propto Gb^3$, where $\propto \cong 1$. The average distance between dislocation ring groups will be $N^{-1/3}$, and, if we add the jog energy and the contribution from the applied stress, we obtain the activation energy

$$U = \propto Gb^3 - \frac{\sigma b^2}{N^{1/3}} \tag{2}$$

For plastic flow to be rapid, the flow stress must be

$$\sigma \cong GbN^{1/3} \tag{3}$$

which is the same as Equation 1. In this case, the flow stress should be temperature-dependent. In order to cut through the dislocation ring, however, the partial dislocations in h.c.p. and f.c.c. metals will have to coalesce; otherwise, a complex stacking

fault at the place of intersection will be formed. The stress necessary to force the two partial dislocations of an extended dislocation together is quite high even for metals with high stacking fault energies, such as aluminum. The dependence of the width of an extended dislocation on stress during intersection of dislocations has not been considered, but this will affect the activation energy U.

Equation 2 indicates that the critical shear stress at constant strain rate will be directly proportional to the absolute temperature of the specimen. In the case of metals with low stacking fault energy such as copper, the temperature-dependence of the critical shear stress will be more complicated, since different rate-determining processes occur in different temperature intervals. Indeed, Blewitt[10] observes that the critical shear stress of copper single crystals irradiated with neutrons is approximately proportional to the square root of the absolute temperature of the specimen.

DISCUSSION OF THE THEORY

The number of dislocation ring groups should be proportional to the number of temperature spikes and, therefore, proportional to the integrated fast neutron flux. The critical shear stress from Equation 1 or Equation 3, then, is proportional to the cube root of the integrated fast neutron flux, in agreement with the results that Blewitt[10] has obtained for 99.999 percent pure copper single crystals irradiated up to an integrated fast neutron flux of $2(10^{19})$nvt. Calculation of the number of displacement spikes produced during bombardment shows that there should be enough of the dislocation ring groups to account for the amount of hardening observed. Thus, it is possible to explain the general features of radiation-hardening on the basis of the dislocation rings caused by temperature spikes. The value of a new theory is determined by how well it can account for observed facts and how well it can predict experimentally verifiable phenomena. Some of the effects to be expected on the basis of the theory are as follows:

1. The generation of dislocation rings around temperature spikes depends on the existence of the high stresses in the vicinity of the spike. Furthermore, a glide dislocation in this high stress region will relieve the stress by moving. Therefore, no dislocation rings will be formed if a dislocation happens to be in the high stress region. The more a metal has been work-hardened, the more chance there is for a dislocation to be in the high stress region. For a fully work-hardened metal, exceedingly few

dislocation rings will be produced by the temperature spikes. Thus, it is possible to explain on the basis of the dislocation ring mechanism the fact that irradiation of a work-hardened metal raises the flow stress by a small amount compared with the change due to irradiation of an annealed metal.

2. Since the dislocation rings are produced directly by the irradiation, radiation-hardening of a metal should take place at the lowest temperatures.

3. Because the dislocation rings will disappear from the lattice by climbing of the jogs on shear dislocation rings or by climbing of the small prismatic dislocations recovery of the critical shear stress to its pre-irradiation value should be by self-diffusion.

4. Only heavy, energetic particles will produce thermal spikes. Therefore, bombardment of a metal with particles such as fast neutrons should result in considerable hardening of the metal. Bombardment with electrons that produce single atomic displacements only or with gamma rays should produce at most a slight hardening of the metal.

5. For annealed metals, there should be no saturation of the increase in critical shear stress with integrated flux, up to very high levels of irradiation. Likewise, there should be practically no radiation annealing.

6. There should be little radiation-hardening until either the separation distance of the dislocation ring groups becomes less than the length of the Frank-Read sources in the metal, or the effect of the dislocation rings becomes large enough to exceed the normal slip resistance of the lattice.

7. The radiation-induced increase in the critical shear stress will be sensitive to temperature if the glide dislocations cut through the dislocation rings.

8. According to the dislocation ring model, growth of slip lines, under certain conditions, should be more difficult in an irradiated metal; i.e., there should be a lattice-hardening. Some metals, for example nickel, seem to show this effect.

The coarse slip lines and the yield point effect sometimes observed in irradiated metals indicate that nucleation of slip lines is more difficult than their growth. Ordinarily, this would not be expected from the dislocation ring model. However, if a glide dislocation cuts through a dislocation ring group in a manner such that point defects are left behind by the jogs so formed on the glide dislocation, the next glide dislocation that cuts through the dislocation ring group will lay down a row of point defects next to the row left by the first dislocation. Since the formation of rows of point defects by succeeding glide dislocations under these conditions takes less and less energy, there would be a drop in stress corresponding to the yield point effect. This should happen only under conditions in which the glide dislocation can produce point defects as a result of being jogged and in which the strain rate is high enough. Other processes such as cross-slip or pinning by point defects may be involved and, since detailed observations of the yield point effect have not been made, the above explanation must be regarded as tentative.

The strength of metal single crystals after extensive plastic flow is nearly the same for both irradiated and nonirradiated specimens. Moreover, the work-hardening rate at this point becomes nearly the same. This is due to the mutual interference of glide dislocations. As deformation proceeds, more glide dislocations are produced and the mobility of the dislocations becomes more sensitive to the presence of other glide dislocations than to dislocations introduced by irradiation.

The purpose of this paper is to point out that most of the observed effects of irradiation on the critical shear stress of a metal single crystal can be explained by a model of radiation-hardening caused by small dislocation rings introduced into the lattice of a metal by the irradiation. It is difficult to see how any other defect that might be produced by irradiation could be responsible for both effect 1 and effect 2 mentioned above. The small amount of radiation-hardening displayed by a work-hardened metal might be explained by a theory based on some other radiation-induced structural defect, if it is assumed that the number of dislocations due to the work-hardening is considerably larger than the number of such defects caused by irradiation. This implies that the strength of a highly work-hardened metal could be considerably increased by irradiating it to a sufficiently high level, while the dislocation-ring model indicates that the strength of a fully work-hardened metal will be increased only a little for any amount of irradiation.

REFERENCES

1. Broom, T., Nature 181, 449 (Feb. 15, 1958).

2. Thompson, D. O., and Holmes, D. K., J. Appl. Phys. 27, 713 (1956); also, with Blewitt, T. H., J. Appl. Phys. 26, 1188 (1955).

3. Barnes, R. S., and Hancock, N. H., Effect of Neutron Irradiation Upon the Internal Friction of Copper Single Crystals at Liquid Nitrogen Temperature. Atomic Energy Research Establishment Report AERE M/R 2436A (Nov. 1957).

4. Blewitt, T. H., discussion of article by P. Coulomb and J. Friedel, "On the Formation of Cavities Along Dislocations," Dislocations and Mechanical Properties of Crystals. New York: John Wiley and Sons (1957), 573.

5. Takamura, J., Metal Phys. 2, 112 (1956).

6. Brinkman, J. A., Am. J. Phys. 24, 246 (1956).

7. Snyder, W. S., and Neufeld, J., Phys. Rev. 97, 1636 (1955).

8. Seitz, F., and Koehler, J. S., "Displacement of Atoms During Irradiation," Solid State Physics. New York: Academic Press, Inc. (1956), Vol. II, 305.

9. Orowan, E., Discussion, Symposium on Internal Stresses. London: Inst. Metals (1947), 451.

10. Holmes, D. K., Redman, J.K., Blewitt, T. H., Coltman, R. R., Bull. Am. Phys. Soc. II 1, No. 3, 130 (1956).

MEASUREMENT OF THE RANGE OF RECOIL ATOMS

by

R. A. Schmitt and R. A. Sharp

John Jay Hopkins Laboratory for Pure and Applied Science,
General Atomic Division of General Dynamics Corporation,
San Diego, California

An important problem in the interpretation of radiation-damage and sputtering phenomena is the evaluation of the range of an atom which moves through a lattice after having received an initial energy of 10 to 100 kev. An initial energy of about this amount is acquired by an atom which has been struck by a fast neutron ($\sim$1 Mev). The kinetic energy of such atoms will be transferred to the lattice largely by thermal vibrations and the creation of lattice vacancies and displacements. If the collision cross section is very large, the displaced atoms and/or vacancies will be separated by only an atomic lattice spacing. On the other hand, separations of many atomic diameters are expected for low collision cross sections. Annealing of such a perturbed lattice is achieved by the diffusion of lattice vacancies and interstitial atoms.

A theoretical evaluation of the collision cross section is difficult because (1) such a calculation essentially involves a many-body problem of the interpenetration of orbital electron clouds during collision, and (2) the atomic charges of moving atoms through solid lattices are unknown. Everhart, et al.,[1-3] have measured the differential cross sections for the scattering of singly ionized noble gases (25 to 138 kev) in noble gases and also have determined the charge states of the scattered atoms after single collisions. Since a crystal lattice is a condensed medium and atomic stopping power is larger in crystalline lattices than in gaseous media,[4] it is doubtful whether the scattering data of gaseous atomic interactions may be used to theoretically calculate scattering cross sections in solids.

Experimentally, a direct observation of recoil atoms in solids is difficult because of the uncertain charge states. At present, the motion of an uncharged atom in a lattice does not produce effects that are amenable to detection. Only by measurements of density, electrical conductivity, elastic moduli, etc., are we able to study the effects of radiation damage.[5] A study of the range of recoil atoms is one unknown in the general problem of radiation damage.

Investigations of the ranges in metals and gases of the light atom, helium, in its two charge states have been reported.[6] Also, considerable work has been devoted to measurements in solids of highly energetic (in the tens-of-Mev region) fission products.[7-9]

By using an electromagnetic isotope separator, Thulin[10] has measured the penetration depth of 50-kev Xe^{135} atoms in Formvar absorbers. Following the discussion of Bohr[11] in his classic paper on atomic-particle penetration, Nielsen[12] has shown that the calculated ranges agreed fairly well with the observed ranges found by Thulin. Furthermore, Nielsen successfully correlates the depth of ion penetration of a number of ions into various foils with the width of the energy distribution of light charged particles scattered from the ions deposited in the foils.[13]

A novel experimental technique has been applied to the problem of determining the ranges of atoms in the kev region. Atoms with initial energies in this region are produced by irradiating suitable targets with high-energy bremsstrahlung gamma rays, and the products of photonuclear reactions, such as photoneutron (γ, n) transmutations, are observed. The bremsstrahlung gamma rays used in this work were generated by a 24-Mev Allis-Chalmers betatron.[a] The photon spectrum of gamma rays is continuous from 0 to 24 Mev; the energy spectra of evaporated neutrons from copper[14] and lead[15] are centered at about 1.5 Mev, with a full width at half maximum of about 2 Mev. Since (1) the energy thresholds for the photoneutron reactions of the majority of the elements reported in Table I, below, are well below 24 Mev and near the copper and lead photoneutron thresholds and (2) all the photonuclear absorption cross sections of elements in Table I nearly resemble the familiar bell-shaped or resonance cross-section curve of copper and lead, it is anticipated that the spectra of evaporated neutrons for all the targets studied here are centered at about 1.5 Mev, with corresponding half-widths of 2 Mev.

The nucleus receives a negligible amount of momentum from the incoming gamma ray ($\sim$2 kev and $\sim$0.7 kev for a 16-Mev photon absorbed by copper and gold, respectively). However, the nucleus (atom) recoils from neutron emission with an energy E_R, given by the formula

$$E_R = E_N \frac{M_N}{M_A} ,$$

where E_N is the neutron energy and M_N and M_A are the masses of the neutron and atom, respectively. For representative atoms, such as fluorine (A = 19), copper (A = 63 and 65), and gold (A = 197), the most probable recoil energies are about 75, 25, and 10 kev, respectively. As a result of photoneutron emission, the nuclei of the recoiling atoms are usually unstable to beta (positron) decay and, therefore, are amenable to detection by standard scintillation and beta-counting methods.

The ranges were determined for carbon (C^{11} in polystyrene, CH), fluorine (F^{18} in Teflon, CF_2), chlorine (Cl^{34} in saran, CHCl), and the metals titanium, iron, zinc, copper, molybdenum, silver, and gold in their respective metallic

[a]We wish to acknowledge the generous cooperation of Dr. Waldo K. Lyon and Mr. R. B. Doherty of the U.S. Navy Electronics Laboratory, San Diego, California, in the performance of these irradiations.

lattices. The method used was somewhat similar to the stacked-foil technique commonly used in charged-particle excitation-function studies. Thin elemental or plastic target foils about 0.001 in. thick were interleaved between 0.0008-in.-thick aluminum catchers (Alcoa 1199-0, 99.986% pure). Before use, the metallic foils were thoroughly cleaned with organic solvents and etched with appropriate acids; plastic foils were detergent-cleaned. In order to evaluate the background activities present in the aluminum catchers, an equal number of aluminum foils without targets were simultaneously irradiated. About 2000 roentgens per minute of 23-Mev bremsstrahlung were incident on the sandwiched targets.

Immediately after irradiation, the sandwich was disassembled and the radioactivities of the target foils, aluminum catcher foils, and aluminum background-monitoring foils were measured by scintillation-counting the annihilation radiation (0.51 Mev) of the positrons. The recoiling atoms which are close to the target-foil surface are caught in the aluminum foils. If the range of the recoil atoms is small compared with the foil thickness, the range, R, is related to the fraction N_c/N_f of atoms which recoil out of the target foil and to the foil thickness, x, by $R = 2(N_c/N_f)x$, where N_c and N_f are the numbers of atoms that recoil into the catcher and that are retained in the target foil, respectively. By counting nearly equal thicknesses of target foils and aluminum catchers, the errors in the ratio N_c/N_f are less than 5%. Subsidiary experiments showed that scattering of the recoil atoms back into the target foils by air between the target foils and aluminum catchers is negligible.

In Table I are listed the experimental data and other information relevant to this paper. The first column lists the recoiling atoms and their mass numbers. The most probable recoil energy (in kev) is given in the second column, with the average recoil energies for all atoms assumed to be about 1.5 times the most probable recoil energies, as was observed for the copper and lead photoneutron spectra. The third column gives the fraction of activated atoms that recoil out of a 0.001-in. foil with 23-Mev bremsstrahlung incident on the foils. (A graphic representation of N_c/N_f is displayed in Fig. 1, below.) In the fourth and fifth columns the corresponding ranges are shown, calculated by the formulae $R = 2(N_c/N_f)x$ (Å units, 10^{-8} cm) and $R\rho$ ($\mu g/cm^2$), respectively.

The ranges, calculated by the formula $2(N_c/N_f)x$, are the vector sums of the tortuous paths traveled by the recoiling atoms. Theoretical ranges, calculated by assuming billiard-ball collisions, were made according to Seitz and Koehler,[5] and, in general, the theoretical ranges were many times higher than those given in Table I. Nielsen,[12] following the lines of Bohr,[11] obtains the following theoretical expression for the range:

$$R = 0.6 \cdot \frac{\left(Z_1^{2/3} + Z_2^{2/3}\right)^{1/2}}{Z_1 Z_2} \cdot \frac{A_1 + A_2}{A_1} \cdot A_2 \cdot E_1 \ (\mu g/cm^2) ,$$

where Z_1, A_1 and Z_2, A_2 are the atomic numbers and masses for the incoming particles and the target atoms, respectively, and E_1 is the energy of the

Table I

FRACTION (N_c/N_f) OF ACTIVATED ATOMS RECOILING OUT OF 0.001-IN. FOILS AND CALCULATED RANGES OF THE RECOIL ATOMS (23-Mev BREMSSTRAHLUNG INCIDENT ON FOILS)

Recoiling Atom	Most Probable Recoil Energy (kev)	$N_c/N_f \times 10^4$[a]	R, Calc. Range in Å (10^{-8} cm)	R, Calc. Range in $\mu g/cm^2$[b]	Theoretical Range in $\mu g/cm^2$[c]
C^{11}	130[d]	216 ±20	11,000[e,f]	117	216[g]
F^{18}	85[d]	182 ±18	9,200[e]	200	118
Cl^{34}	45[d]	104 ±10	5,300[e]	90	31[g]
Ti^{45}	33[d]	6.1 ±0.8	310	14	24
Fe^{53}	30[d]	11.0 ±1.7	560	44	19
Zn^{63}	25[d]	2.7 ±0.3	137	9.8	15
Cu^{62}	25 ±16	3.1 ±0.2	163	14.5	16
Cu^{64}	25 ±16	3.2 ±0.2	157	14.0	16
Mo^{91}	16[d]	1.4 ±0.4	71	7.5	8.1
Ag^{106}	14[d]	1.4 ±0.3	71	7.5	6.5
Au^{196}	9 ±6	0.55 ±0.06	28	5.4	3.2

[a] Errors are two standard deviations of counting statistics only.

[b] Calculated from the previous column by the formula $R\rho$, where ρ is the density of the target foil.

[c] Calculated theoretical expected range given by K. O. Nielsen (Reference 12, p. 73, Eq. (13)), where

$$R = 0.6 \cdot \frac{(Z_1^{2/3} + Z_2^{2/3})^{1/2}}{Z_1 Z_2} \cdot \frac{A_1 + A_2}{A_1} \cdot A_2 E_1 \ (\mu g/cm^2) ,$$

a formula based on a paper by N. Bohr.[11] The energy inserted in the formula is the average recoil energy.

[d] Estimated by assuming that the respective evaporated-neutron spectra were similar in shape to those observed for copper and lead. The average recoil energy is assumed to be about 1.5 times the most probable recoil energy.

[e] Range for C^{11} is in polystyrene (CH); for Cl^{34}, in saran (CHCl); and for F^{18}, in Teflon (CF_2). Other ranges are in their respective metallic lattices.

Table I--continued

[f] Range of C^{11} (for same recoil energy) in polyethylene (CH_2) and in cellulose acetate ($C_{1.0}H_{1.3}O_{0.7}$) are 10,600 ±1,100 Å and 11,900 ±1,800 Å, respectively.

[g] With the exception of the hydrogen atoms, it was assumed that the target atoms shared equally in stopping the recoiling atoms. Hydrogen atoms were neglected in the calculations.

incoming particle in kev. In the application of Nielsen's equation to the data of Table I, we have let Z_1, A_1, E_1 represent the recoiling atom and Z_2, A_2 represent the target atoms. For the data pertaining to the metals, Z_1 equals Z_2 and A_2 equals $A_1 + 1$. In calculating the theoretical ranges for the nonmetals (C^{11}, F^{18}, and Cl^{34}) in their respective plastic matrices, Z_2 and A_2 have been averaged stoichiometrically over the target-foil atoms, excluding the hydrogen atoms. Theoretical ranges calculated according to Nielsen are given in the last column of Table I. Agreement between calculated- and theoretical-range values is rather surprising (within a factor of two for most ranges), in view of the claim by Nielsen that the theoretical-range formula is not applicable when the recoiling atom and the target atoms are common--i.e., having the same Z, A--because the recoil atoms may lose all of their energy in a head-on collision with a common target atom.

Figure 1 shows that the fraction of metal atoms that recoil out of 0.001-in. foils varies exponentially with 1/A, while fluorine, chlorine, and carbon in the plastic matrices increase slowly with 1/A. If it is assumed that the photoneutron spectra of all the elements are centered at the same energy and have the same shape, then the abscissa of Fig. 1 essentially represents the energy of the recoil atoms. No explanation is offered for the data of Fig. 1, which depend on parameters, mass, energy, and lattice structures. By performing recoil experiments with photoproton, photodeuteron, and photoalpha transmutations, it will be possible to see the effect on N_c/N_f by varying the recoil energy only.

It should be noted that the N_c/N_f fractions for Cu^{62} and Cu^{64} agree well within experimental error. Since the photoneutron thresholds for Cu^{62} and Cu^{64} are nearly equal (10.7 and 10.0 Mev, respectively) and the corresponding photoneutron cross sections are roughly superimposable after normalization by a constant factor, the kinetic energies of the evaporated neutrons are expected to be identical. By measuring the average evaporated photoneutron energy, using the simple recoil technique outlined in this paper, it is possible to compare the nuclear temperatures of pairs of excited nuclei. The comparison should be restricted to a narrow range of atomic numbers because of the variation in recoil range with electronic structure.

Proton-energy spectra resulting from 22-Mev bremsstrahlung have been measured for at least fourteen photoproton reactions by nuclear-emulsion techniques. In general, the most probable proton energy is about 6 Mev.

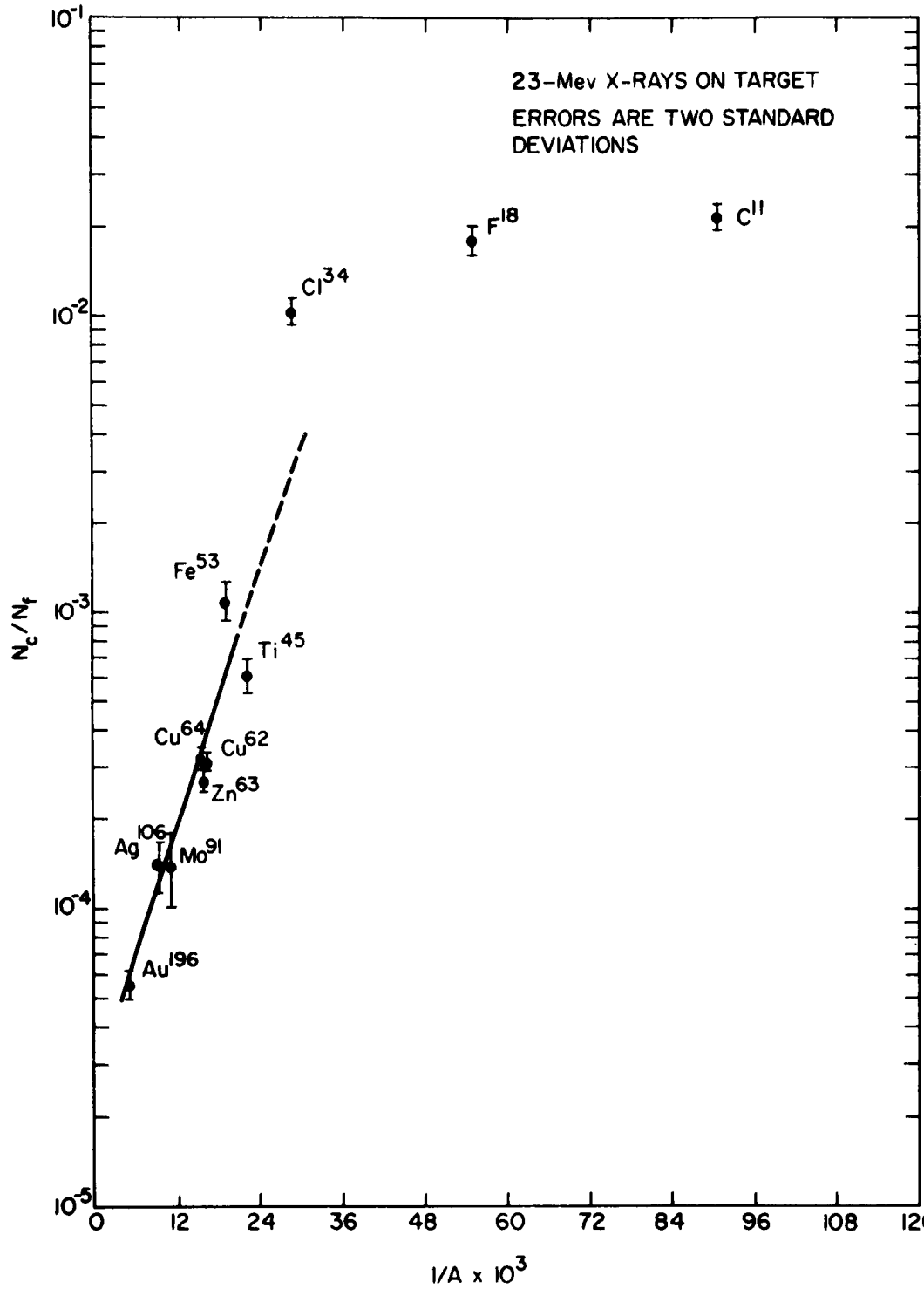

Fig. 1--Fraction of atoms, N_c/N_f, recoiling out of 0.001-in. foils as a function of inverse mass of recoiling atom, 1/A

The most probable proton energy and the corresponding energy width may be converted to the most probable recoil energy for the residual atom and the corresponding energy width. For example, recoil energies of such typical atoms as Li^{8}, Nb^{91}, and Hf^{180} have been observed to be about 200 ±80,[16] 60 ±40,[17] and 40 ±15 kev,[18] respectively. About 80% of the recoils are within the respective energy limits. Even higher recoil energies may be expected from photodeuteron, phototriton, and photoalpha reactions because the emitted particles are heavier and, in the case of photoalpha emission, more highly charged. By choosing the proper photoreaction, measurements may be made of the energies of other recoil atoms in the range 10 to 100 kev in lattices composed of similar materials and also in lattices of dissimilar materials, such as alloys and crystals.

REFERENCES

1. Everhart, E., G. Stone, and R. J. Carbone, Classical Calculation of Differential Cross Section for Scattering from a Coulomb Potential with Exponential Screening, Phys. Rev. 99, 1287 (1955) August 15.

2. Carbone, R. J., E. N. Fuls, and E. Everhart, Charge Analysis and Differential Cross Section Measurements for Large-Angle Argon Ion-Argon Atom Collisions with Energies between 25 and 138 kev, Phys. Rev. 102, 1524 (1956) June 15.

3. Fuls, E. N., P. R. Jones, F. P. Ziemba, and E. Everhart, Measurements of Large-Angle Single Collisions between Helium, Neon, and Argon Atoms at Energies to 100 kev, Phys. Rev. 107, 704 (1957) August 1.

4. Neufeld, J., Electron Capture and Loss by Moving Ions in Dense Media, Phys. Rev. 96, 1479 (1954) December 15.

5. Seitz, F., and J. S. Koehler, Displacement of Atoms during Irradiation, in F. Seitz and D. Turnbull (eds.), Solid State Physics, Vol. 2, Academic Press, Inc., New York (1956).

6. Allison, S. K., and S. D. Warshaw, Passage of Heavy Particles through Matter, Revs. Modern Phys. 25, 779 (1953) October.

7. Finkle, B., E. J. Hoagland, S. Katcoff, and N. Sugarman, Ranges of Fission-Recoil Fragments of Known Mass Numbers (III), in C. D. Coryell and N. Sugarman (eds.), Radiochemical Studies: The Fission Products, Book 1, National Nuclear Energy Series, Div. IV, Vol. 9, McGraw-Hill Book Company, Inc., New York (1951), p. 471.

8. Suzor, F., Parcours dans divers matériaux de fragments déterminés de fission de l'uranium, Ann. phys. 4, 269 (1949).

9. Leachman, R. B., and H. W. Schmitt, Fine Structure in the Velocity Distributions of Slowed Fission Fragments, Phys. Rev. 96, 1366 (1954) December 1.

10. Thulin, S., Studies in Nuclear Spectroscopy with Electromagnetically Separated Gaseous Isotopes. I. Isotope Separator and Sample Preparation, Arkiv Fysik 9, 107 (1955).

11. Bohr, N., The Penetration of Atomic Particles through Matter, Kgl. Danske Videnskab. Selskab, Mat.-fys. Medd. 18, No. 8 (1948).

12. Nielsen, K. O., Electromagnetically Enriched Isotopes and Mass Spectrometry, Academic Press, Inc., New York, and Butterworth and Co., London (1956), Paper No. 9, pp. 68-81.

13. Mileikowsky, C., Reaction Energy of O^{18} (p, α)N^{15} and the Atomic Mass of Oxygen 18, Arkiv Fysik 7, 89 (1954).

14. Byerly, P. R., Jr., and W. E. Stephens, Photodisintegration of Copper, Phys. Rev. 83, 54 (1951) July 1.

15. Toms, M. E., and W. E. Stephens, Photoneutrons from Lead, Phys. Rev. 108, 77 (1957) October 1.

16. Cohen, L., A. K. Mann, B. J. Patton, K. Reibel, W. E. Stephens, and E. J. Winhold, Photoprotons from Be, C, and O, Phys. Rev. 104, 108 (1956) October 1.

17. Butler, W. A., and G. M. Almy, Photoprotons from Mo^{100} and Mo^{92}, Phys. Rev. 91, 58 (1953) July 1.

18. Hoffman, M. M., and A. G. W. Cameron, Angular and Energy Distribution of Photoprotons from Aluminum and Tantalum, Phys. Rev. 92, 1184 (1953) December 1.

THE EFFECTS OF NUCLEAR IRRADIATION ON METALLIC AND NONMETALLIC MAGNETIC MATERIALS

by

E. I. Salkovitz, A I. Schindler, G. S. Ansell

U. S. Naval Research Laboratory
Washington, D. C.

Extensive investigations of the effects of nuclear environments upon magnetic materials have been undertaken. A major aim of the program is to obtain basic information concerning the mechanisms producing the observed effects. More than 100 samples have been irradiated in the Brookhaven graphite reactor at an integrated flux of 10^{17} NVT. The materials studied have been in the form of toroids or rods and have consisted mainly of various ferrites and square loop and high permeability alloys. In addition, discs of permanent-magnet type ferrites and portions of magnetic devices have been irradiated. A detailed discussion will be given of the method of canning temperature control,and the means by which pre- and post-irradiation magnetic measurements were made.

During the past decade there have appeared many papers on irradiation effects in many materials. Such effects on magnetic materials, however, have escaped concerted attention. A notable exception has been the work of Sery, Fischell, and Gordon[1] dealing primarily with several alloys. Consequently at the U. S. Naval Research Laboratory a broad program is underway to determine the changes which may occur in typical magnetic substances due to nuclear irradiation, and to investigate mechanisms which may account for these changes. The need for such a study is obvious. From the theorist's point of view, new information on the behavior of matter will be obtained. And from the practical point of view, there is a considerable degree of urgency for this type of data. As the application of nuclear energy increases there will be an accompanying increase in the use of magnetic devices operating in radiation fields. For example, it has come to the authors' attention that an accelerator is to be constructed using nearly a ton of a nickel ferrite. How such a ferrite will behave in a billion electron volt accelerator at the operating frequency is an unanswered question because the appropriate investigations have not been conducted yet.

At the outset it must be appreciated that an investigation of irradiation effects is in a sense an investigation of environmental effects. Consequently, it is not only mandatory to know as much as possible about the material under study, it is

equally necessary to be able to delineate the various environmental parameters. Unfortunately this latter task is a very formidable one. If a given reactor is used for the study it is desirable to state the power level (which may vary during the test), the ambient temperature in the vicinity of exposure, the energy spectrum of radiation, and the total flux received by the material studied. On the other hand the research should be so conducted that the effects may be discussed in terms of the influence of the specific variables already mentioned and in addition to these such parameters as dose rate and recovery processes which may occur during and after irradiation. It should be clear therefore that the program discussed here is to be considered still in the exploratory stage. Sufficient results have been uncovered which are worth reporting, but which indicate that further study is required.

To complement an investigation of the behavior of irradiated ferrites in the microwave region, it is desirable to examine the behavior in the D.C. and 60 cycle region. For the sake of expediency a variety of commercially available ferrites have been studied. Very serious disadvantages exist with this approach. Usually the exact chemical composition and manufacturing procedures are complicated and trade secrets. Studying commercial ferrites however furnishes immediate information on materials of practical importance. Suffice to say that experiments on more controllable ferrites are underway and will be reported in the near future.

Four separate sets of experiments were conducted using the Brookhaven reactor operating between 15 and 22 megawatts. During each run, ferrites and magnetic alloys (which were also studied) were distributed in aluminum cans over a 3 or 4 foot portion of a channel in the reactor. Consequently the total integrated flux (fast) received by the different samples varied between the limit of 6×10^{16} NVT and 3×10^{17} NVT. By means of forced air cooling the temperatures of all samples were kept below 75°C and some as low as 30°C. Approximately 100 ferrite samples of about 20 different compositions were studied, as well as 35 metal alloy samples of 9 different compositions.

To obtain 60 cycle hysteresis loops, toroids were wound with appropriate primary and secondary coils. Groups of 4 to 7 such toroids were then mounted on a sample holder. Figure 1 shows such a sample holder patterned after that of the early work of Sery, Fischell and Gordon. As can be seen, leads from the coils were connected to ceramic octal receptacles. Electrical connections could then be made with a hysteresis loop-tracer[2] and the loops presented on an X-Y recorder. These measurements were made remotely, both before and after irradiation, using the same equipment and all measurements were made in the hot cell facilities of the U. S. Naval Research Laboratory. When the "before" measurements were completed, the

toroids mounted on their sample holders were placed in aluminum cans, shipped to the Brookhaven National Laboratory and inserted in the reactor with coils intact. After exposure the units were returned, their radioactivity measured and hysteresis loops again obtained. Figures 2 through 8 are representative of the effects of the irradiation upon several different types of ferrites. The hysteresis loops shown are direct reproductions of the loops presented on the X-Y recorder. For purposes of comparison we note in Table I, changes in the remanence Br, the coercive force H_C and the ratio B_m/Br where B_m is the maximum flux density. If a 10 percent change in any of these parameters arbitrarily is considered to be insignificant, then Samples IV and II which are nickel, zinc, manganese ferrites, and Sample VI which is a complex ferrite containing mixtures of oxides of nickel, zinc-manganese, magnesium, and copper may be assumed to have been unaffected. All other ferrites showed larger changes.

The kinks which appeared in the hysteresis loops of Sample VIII (Mn, Zn ferrite) and Sample IX (Ni, Zn, Cu ferrite) after irradiation, are reproducible. Such kinks appeared in more pronounced fashion in several irradiated alloys. Although the work on alloys will be covered in detail in a paper in preparation it is germaine to indicate a similarity between the "kink" phenomena in irradiated ferrites and in alloys. Such "kinks" in hysteresis loops have been found in unirradiated permalloys and have been studied elsewhere. These kinks may be associated with the order-disorder processes which occur during the thermal history of the material. Figure 9 shows loops for a 4-79 Mo Permalloy before and after irradiation. The kinks in the "after" curve are quite apparent. In Figure 10 are the loops for a sample of Mumetal. Figure 10a shows the "before" curve, Figure 10b and Figure 10c show "after" irradiation loops obtained for two different exposures. Since these were exploratory experiments, the radiation flux was not carefully monitored, so that it was quite possible that the radiation environment was very different for the two runs. The important feature is that the two loops are different (Figures 10b and 10c) but are the types of loops which are found when the ordering treatment is interrupted and hysteresis loops obtained for permalloy type of alloys. It is conceivable that for the ferrites a similar explanation may be offered. However, this phenomena is under investigation and should not be discussed until further data is available. Additional results on a variety of commercial alloys are shown in the succeeding figures.

As an exploratory experiment in which the ratio of thermal, to epi-thermal, to fast neutrons was varied, two samples of a particular ferrite were placed in close proximity in the reactor. One of these however was wrapped in cadmium foil. Table II indicates that the energy spectrum of the neutrons

does influence the effects observed. Obviously more work of this nature is desired.

The effect of irradiation upon the Curie temperature of all the ferrites were investigated by Mr. Glenn C. Bailey of this Laboratory. For this experiment the samples received a total flux of 1.24×10^{17} NVT (fast). No change in the Curie temperature was found for any of the ferrites.

The preliminary results of still another experiment may be of interest. The effect of irradiation (1.24×10^{17} NVT fast) upon the magnetic moment of α Fe_3O_4 and γ Fe_2O_3 has been obtained by Dr. W. E. Henry and one of the authors (EIS). Whereas the moment was found to decrease by 25 percent in the case of α Fe_3O_4 a decrease of only 2 percent was found for γ Fe_2O_3. This strongly suggests, as would be expected, that the radiation produces a redistribution of the cations. Neutron diffraction experiments are underway to determine if this is the case.

From the foregoing it is apparent that certain magnetic properties of the materials investigated may be altered by neutron irradiation. These are primarily the structure sensitive properties. The degree of the effect varies with the chemical composition and past history of the material. Both factors of course determine the cation distribution. Sufficient variables however have been uncovered that until further controlled experiments are conducted it would be unwise to dogmatically advance mechanisms for the observed effects. Having uncovered these effects in the very low frequency region it is now desirable to investigate the behavior of irradiated ferrites at higher frequencies. This will be discussed in a forthcoming paper.

ACKNOWLEDGEMENTS

We wish to thank Mr. L. Steele, LT. R. Howthorne and Mr. F. Newman, for furnishing considerable assistance in getting the materials irradiated, in performing many of the operations in the hot cell, and for taking care of numerous details which were required to successfully perform the experiments.

We also wish to thank the General Ceramics Corporation, Radio Corporation of America. Indiana Steel Products Company, Ferroxcube Corporation of America, Allegheny Ludlum Steel Corporation, and Crucible Steel Company for furnishing many of the samples studied in this investigation.

REFERENCES

(1) Sery, R. S., Fischell, R. E., and Gordon, D. I., Conference on Magnetism and Magnetic Material, Oct 1956 (AIEE, Feb 1957).

(2) Geyger, W. A., Proc. Natl. Electronics Conference (1956), Vol. 12.

FIGURE CAPTIONS

Fig. 1 - Sample holder used for irradiation experiments.
Fig. 2 - Hysteresis loops before and after irradiation for a commercial nickel ferrite.
Fig. 3 - Hysteresis loops before and after irradiation for a commercial nickel, zinc, manganese ferrite.
Fig. 4 - Hysteresis loops before and after irradiation for another commercial nickel, zinc, manganese ferrite.
Fig. 5 - Hysteresis loops before and after irradiation for a commercial nickel, zinc, manganese, magnesium ferrite.
Fig. 6 - Hysteresis loops before and after irradiation for a commercial nickel, zinc, copper ferrite.
Fig. 7 - Hysteresis loops before and after irradiation for another commercial nickel, zinc, copper ferrite.
Fig. 8 - Hysteresis loops before and after irradiation for a commercial manganese, zinc ferrite.
Fig. 9 - Hysteresis loops before and after irradiation for a commercial 4-79 Permalloy.
Fig. 10 - Hysteresis loops before and after irradiation for a commercial Mumetal. (b) and (c) represents two different samples irradiated at different times.

Figs. 11 thru 16 - Hysteresis loops before and after irradiation for commercial alloys as indicated.

TABLE I

Effect of Irradiation on the Coercive Force, Remanence and B_m/B_r for Various Ferrites

Fig. No.	Sample No.	Oxide Constituents	Applied H Max.	ΔH_c	ΔB_r	$\Delta \frac{B_m}{B_r}$
2	XII	NiO, Fe_2O_3	14 oersteds	- 8%	- 36%	+ 25%
-	X	NiO, ZnO, Fe_2O_3	7 oersteds	+ 22%	- 9%	+ 9%
3	IV	NiO, ZnO, Mno, Fe_2O_3	20 oersteds	0	+ 5%	- 3%
4	II	NiO, ZnO, MnO, Fe_2O_3	25 oersteds	0	+ 7%	- 3%
-	V	NiO, ZnO, MnO, MgO, Fe_2O_3	14 oersteds	+106%	- 15%	- 4%
5	III	NiO, ZnO, MnO, MgO, Fe_2O_3	6 oersteds	+ 14%	- 12%	+ 6%
6	IX	NiO, ZnO, CuO, Fe_2O_3	3 oersteds	+ 30%	- 17%	+ 18%
7	VII	NiO, ZnO, CuO, Fe_2O_3	25 oersteds	+ 21%	- 15%	+ 20%
-	XI	NiO, ZnO, MnO, MgO, Fe_2O_3	9 oersteds	+ 40%	- 6%	+ 6%
-	XIII	MgO, MnO, Fe_2O_3	25 oersteds	+ 48%	- 1%	+ 1%
8	VIII	MnO, ZnO, Fe_2O_3	5 oersteds	+ 6%	- 20%	+ 24%
-	VI	NiO, ZnO, MnO, MgO CuO, Fe_2O_3	2 oersteds	+ 5%	0	+ 2%

TABLE II

Sample	Total Thermal Flux (NVT)	Total Epi-Thermal Flux (NVT)	Total Fast Flux (NVT)	ΔH_c	ΔB_r	$\Delta \frac{B_m}{B_r}$
X	5.4×10^{18}	8.0×10^{17}	12.0×10^{16}	+246%	+232%	-69%
Y	3.2×10^{18}	14.0×10^{17}	6.0×10^{16}	+146%	+325%	-75%

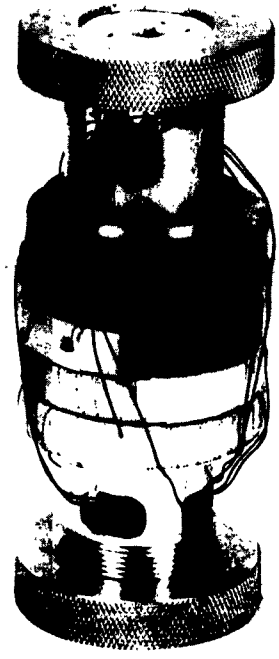

Figure 1

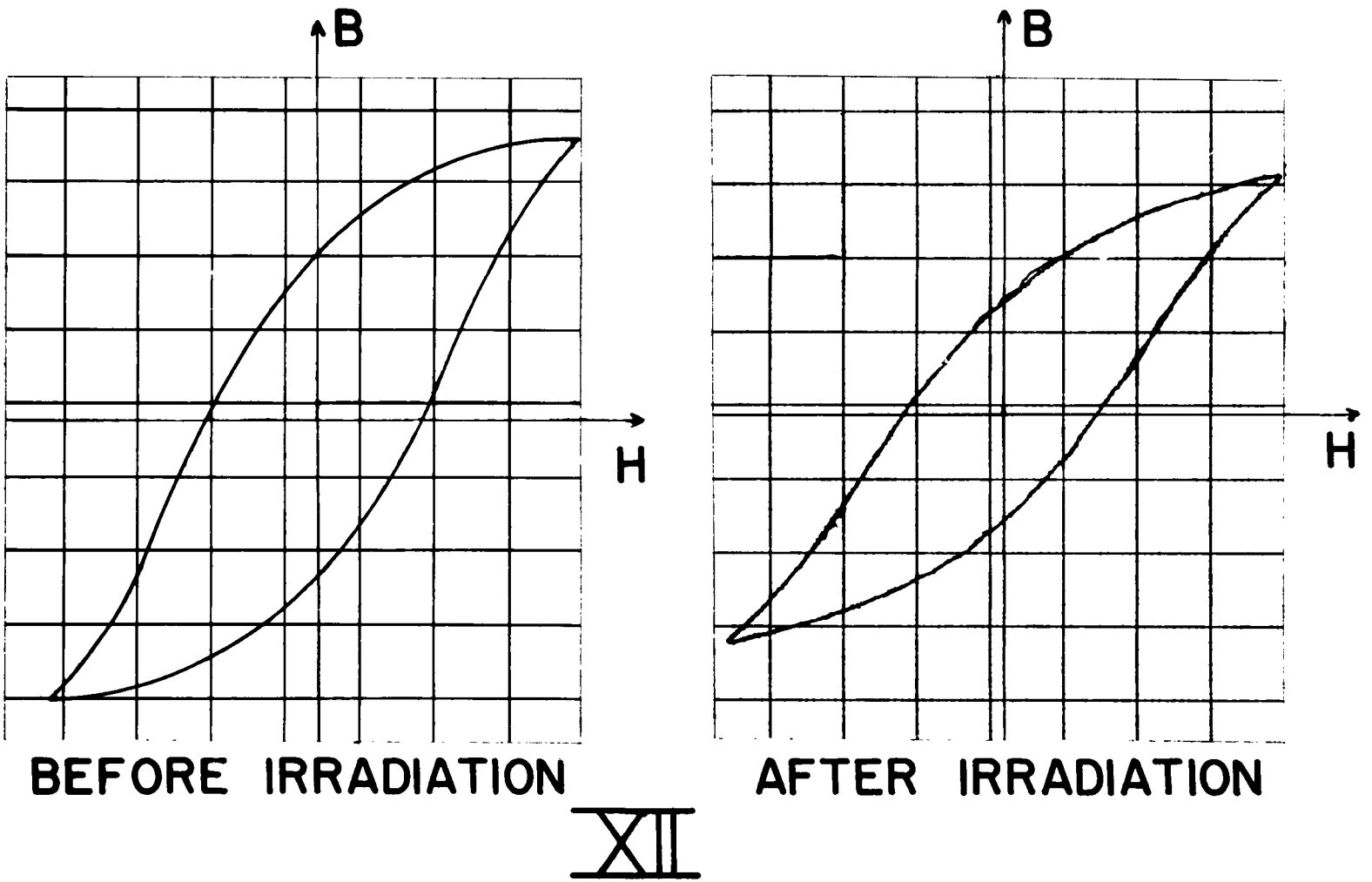

Figure 2

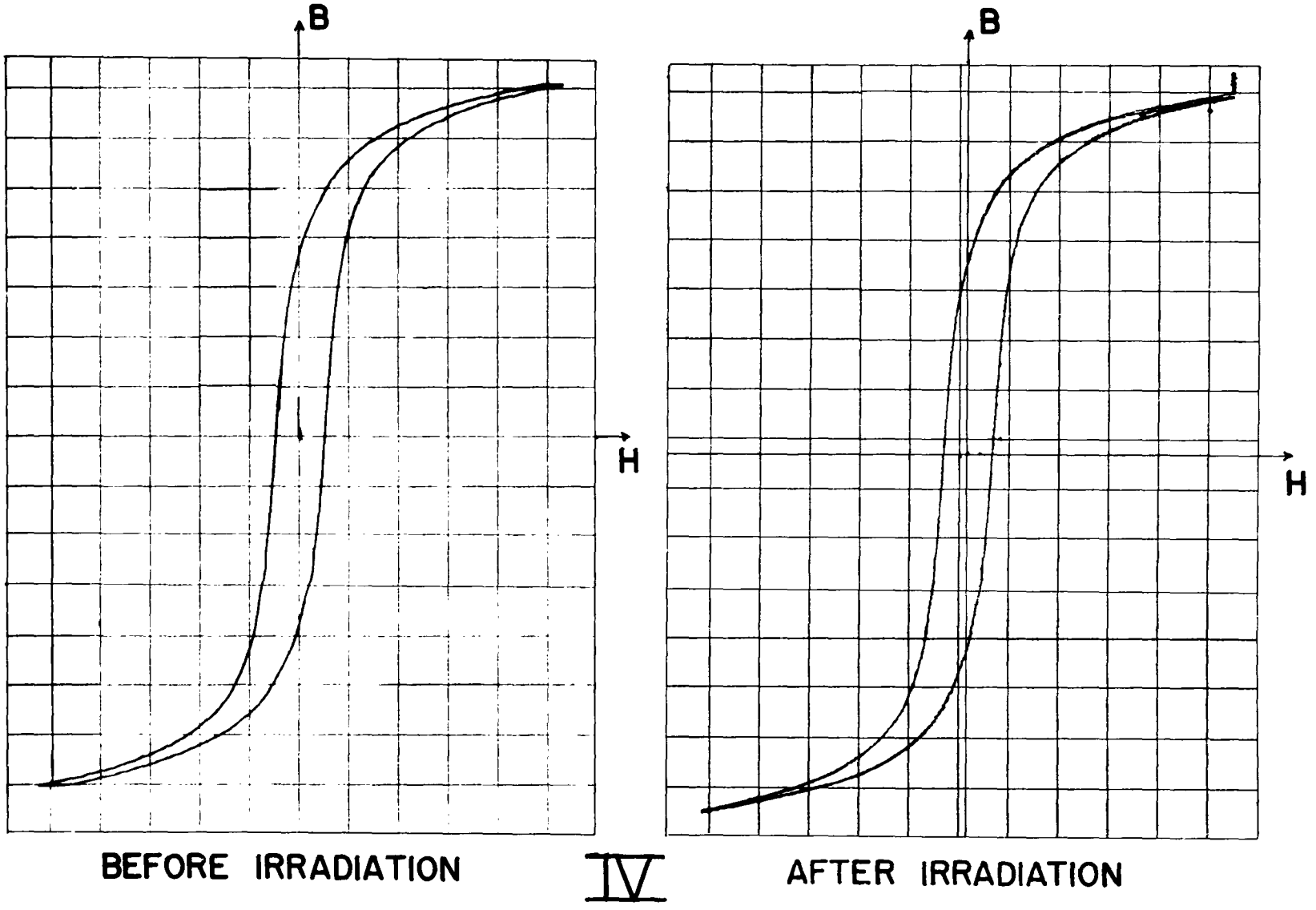

Figure 3

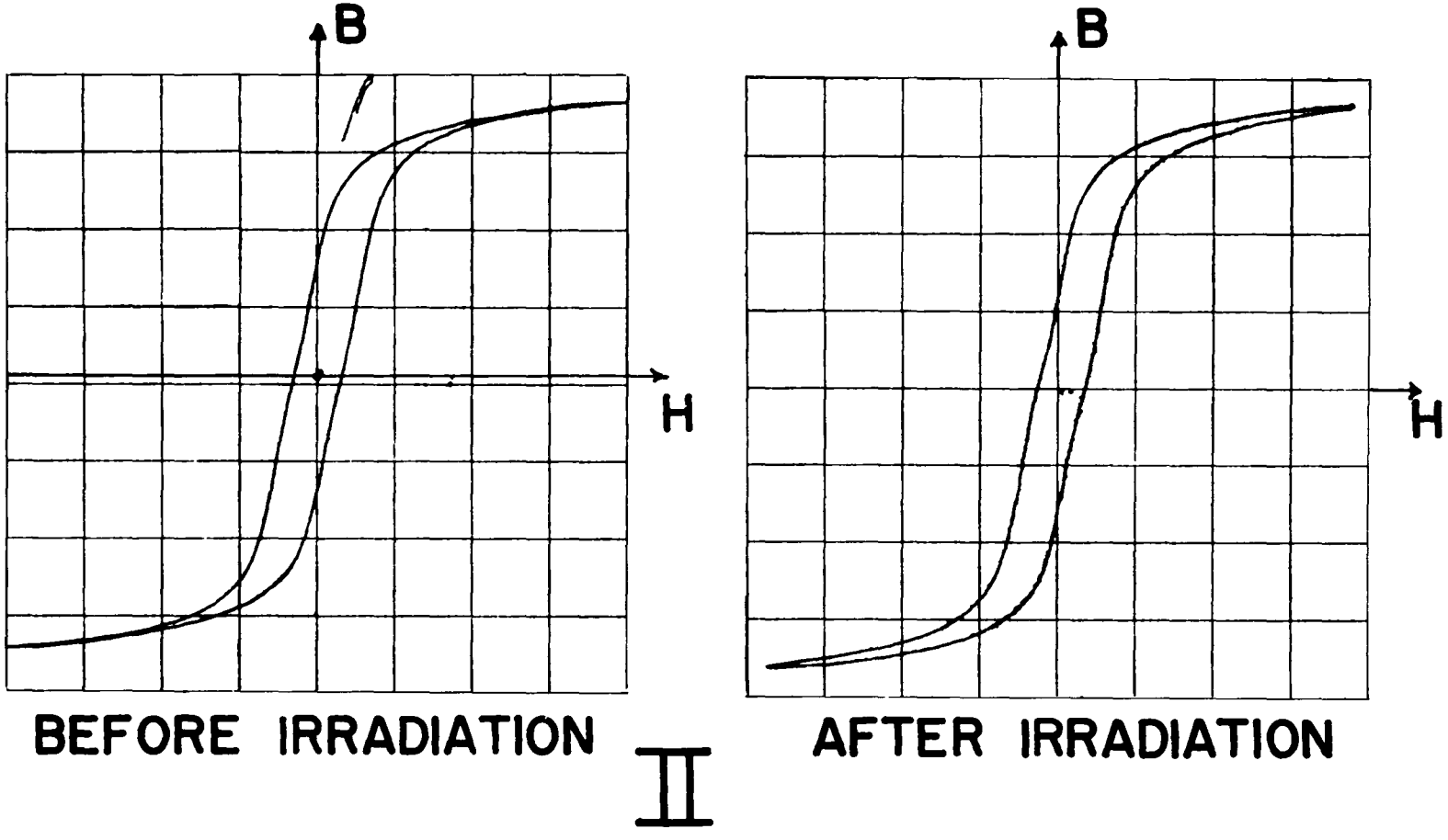

Figure 4

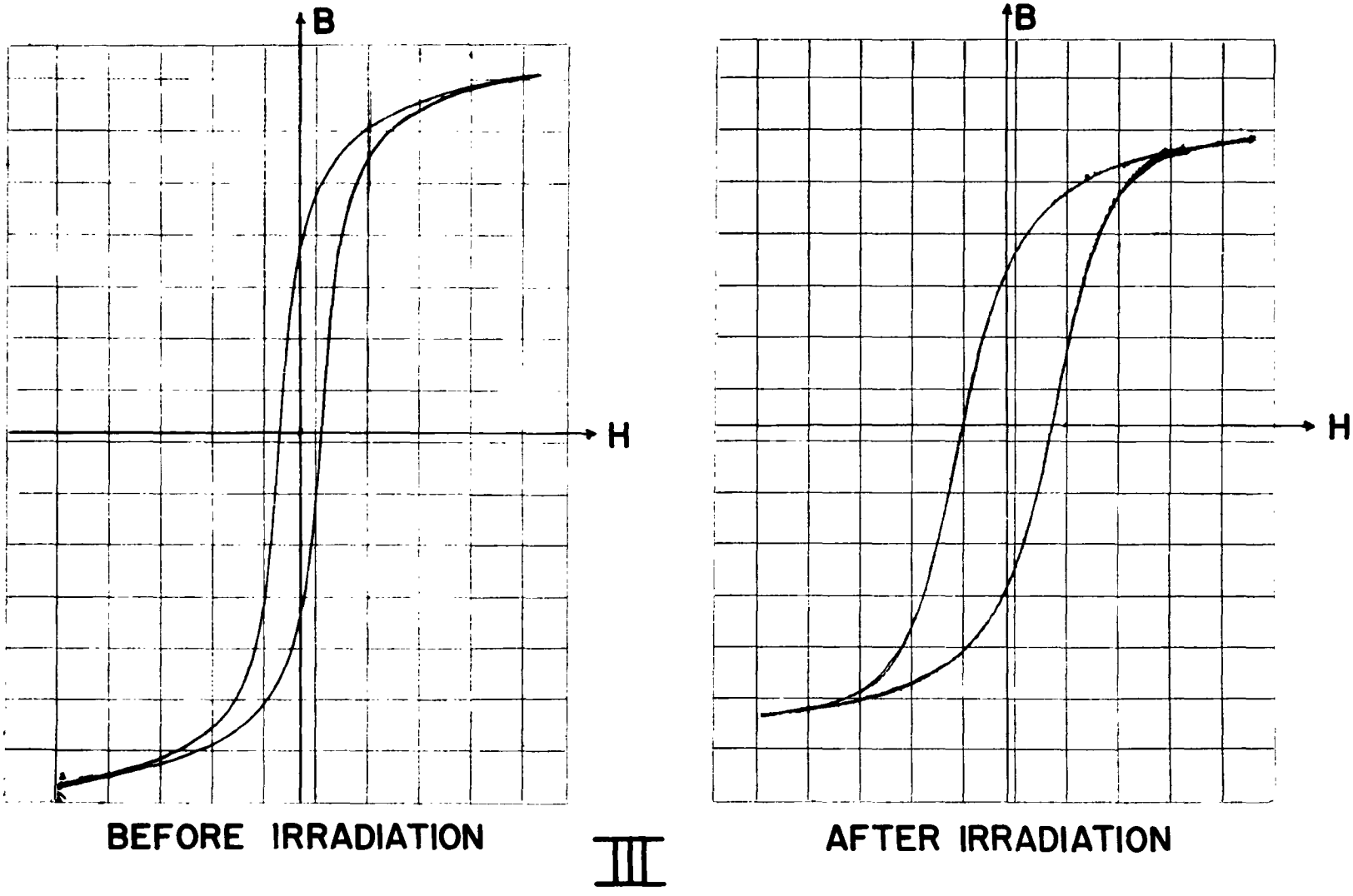

Figure 5

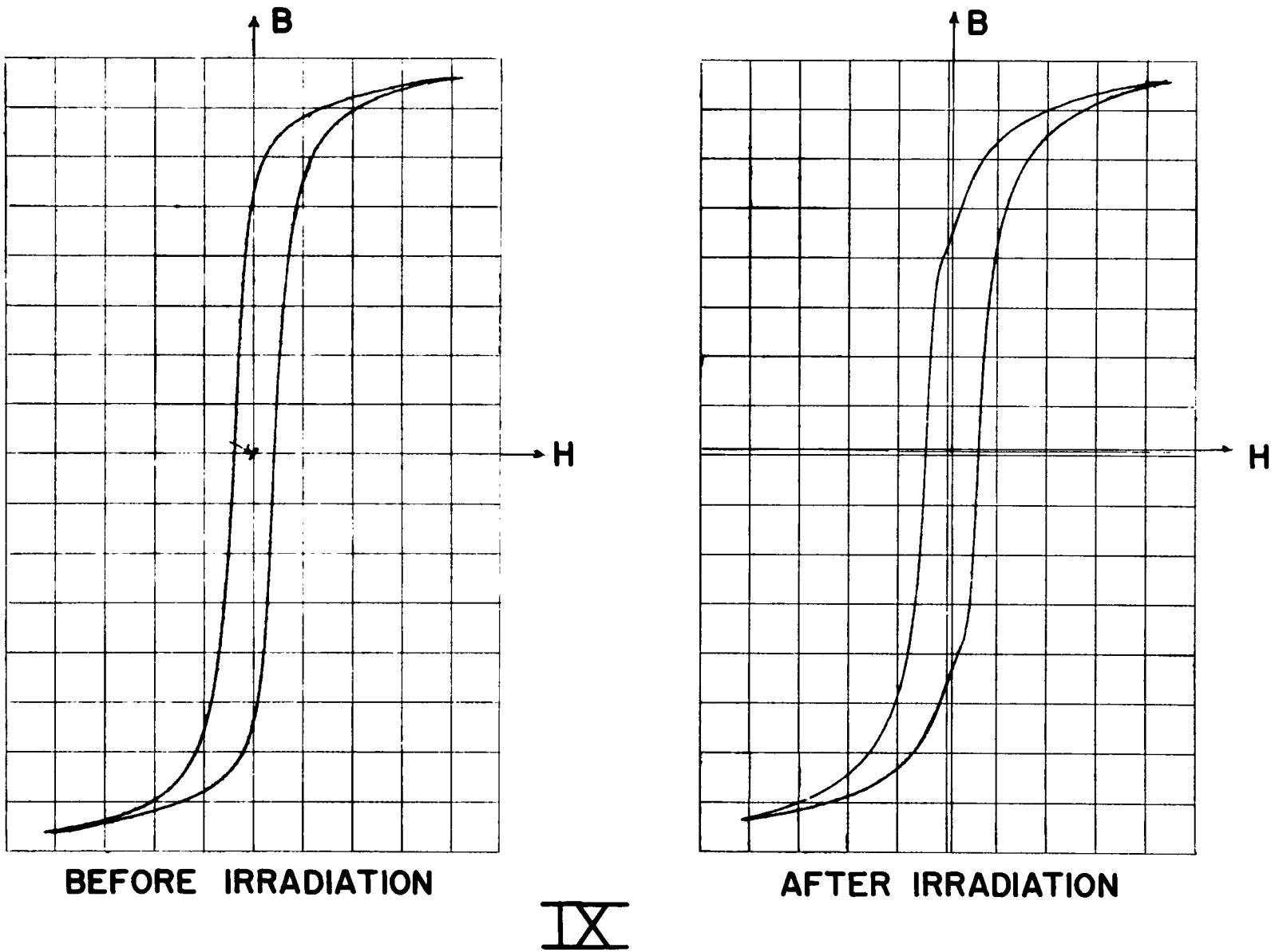

Figure 6

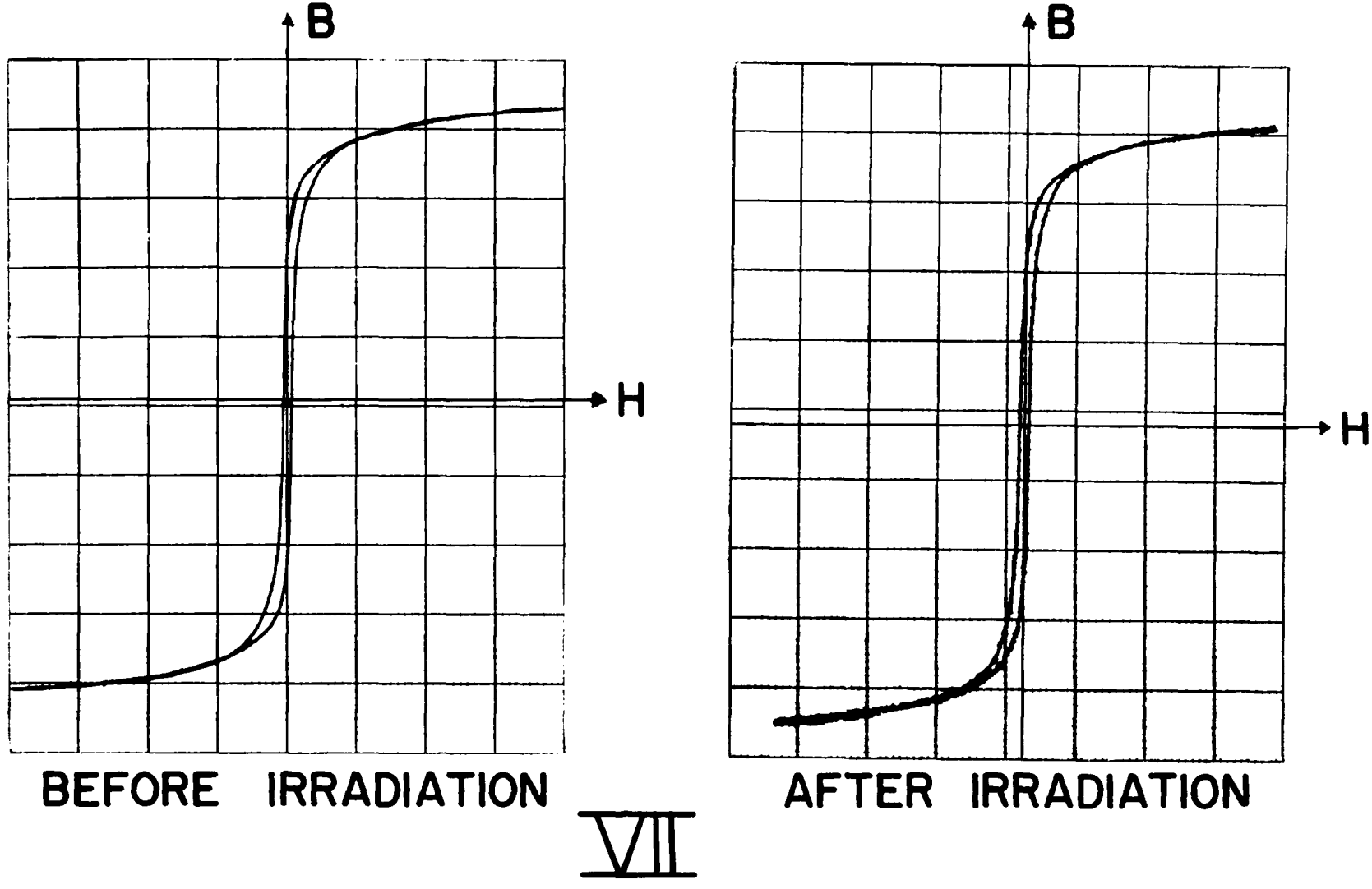

Figure 7

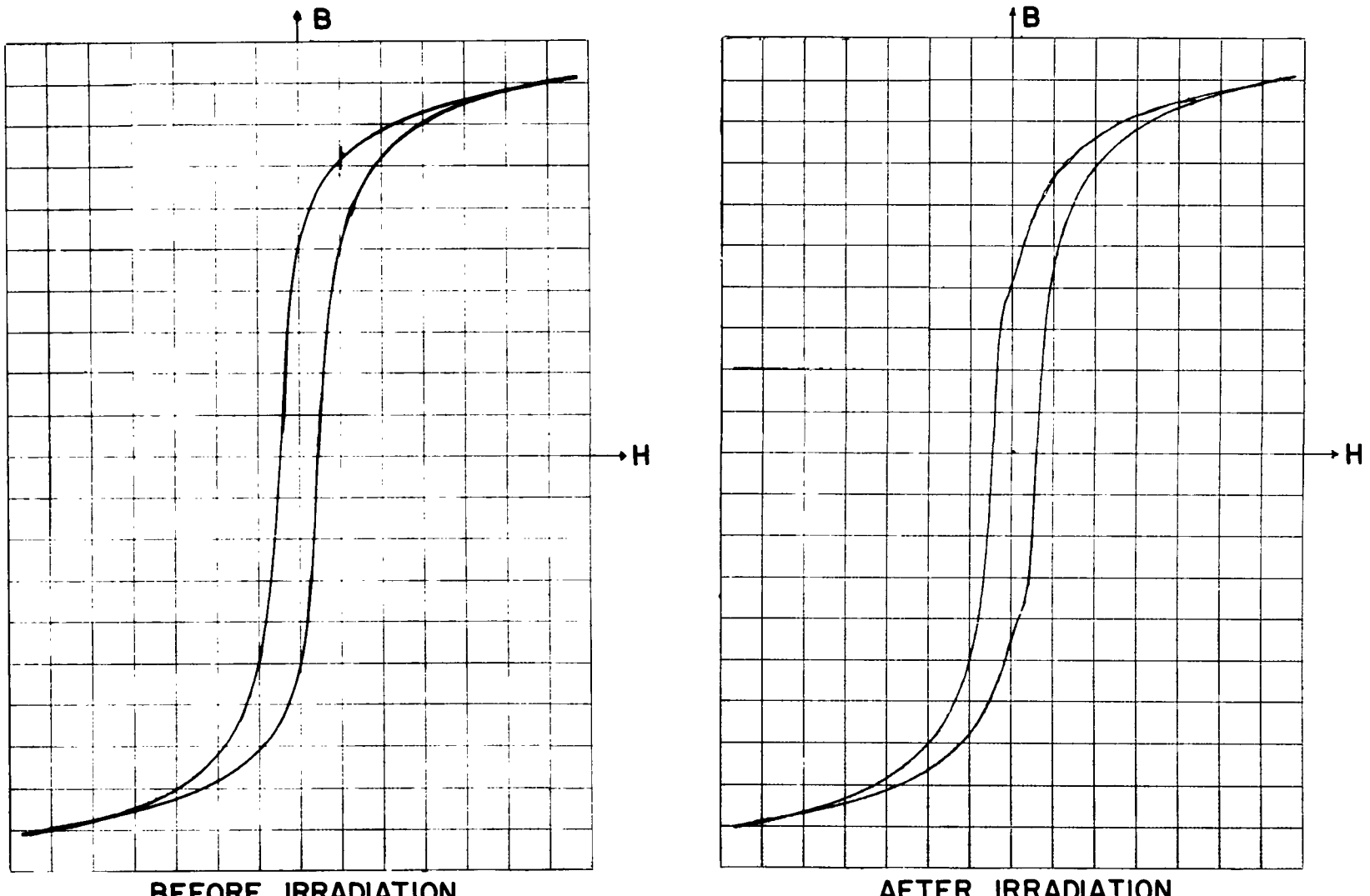

Figure 8

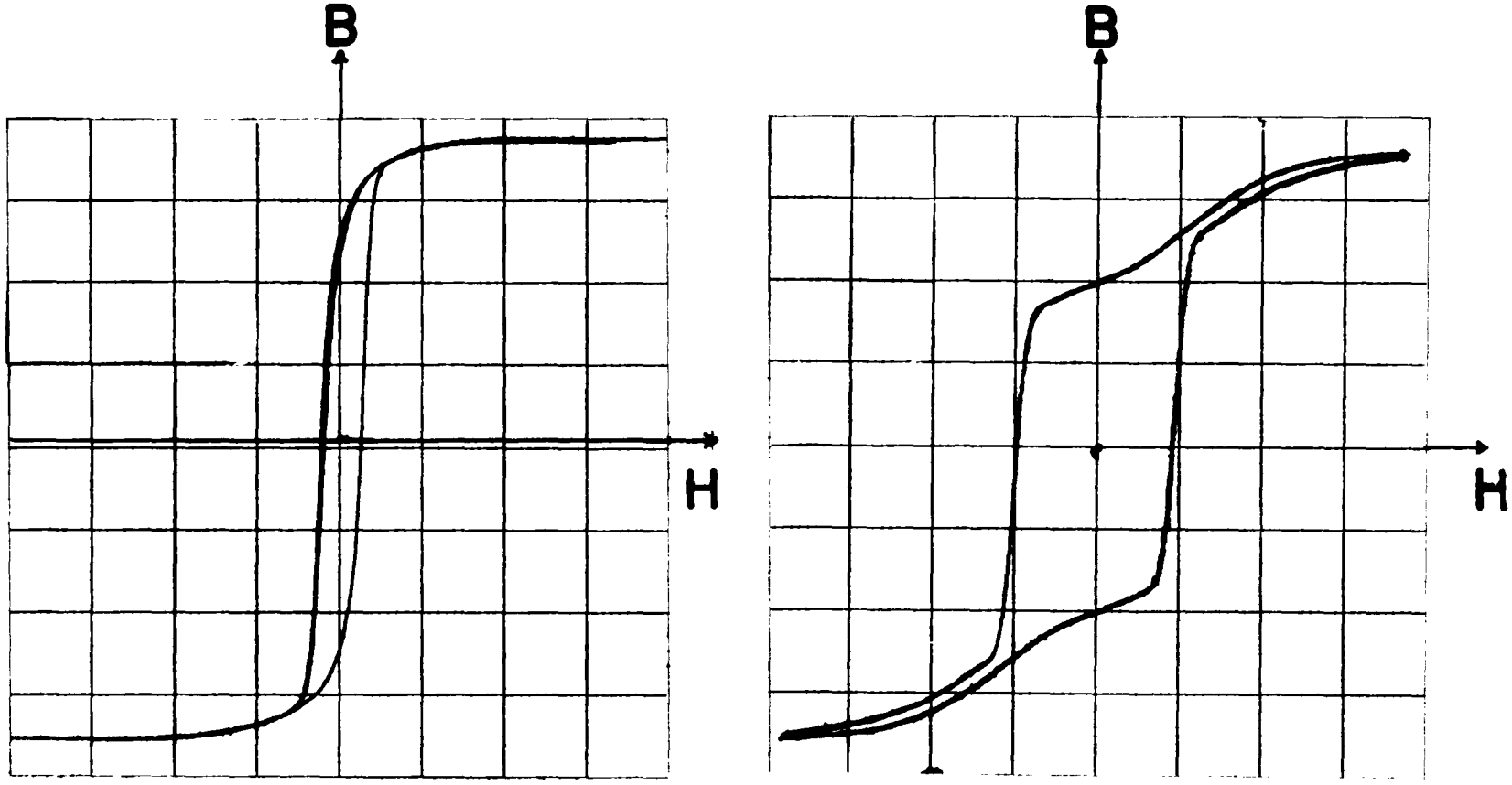

Figure 9

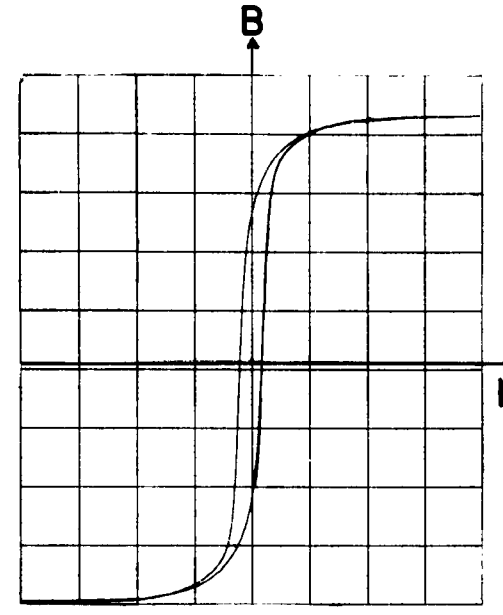

BEFORE IRRADIATION

(a)

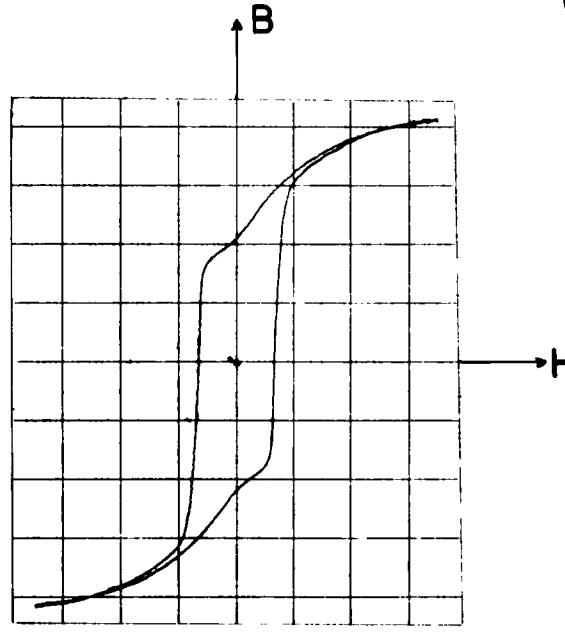

AFTER IRRADIATION

(b)

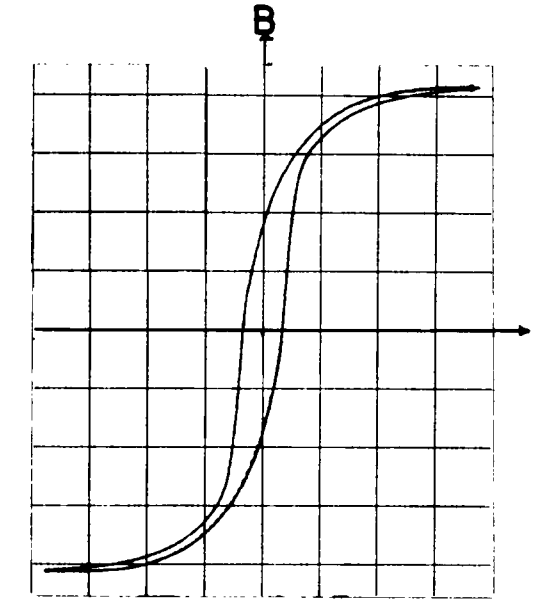

AFTER IRRADIATION

(c)

MUMETAL

Figure 10

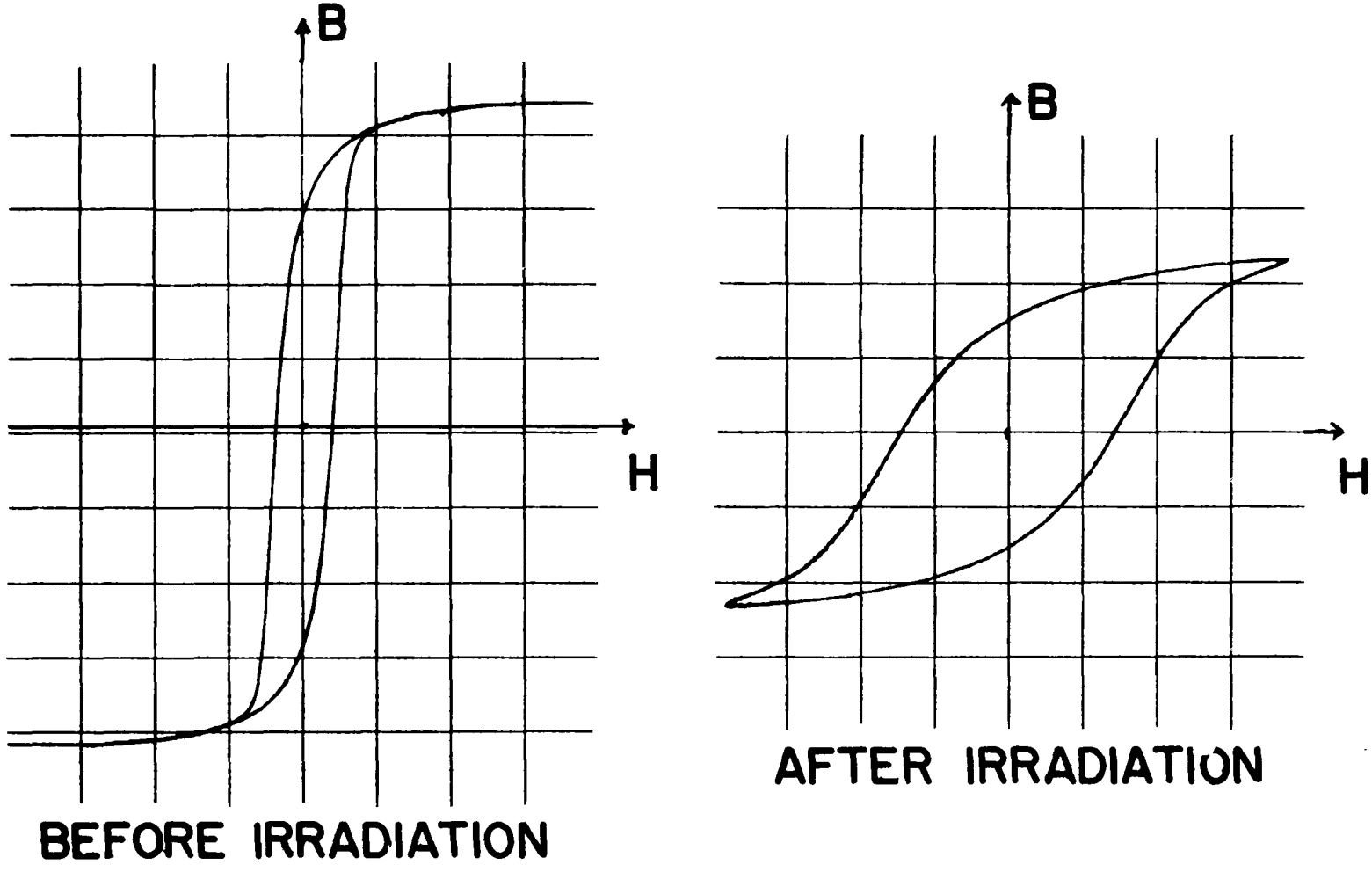

Figure 11

5-79 Mo PERMALLOY

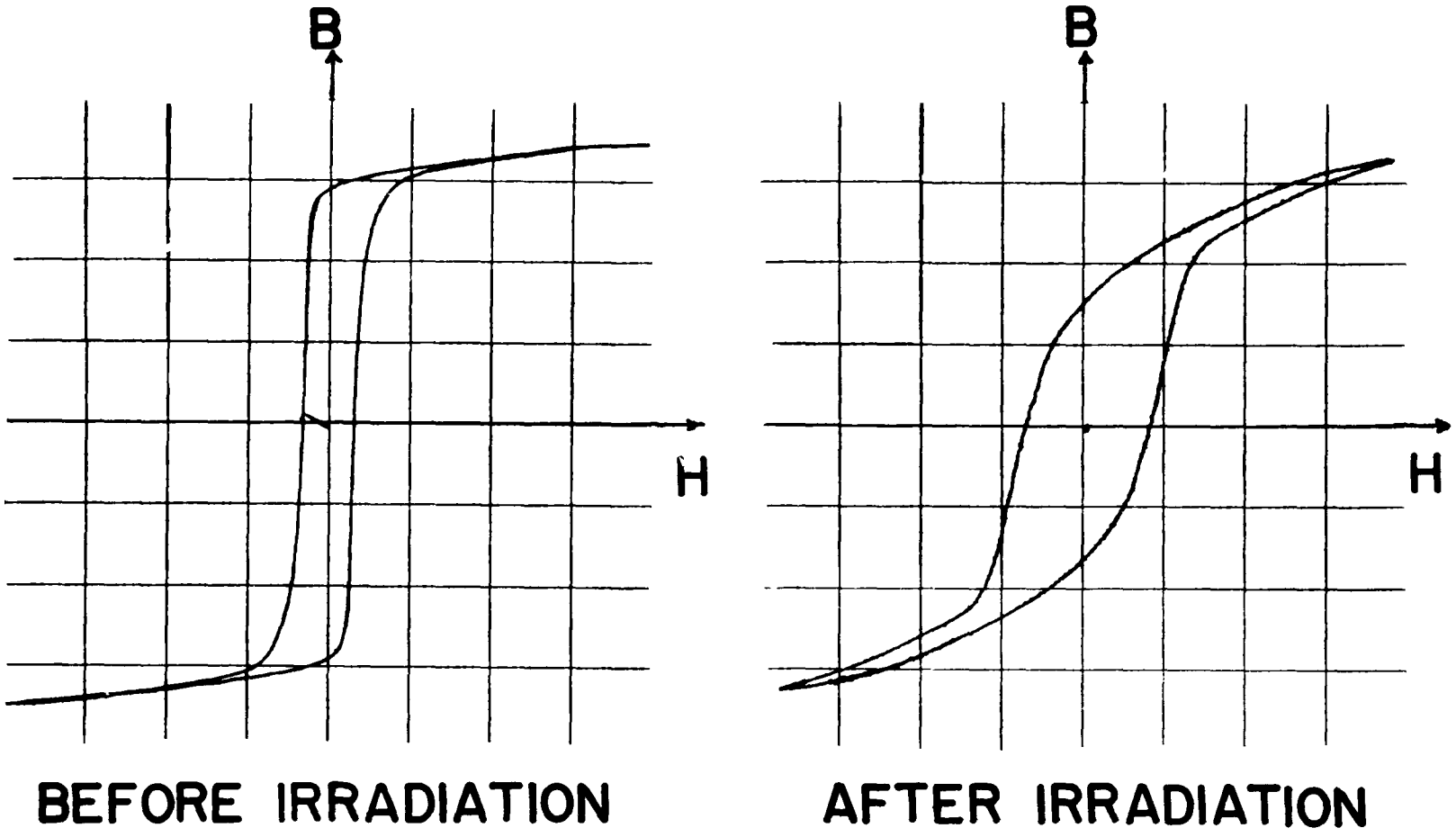

Figure 12

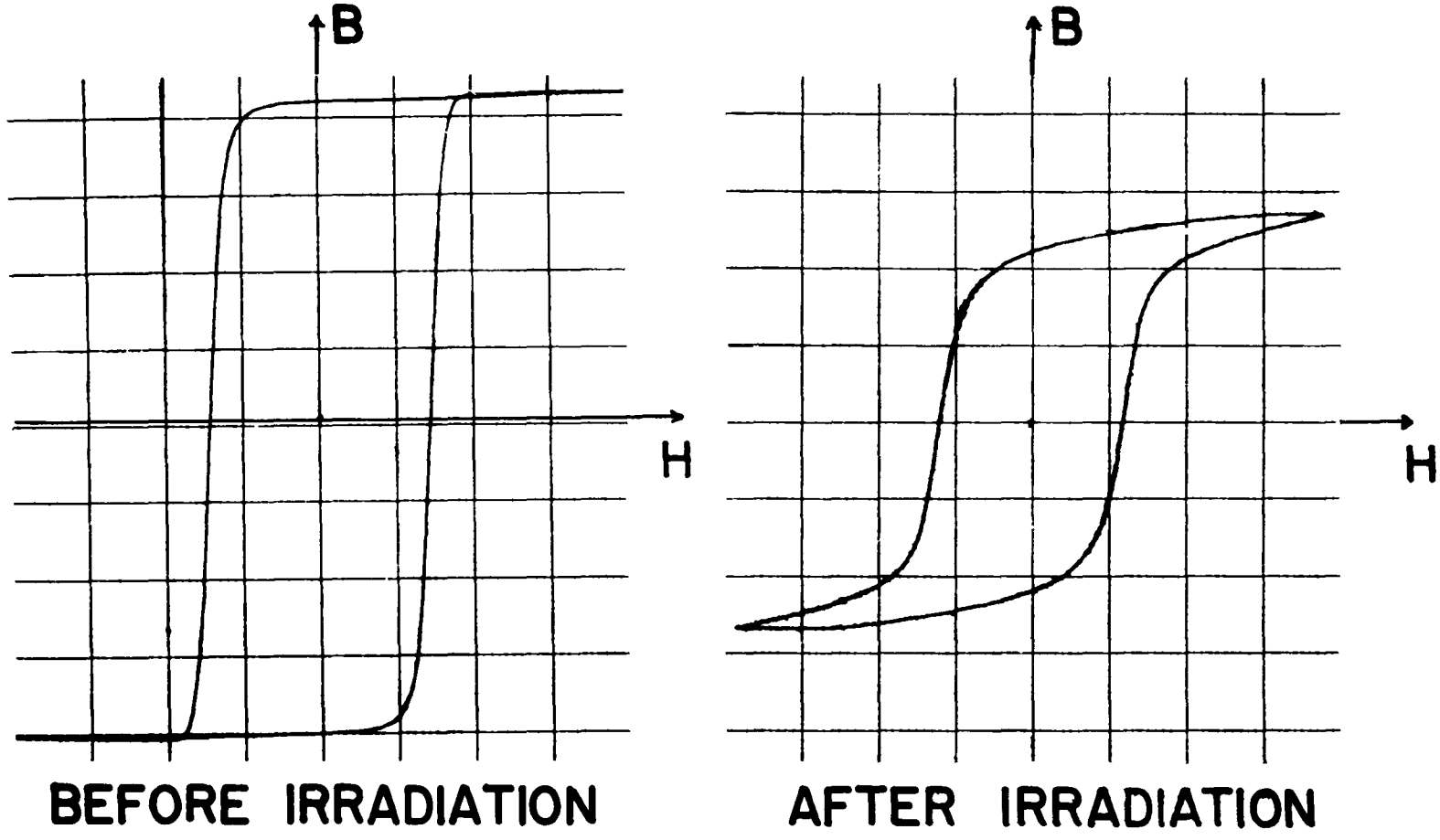

SQUARE LOOP Fe Ni

Figure 13

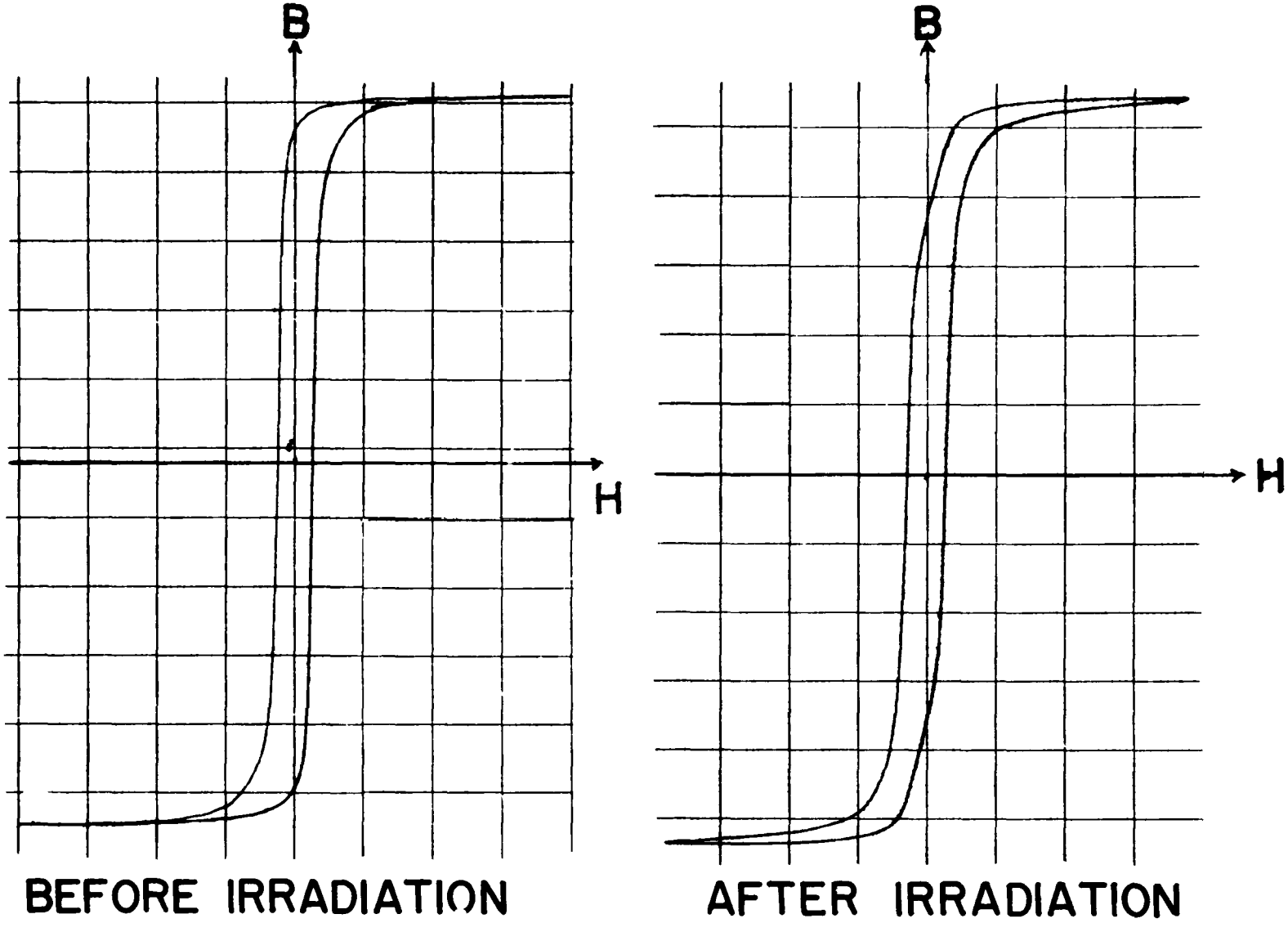

3 Mo 47 Ni 50Fe

Figure 14

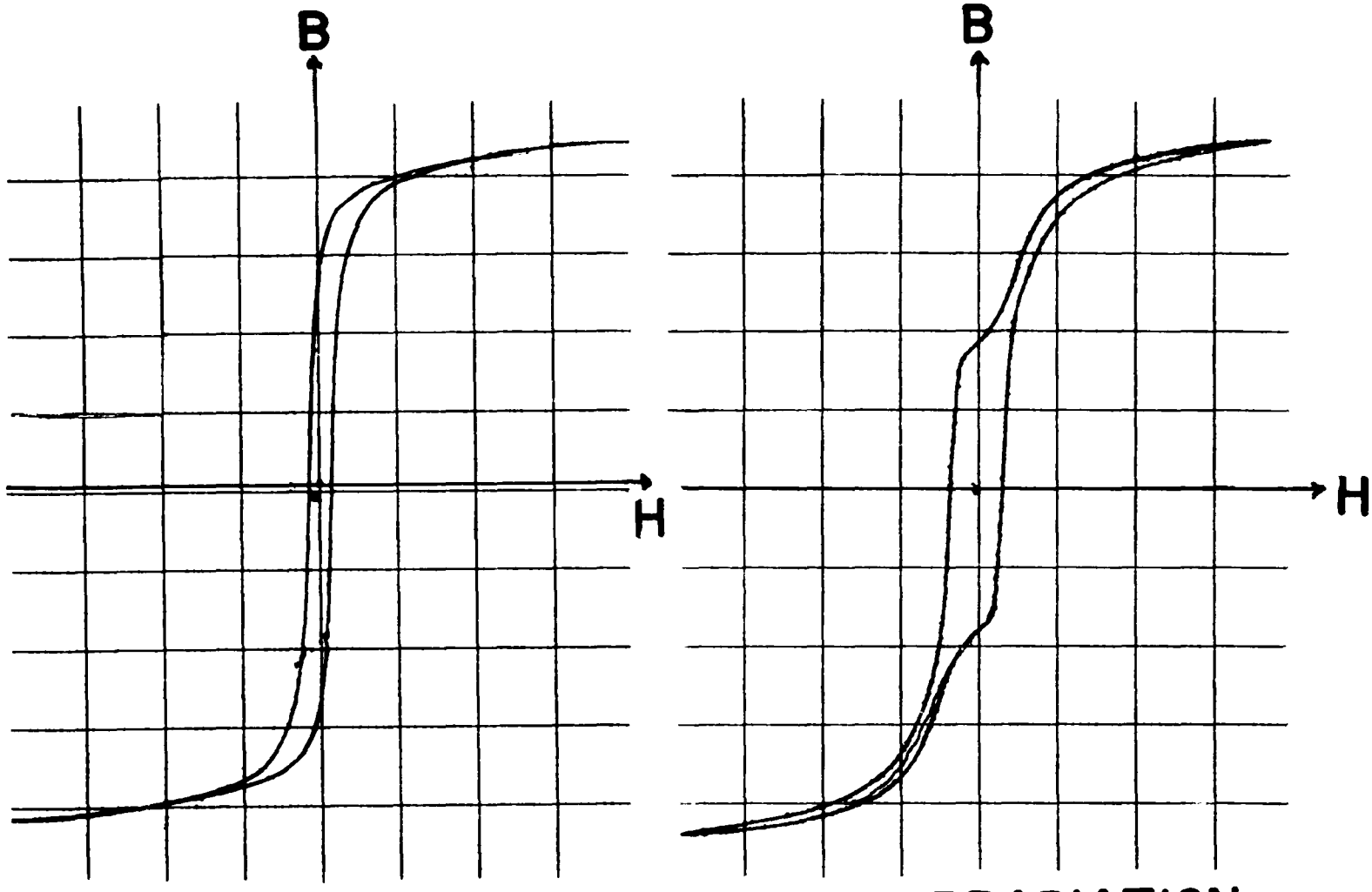

Figure 15

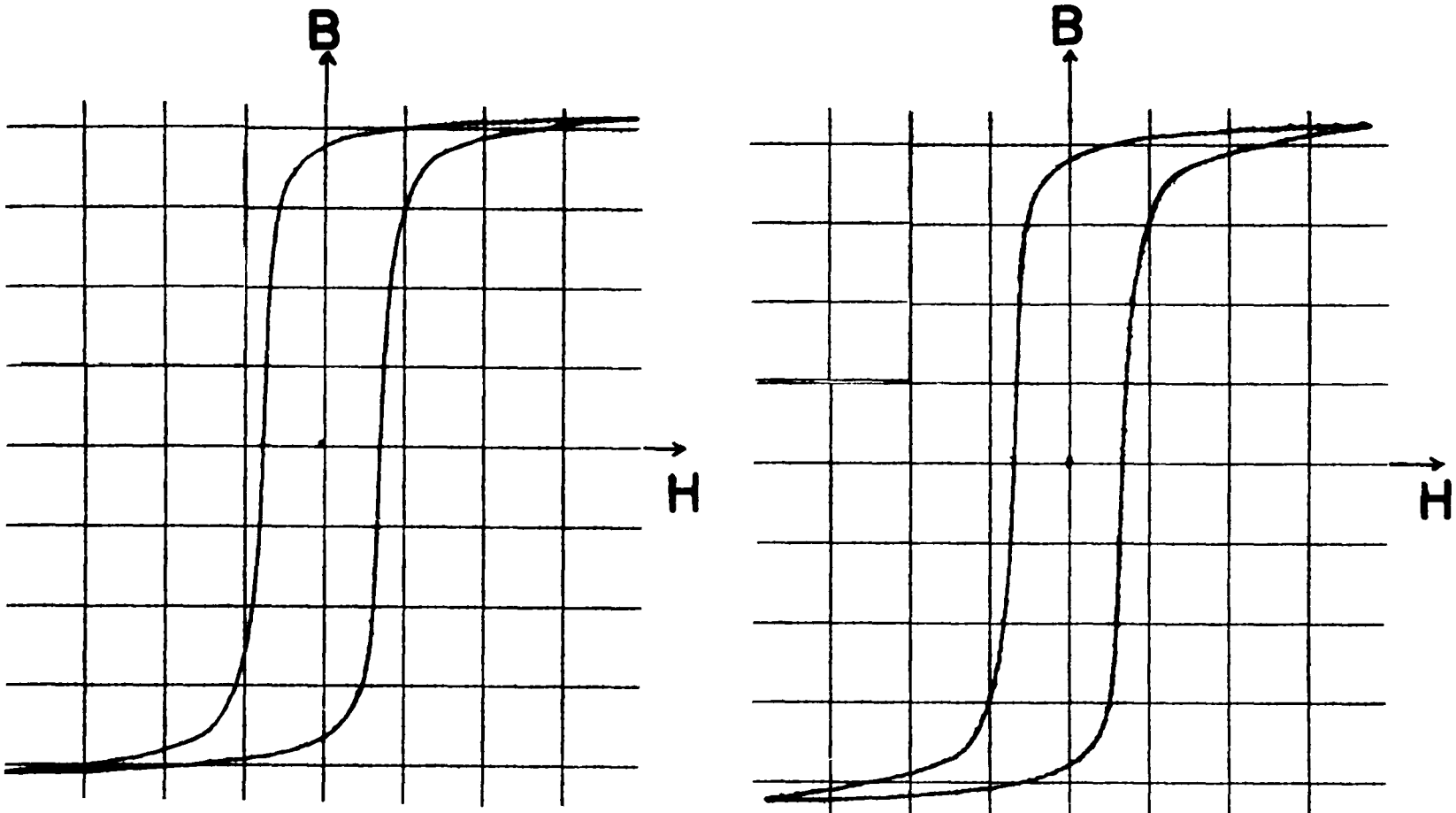
B
H
B
H
BEFORE IRRADIATION
AFTER IRRADIATION
3% GRAIN ORIENTED SILICON STEEL

Figure 16

THE EFFECT OF NUCLEAR RADIATION ON COMMUNICATIONS SET AN/ARC-34

by

D. L. JACOBS

Convair
A Division of General Dynamics
Fort Worth, Texas

Two AN/ARC-34 UHF Command Communications Systems were exposed to high energy neutron and gamma radiation from the Ground Test Reactor. When set number C-3735 failed due to radiation induced damage to a 1N69 crystal diode it had received an integrated epicadmium neutron flux of 4.68×10^{13} neutrons/cm^2 and an integrated gamma dose of 4.71×10^{6} Roentgen. When set number C-3731 failed due to radiation induced damage to a 1N69 crystal diode it had received an integrated epicadmium neutron flux of 4.22×10^{13} neutrons/cm^2 and an integrated gamma dose of 7.03×10^{6} Roentgen. A second failure occurred in set number C-3731 at an integrated epicadmium neutron flux of 2.82×10^{14} neutrons/cm^2 and an integrated gamma dose of 4.7×10^{7} Roentgen when a 0.22 microfarad paper capacitor failed. No transient responses were noted in system performance while subjected to radiation.

This paper is classified and is bound in Volume Six.

RADIATION TESTING OF J-79 ORGANIC ENGINEERING MATERIALS AND COMPONENTS

by

D. E. BARNETT
Aircraft Nuclear Propulsion Department
General Electric Company
Cincinnati, Ohio

A number of organic engineering materials and components used by the General Electric Company on J-79 turbojet engines have been and are presently being irradiation tested at the ANPD in an effort to determine the applicability of these materials in propulsion machinery for nuclear powered flight. The materials and components are irradiated in anticipated thermal environments while being subjected to functional pressure and fluid flow. The materials and components under investigation include a turbojet lubricant, hydraulic fluid, fuel, elastomer seals, gaskets, and hoses. The elastomer materials consist of seven commercial products in the form of fabricated O-rings, gaskets and flexible hoses.

This paper will present the past, present and planned materials and components irradiation programs, post-irradiation materials evaluation, the necessity for information of this kind, and other problems and considerations associated with applications proving radiation tolerance of organic engineering materials.

This paper was not available for publication.

THE EFFECT OF NUCLEAR RADIATION DURING ESCAPE ON F-104

by

F. L. BOUQUET, JR.
Lockheed Aircraft Corporation
California Division, Burbank, California

This paper is classified and is bound in Volume Six.